AFCRL 681

THE UNIVERSITY OF MICHIGAN

COLLEGE OF LITERATURE, SCIENCE, AND THE ARTS
Department of Physics

Technical Report

STARK EFFECTS IN THE NEAR INFRARED SPECTRA OF SIMPLE POLYATOMIC MOLECULES

P. D. Maker

ORA Project 03640

under contract with:

AIR FORCE COMMAND AND CONTROL DEVELOPMENT DIVISION
AIR RESEARCH AND DEVELOPMENT COMMAND
CONTRACT NO. AF 19(604)-6125
LAURENCE G. HANSCOM FIELD
BEDFORD, MASSACHUSETTS

administered through:

OFFICE OF RESEARCH ADMINISTRATION ANN ARBOR

May 1961

This report was also a dissertation submitted in partial fulfillment of the requirements for the degree of Doctor of Philosophy in The University of Michigan, 1961.

ERRATA

STARK EFFECTS IN THE NEAR-INFRARED SPECTRA
OF SIMPLE POLYATOMIC MOLECULES

Paul Donne Maker

ORA Report 03640-1-T

Page 42 line 8 read "(20)" for "(30)"

Page 43 last line of Table VI read "$\frac{A}{B}$" for "$\frac{C}{A}$".

Page 47 line 3 read $\psi_{JM}^{EXACT} = \sum_{J'} A_{J'J}^{M} \psi_{JM}$

Page 54 line 12 read P(2) for P(1).

Page 95 line 14 read "$\frac{2\mu^2\mathcal{E}^2}{A+C}$" and "$\mathcal{E}$ = 20 KV/cm".

Page 98 line 6 read "1.0" for "10".

Page 102 line 24 read "Edmonds" for "Edwards".

Page 102 line 31 add ref. 21b: Peter and Strandberg, MIT Research Laboratory of Electronics Technical Report 336 (1957).

TABLE OF CONTENTS

LIST OF FIGURES

LIST OF FIGURES (Concluded)

LIST OF TABLES

ABSTRACT

A survey has been made of Stark effects in the vibration-rotation spectra of simple polyatomic molecules. Employing a light guide type Stark absorption cell 90 cm long having front surfaced mirrors as parallel plate electrodes, fields of 120 kV/cm could be obtained with sample pressures below 1/4 mm Hg. The electrode spacing of 0.2 to 0.5 mm was evaluated by examining the fringe systems produced upon passing light through the cell perpendicular to its optical axis. For this purpose, partially transparent mirror electrodes were used. The gap was held to ±1%(± 2.5 microns). An Ebert-Fastie spectrometer of three meter focal length and equipped with a 300 line/mm grating 200 mm long afforded a resolving power in excess of 75,000 when used double passed. Liquid air cooled PbS detectors and synchronous amplifiers were used.

Measurable frequency shifts were observed in the ν_3 fundamental of hydrogen cyanide. Its large dipole moment and simple spectrum made possible the resolution and identification of all the 'M' components for the lines R(2) through P(3). Careful measurement (with a relative accuracy of ± .005 cm^{-1}) of the splittings yielded a value of 3.001 ± .007 debye for the dipole moment of hydrogen cyanide in its ν_3 vibrational state. The identification of Stark components in the spectra of methyl fluoride and methyl iodide was made impossible by their dense zero field spectra. The low field Stark difference spectra did, however, show line intensities differing in a predictable way from the normal spectra. This intensity variation eliminated up to 70% of the normally observed absorption lines and could be used to advantage in making

assignments in the zero field spectrum. The Stark effects observed in the ν_1 fundamental of NH_3 resulted from field produced mixing of the wave functions describing adjacent inversion states and consequent vitiation of the $a \not\leftrightarrow a$, $s \not\leftrightarrow s$ selection rule. Near degeneracies which interacted in the presence of an electric field were found to account for the bulk of the Stark signals observed in the ν_1 and ν_3 fundamentals of water vapor.

Stark effect techniques, at present difficult and applicable to only a few molecules, would become valuable new infrared tools if a significant increase in resolving power (as might be obtained by using a Fabry Perot interferometer) were available.

I. INTRODUCTION

An electric dipole placed in a uniform electric field is acted upon by forces tending to orient it in that field. Classically, the dipole would align itself parallel to the field. Quantum mechanically, only certain angular orientations, each with its own energy of interaction, are allowed. Such effects were first observed in 1913 by Stark (1) in atomic spectra with electric fields of the order of hundreds of thousands of volts/cm. Stark effects in the pure rotational spectra of molecules having permanent dipole moments are extensively used in the microwave region (2) where fields of several hundred volts/cm produce sufficient separation of the components. Certain molecular beam experiments also depend upon the Stark effect (3). Stark effects in the vibration-rotation spectra of polar molecules were recently noted for NH_3 and H_2O by Terhune (4). The results, although not directly interpretable due to the large spectral line widths produced by the high gas pressures needed to prevent electrical breakdown, indicated that infrared Stark effect studies could be made provided that an absorption cell could be operated with low sample pressures and high electric fields (of the order of tens of thousands of volts/cm).

II. OUTLINE OF THE WORK

The current investigation began with construction of such an absorption cell. It was learned (5) that fields of several hundreds of thousands of volts/cm had been obtained at low gas pressures with closely spaced parallel plate electrodes under conditions of extreme cleanliness. The relation between these parameters is conveniently displayed by the Paschen curves (6). Here, breakdown voltage is plotted versus the product of sample pressure

and electrode spacing, and it is indicated that for a pressure gap product less than about 2mm x 1mm Hg, depending upon the gas used, the breakdown voltage rises sharply to a limit imposed by field emission at the electrodes. Thus, the necessary conditions on the proposed Stark cell were that the electrode gap be fractions of a millimeter, the length to be sufficient to produce 10% - 50% infrared absorption, with a sample pressure of about 1mm Hg, and that the cell could be incorporated into the foreoptics of a high resolution grating spectrometer.

The final design of the Stark cell had front-surface mirror electrodes spaced 1/5 to 1/3mm apart, some 90 cm long by 4 cm high. Electric fields up to 120,000 volts/cm were obtained at minimum gas pressures (1/2mm Hg or less), but higher pressures (and consequently lower fields) were necessary to obtain adequate absorption strengths for many transitions. Using the Michigan 3-meter double-passed Ebert-Fastie Spectrometer (7,8), observations in the three micron spectral region were made upon fundamentals of HCN, CH_3F, CH_3I, NH_3, and H_2O.

Because of its very favorable dipole moment and moment of inertia, and its simple infrared spectrum, HCN yielded to quantitative Stark effect measurements. Spectral line shifts of as much as 1 cm^{-1} were seen, and measurements of the shifts allowed a determination of the excited ν_3 vibrational state dipole moment.

CH_3F and CH_3I, because of their less favorable molecular constants and much more complicated spectra, did not demonstrate quantitatively measurable Stark effects. However, their Stark effect spectra, when recorded as the difference signal between absorption with electric field on and absorption with electric field off, were considerably simpler and much more easily

interpreted than their normal infrared spectra. In fact, with the aid of the Stark difference spectrum rotational assignments in the ν_4 fundamentals can readily and reliably be given, a task which otherwise would require extensive labor.

The Stark spectrum of NH_3 arises primarily from the inversion duality of the molecule. The spacing between adjacent inversion levels is much smaller than that between adjacent rotational levels, and, consequently, the principal interaction with the electric field is through neighboring inversion levels. These facts imply that the wave functions describing adjacent inversion states will mix strongly in the presence of an electric field, allowing transitions otherwise forbidden. Thus, the Stark spectrum shows not only large line shifts but also new, field produced absorptions.

Observed Stark effects in the spectrum of H_2O were in the main found due to the interaction of nearly degenerate energy levels in the presence of the applied field. Small shifts were also seen for lines arising from transitions between states of low rotational energy. Analysis of the Stark spectrum was complicated by the moderately strong absorption of traces of water vapor remaining in the spectrometer foreoptics, even after dry-nitrogen flushing.

The effects encountered were fully explained on the basis of perturbation calculations except for the case of HCN. Here the small field approximation was unsatisfactory and an exact solution of the Schroedinger equation including the electric field term was needed to account for the observed shifts and intensities.

The Stark shifts produced in the present work are of the order of hundredths of a cm^{-1}, excepting those due to the near degeneracies occurring in NH_3 and H_2O and those found in the first few rotational lines of the HCN

spectrum. The best resolution attainable was about 0.04 cm^{-1} so that quantitative measurements were all but impossible save in the few cases mentioned.

III. EXPERIMENTAL ARRANGEMENT

As the expected Stark shifts were of the order of, or in many cases smaller than the resolution available, it was absolutely necessary to operate the spectrometer at peak resolution. This meant that sample pressures must be kept low enought to limit pressure broadening to a few hundredths of a cm^{-1}. Thus having fixed the pressure (for most gases less than 3mm Hg), the length of the Stark cell must be sufficient to give adequate absorption. However, the transmission efficiency of the cell must also be considered in determining its optimum length.

Consideration of the Paschen curves (6) indicated that at the pressures contemplated, the electrode spacing must be limited to fractions of a millimeter, and further that the maximum field applicable would increase inversely as the second power of the electrode separation. The value of a small gap in this respect had to be balanced against the reduced transmission efficiency of the cell as the spacing decreased. It was decided to fix the cell length at 90 cm and spacings ranged from 0.2mm to 0.6mm.

An appreciable transmission efficiency for such a long, narrow cell could only be achieved by using it as a light guide. In this arrangement an image is formed at the entrance to the cell and the radiation emerging after a multi-reflection traversal is collected to form an image of the exit aperture of the cell onto the entrance slit of the spectrometer. The incident beam must be confined to as narrow a cone as possible, and the cell walls must be extremely flat and highly reflecting. Since a minimum cell

width of 0.2mm was anticipated, and the slit width of the spectrometer at maximum resolution was 0.04mm, a demagnification of 4X was indicated. The slit height was 1 cm, so that a cell height of 4 cm was necessary. The spectrometer operated at f/15, the cell at f/60. At this aperture, the extreme rays of the beam would strike the electrode at an angle of about 0.5° from grazing incidence, a condition which seemed suitable. Calculations based on the optical constants of freshly deposited aluminum surfaces (9) indicated that a 90 cm Stark cell with a gap of 0.25mm operated at f/60 would have a theoretical efficiency of 90% for 3 micron radiation polarized with its electric vector perpendicular to the plane of incidence, and 43% for the parallel polarization. These figures are extremely sensitive to the reflectivities used and severe downgrading of them is to be expected in practice where the reflecting surfaces are anything but 'freshly deposited' and plane parallel.

With these requirements for the Stark cell firmly in mind, the most promising electrode seemed to be a front surface mirror. Thus the original Stark cells, Model 'A', employed strips of 1/4" thick plate glass 36" long by 2-1/2" wide, selected for flatness, and aluminized in an especially constructed vacuum evaporator. There remained the problems of setting the gap uniformly over the length of the cell consistent with good electrical insulation, and naking electrical contact to the films without disrupting either the flatness of the plates, their reflectivity, the uniformity of the gap, or the electrical insulation. The first solution to these problems, which met with reasonable success, used two 1/2" by 36" strips of 0.008" Lufkin feeler gauge stock running lengthwise of the cell, one at the top and one at the bottom, to establish the gap. The aluminized electrode area extended

to within 1/4" of the ends of the cell, and to within 1/8" of the steel spacers. Small holes were bored through the glass electrodes at their centers, the electrical leads brought through these holes and soldered into place with indium. Each hole was carefully filled with the solder and pared smooth at the surface to be aluminized. The pair of plates, separated by the spacers, was pressed together between the rails of two pieces of surface-ground 2-1/4" channel iron and cemented along the top and bottom edges with Araldite epoxy resin. Pressure supplied by a host of C-clamps over the spacers was uniformly distributed by inserting a strip of rubber between rail and glass. Once the resin set, the clamps were removed and the unit was secured in place inside a vacuum-tight shell made of a piece of brass S-band waveguide having removable end plates with glyptal sealed rock salt windows. One electrode lead was internally attached to the vacuum shell which was grounded while the other was brought directly into the atmosphere through a vacuum seal to the glass electrode plate. The gas sample was admitted, and its pressure measured via a glass tubing system incorporating a differential oil manometer which was Araldited directly to the vacuum shell. The manometer could be read to about $\pm$ 30 microns Hg and had a range of 0 - 5mm Hg above the reference vacuum. This housing with its attachments was used without modification throughout the experiment.

This cell allowed fields up to 70 kV/cm to be applied to several mm Hg of gas, enough to produce a 0.7 cm^{-1} shift of a 50-60% absorption line in the spectrum of HCN. The breakdown voltage versus pressure-gap characteristics of this and subsequent cells fell far short of that expected from consideration of the available Paschen curves. It was felt that dust specks between the electrodes initiated the discharge in the cells. Indeed, attempts

to produce dust-free cells by washing and assembling them in an air-tight dry box did yield slightly improved performance. C. C. Costain (5) recognized this as the limiting factor and was able to attain fields of 500 kV/cm only after removing all traces of dust by immersion-washing his entire cell in purified liquids just prior to use. Considering the size and complexity of our cells, these operations were not feasible, and it seemed that dust specks would remain the field-limiting factor.

The estimated transmission efficiency of this cell was 15 - 20% with a polarization ratio of about 6:1.

The cell soon failed when intermittent sparking along the length of the electrodes caused immense current densities at the periphery of the solder spot which eventually melted down the thin aluminum film, isolating the high voltage lead from the electrode. This weakness was corrected in later designs by using the spacer itself (or a narrow strip of 0.001" feeler gauge stock placed between spacer and electrode for those cells having insulating spacers) to conduct current into the film. The plates of Model 'B' cells were aluminized to within 2mm of the ends and one edge was masked off to prevent electrical continuity through the steel spacer, a gap of about 1mm being left between the aluminum film of one electrode and the spacer-lead of the opposing electrode. The high voltage lead-out, a piece of enameled magnet wire, was soldered directly to the spacer, the joint sealed in epoxy and Apiezon W-100, and the lead brought out through a lucite observation port in the side of the vacuum shell. The enamel coating alone sufficed to prevent discharge from the lead in the space between electrode and shell wall at all vacuums and voltages encountered. This type of cell invariably failed due to intense sparking originating along the edge of the aluminum paralleling

the spacer. This led to the final electrode configuration, Model 'C', shown in Figure 1. The steel spacers, at some sacrifice in gap uniformity, were replaced with ones made of Dupont Mylar, permitting the aluminized area to extend up to and beneath both spacers, eliminating the troublesome source of breakdown and at the same time minimizing electric field fringing effects. The strips were prepared by tightly winding an 8" x 96" piece of Mylar around a 2" spindle chucked in a lathe, facing one end of the bundle and slicing off the required width with a razor blade cutoff tool. This produced a straight, square, and extremely smooth edge, necessary since the spacer edge serves also to reflect the vertically divergent light beams within the absoption cell.

Having established a satisfactory design for the Stark cell, it remained to determine the optimum gap and electrode film material. It was found that the breakdown voltage was inversely proportional to the sample pressure (for small enough pressures and moderate fields) as would be predicted from the Paschen curves. Figure 2 shows the variation of breakdown voltage with pressure for a typical case. The upper voltage limit is evidently determined by the state of cleanliness of the electrodes but does show a distinct dependence upon the cell gap, varying approximately as the reciprocal of the electrode separation. This data was not particularly dependable as it involved a series of cells with different gaps, but there was no way to insure that the cells would all have equally clean (dirty) electrodes.

Transmission measurements revealed efficiencies well below the theoretical maximum. As previously concluded, the chief reason for this discrepancy is undoubtedly due to the fact that the calculated value was based upon the optical constants for 'freshly deposited', clean, unoxidized films. Even the vanishingly thin oxide film present on all aluminum surfaces exposed to

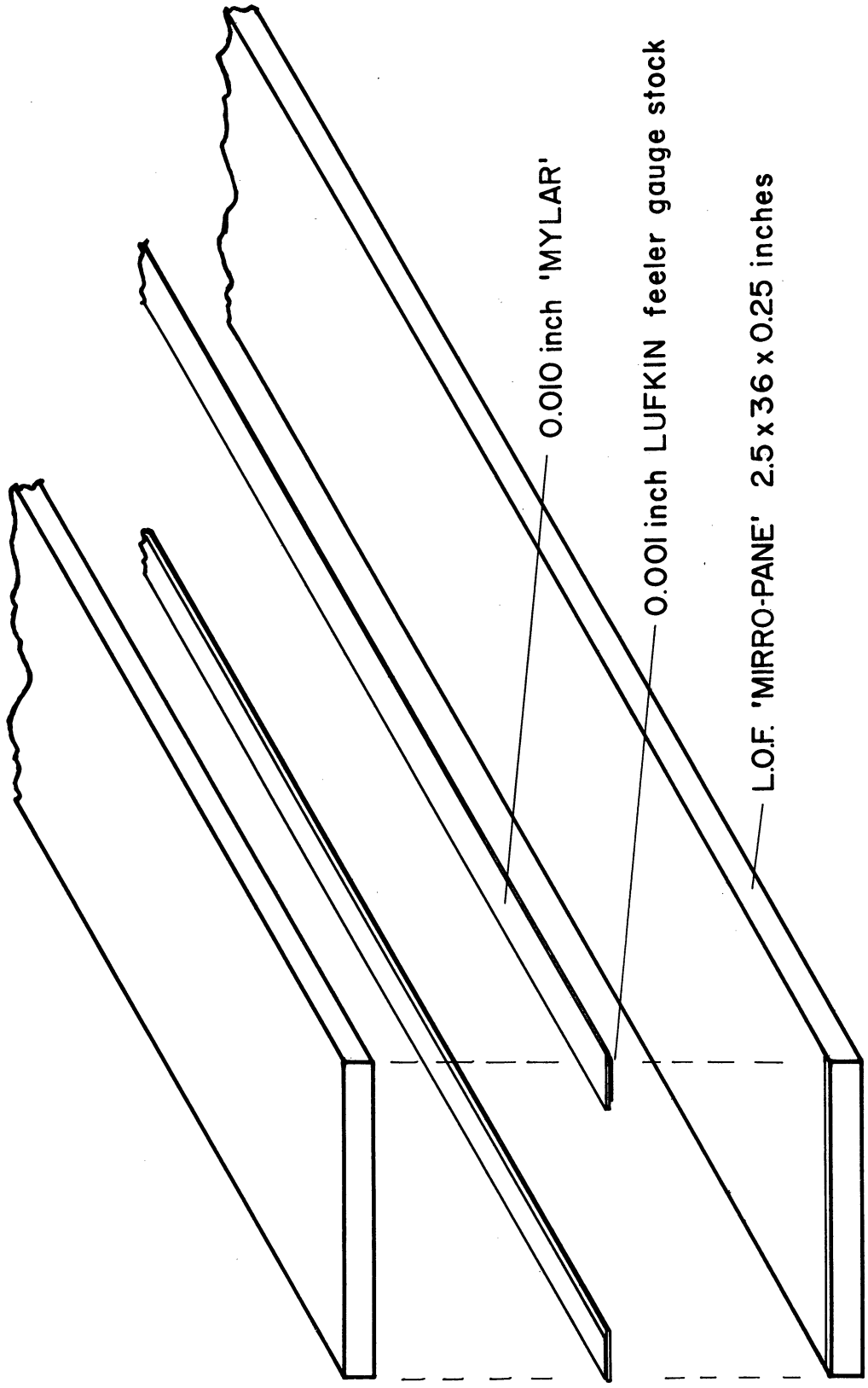

Figure 1 HIGH FIELD STARK CELL

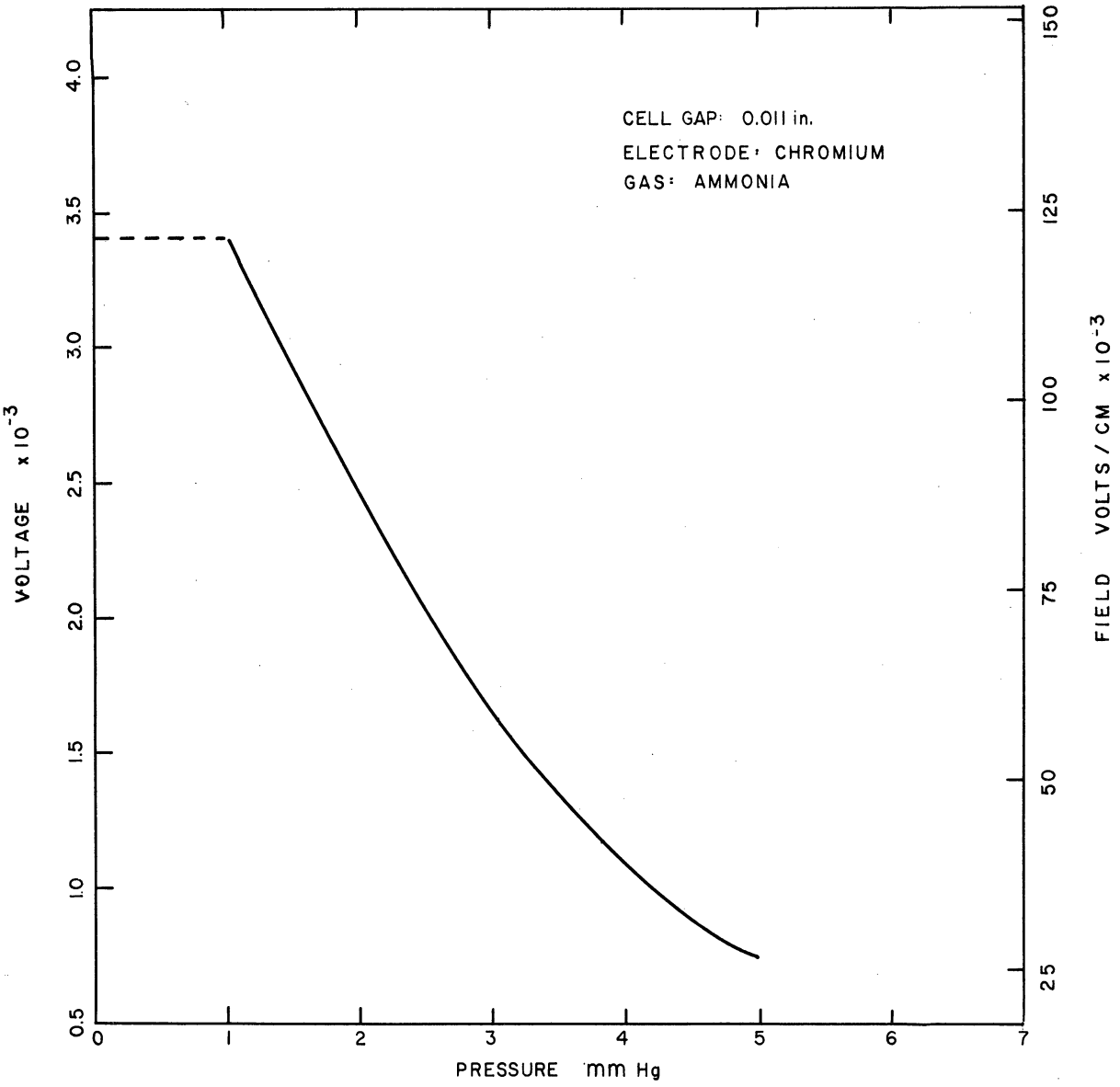

Figure 2 CELL BREAKDOWN VERSUS SAMPLE PRESSURE

the air will sharply reduce the calculated efficiency by refracting the light so as to increase its angle of incidence at the actual metallic surface. This does not increase N, the total number of reflections suffered upon traversal of the cell length, but does lower the reflectivity, R, which decreases linearly as the angle of incidence increases from grazing (for small enough departures from grazing). The transmission efficiency depends upon R^N, and since N is typically 30, even a small decrease in R will have a large net effect. Aside from using idealized optical constants, the calculated value failed to include losses due to reflections from either the unsilvered portions of the light guide or from the Mylar surfaces. Also not taken into account was the fact that slightly nonflat plates would increase the number of reflections.

The possibility of improving cell performance in both transmission and voltage characteristics by changing the film material was investigated. The only substance having optical constants materially superior to aluminum in the three micron region is gold. A cell was made having evaporated gold surfaced electrodes, and a slight increase in transmission over aluminum was noted. However, the gold films seemed to be destroyed much more readily by the action of random breakdown sparking with resultant poor electrical characteristics and short operating life.

Chromium was known to have superior characteristics as a high voltage electrode material (10). Although it was difficult to produce good uniform chromium films in our equipment because of the high temperatures needed in evaporation, a high quality front surface chromium mirror was available from Libbey-Owens-Ford under the trade name Mirro-pane. Tests with Mirro-pane cells revealed somewhat lower transmission efficiencies than for aluminum,

but generally improved electrical properties. Microscopic examination of the surface of an electrode in the neighborhood of a point at which a discharge had occurred revealed a dendritical pattern etched through the metallic film accompanied by random globular deposits, evidently the remains of the detached film. With chromium electrodes, the dendrites seemed shorter, and the damage wrought by a single discharge seemed less than with aluminum films; perhaps due to the fact that chromium adheres to glass orders of magnitude better than does aluminum. Thus, with regard to both cell life and to maximum breakdown voltage, the Mirro-pane cells out-performed the aluminum ones. It was concluded that in spite of their somewhat lower transmission efficiency, the chromium cells were to be preferred, and the majority of the Stark measurements were made using these cells. Table I summarizes the voltage and transmission characteristics of the various cells tested.

TABLE I

Summary of the Optical and Electrical Characteristics of the Various Stark Cells

Coating	Model	Gap	Max. Field[a]	Trans.	Pol.[b]	Lifetime
Aluminum	A	.008"	80kV/cm	20%	6:1	poor
	B	.008	80kV/cm	20%	6:1	poor
	C	.011	60kV/cm	25%	4:1	fair
Chromium	C	.0085	120kV/cm	12%	10:1	good
	C	.011	90kV/cm	15%	5:1	good
	C	.016	60kV/cm	20%	3:1	good
Gold	C	.016	40kV/cm	35%	?	poor

a Measured with cell pressure less than one micron

b Ratio of $T_{\perp}/T_{\parallel}$

Moreover, the Mirro-pane was about 10% transparent to visible light. Interference fringes of excellent definition could be seen upon looking through the cell parallel to the field direction into a monochromatic light source. The appearance (or disappearance) of a fringe upon scanning the cell across the line of vision heralded a decrease (or increase) in the gap of one-half the wavelength of the light employed. Thus a relief map of the spacing, in half-wavelength units, could be drawn for the entire cell area. Further, spectroscopic analysis of the light transmitted in this sense through the cell from an incandescent source revealed so-called 'channel' fringes; that is, transmission maxima occurring when the gap is an integral number of half wavelengths. Measurement of these fringes yielded a determination of the electrode separation to one part in fifty thousand at a single point. Using this point as a reference, the relief map could then be employed to establish the mean gap and its tolerance.

Using the above method, it was determined that with due care Stark cells could be constructed with a tolerance equaling either the thickness tolerance of the spacer or the flatness tolerance of the glass used, whichever happened to be larger. Thus, the cells having Lufkin No. 140 feeler gauge stock as their spacer had a tolerance of 2 fringes of sodium D light (1/4% of a 0.010" gap), a limit set by the plate glass. With Mylar spacers, the non-uniformity ranged upward to 2%, but at times was as good as 3/4%, depending upon the care exercised in selecting the spacer. The bulk supply of Mylar seemed good to about 2/10,000". Occasionally the Mirro-pane slabs as supplied were found unsatisfactory and had to be rejected.

The electric field strength also depends upon the applied voltage, which must then be measured and maintained with an accuracy commensurate with that

of the gap. This was accomplished by using a Baird Atomic Model 318 regulated 0-2500 vDC power supply monitored by a Leeds and Northrup type K-2 potentiometer coupled to the supply through a thermally regulated precision calibrated voltage dividing network (2038.8 ±0.2:1) made of wire wound resistors. A Rubicon galvanometer with a sensitivity of 5 x 10^{-4} ua/mm allowed the voltage to be set to ± .05%. Regulation proved better than ± .1% during a given run.

For operation with a 90 cps square wave Stark field, a negative-going 90 cps square wave signal from a Hewlett-Packard generator synchronized to the 60 cps line frequency was applied to the grid of a 6CU6 whose plate was connected directly to the Stark cell's hot electrode and also, through a 1/2 megohm 30-watt resistor, to a 0-3000 vDC 1 amp unregulated power supply. In operation, the supply was set to its maximum voltage and the amplitude of the trigger signal adjusted to provide the desired cell voltage. This arrangement minimized rise and decay times, for the Stark cell discharged through the conducting 6CU6 and charged through the 1/2 megohm resistor toward the full B+ voltage until reaching the preset point at which the tube began to conduct. Rise times of about 0.3 milliseconds and decay times of about 0.01 milliseconds, compared to the 'on' time of 5.5 milliseconds, were achieved at voltages up to 2000vDC. No precision voltage measurements were necessary in this mode of operation and the described 'square' wave was found suitable.

The spectrometer used is that described by Church (11), namely an Ebert-Fastie Spectrometer (7,8) with three meter focal length, double passed, having a 300 line/mm 6" x 8" Bausch and Lomb grating. The source (labeled 'S' in Figure 3) was a 1-1/2" Nernst glower surrounded by a water-cooled vacuum

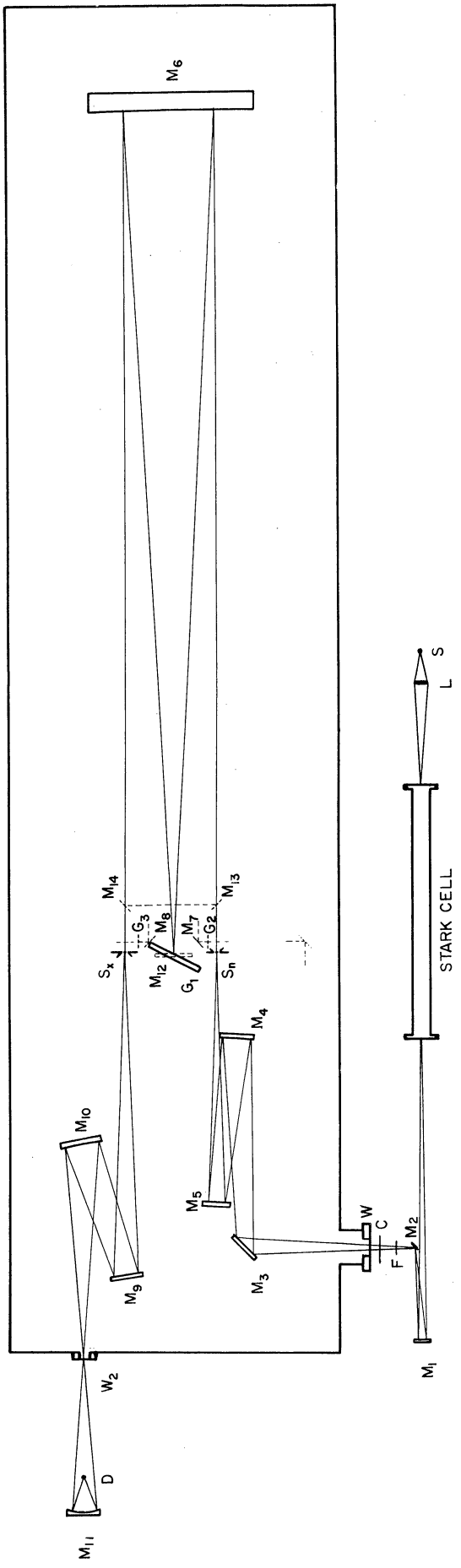

Figure 3 DIAGRAM OF SPECTROMETER AND AUXILIARY OPTICS

tight jacket and operated from a Sorenson regulated Variac delivering one amp. An image of the source was formed on the entrance of the Stark cell by a KBr lens (L) set in a vacuum tight connecting tube. The exit slit of the Stark cell was imaged by a spherical mirror (M_1), demagnified by three, at the surface of a small mirror (M_2) set at 45° to the beam. M_2 was cut from a spectacle lens having the proper radius of curvature, to produce a curved image of the straight exit slit of the Stark cell at the curved entrance slit of the spectrometer. The alignment of the mirror had to be done carefully since the image on the spectrometer slits was not much wider than the 40 micron slit width. The mirror adjustments were cemented with epoxy resin, but building vibrations often interfered with the operation of the instrument.

Leaving the small diagonal, the beam was filtered (F) using anti-reflection coated germanium (>75% transparent for the regions scanned) and chopped (C), all in vacuum tight brass enclosures, before passing into the spectrometer vacuum chamber through its sapphire window (W_1). The foreoptics thus far described were dry-nitrogen flushed, which removed all atmospheric absorption except in the immediate vicinity of strong water vapor lines. Upon entering the spectrometer, the beam is reflected from a flat (M_3) to a sphere (M_4) demagnifying by 4/3 to another flat (M_5) and finally to the entrance slit (S_n). In practice, the image was scarcely wide enough to fill the entrance slit and minute movements of any of the foreoptics after and including the Stark cell had the effect of scanning the image across the slit, causing disasterous signal fluctuations. Sturdy mirror mounts were designed and employed throughout this section of the optical path, ease of adjustment being generously traded for increased

vibrational stability. Once adjusted, the mirrors were cemented in place with epoxy resin (M_1 excepted). This source of noise, except during huge building vibrations, was finally reduced below that of the detector. It remained necessary to refocus (via M_1) on the entrance slit before each run. The entire foreoptics was found to image 80% of the energy passing through a 200 micron slit set at the Stark cell exit, after 4X demagnification and image curving, through a 50 micron entrance slit.

The spectrometer proper had a theoretical resolving power, double passed, of 120,000 corresponding to a maximum resolution of 0.036 cm^{-1} at three microns. Extensive efforts failed to produce spectra exhibiting resolution better than about 0.045 cm^{-1}. Examination of the knife edge pattern produced when scanning the grating through either its central image or through a fifth order sodium line indicated that the cause of this discrepancy was nonflatness in the grating. Attempts to utilize the spectrometer in four-pass configuration thus gave only modest improvements in resolution and not the theoretically expected factor of two, at a sacrifice of about four in energy. A resolution of 0.040 cm^{-1} was observed in four pass with twice the theoretical minimum slit widths and a signal about equal to that obtained at minimum slits when two-passed. Unfortunately, this mode of operation was not practical since the image of the Stark cell exit was not wide enough to fill the expanded slits needed. This multiple passing was accomplished by a set of flat mirrors (M_7 and M_8) aligned to intercept the beam in front of the exit slit, pass it across in front of the grating and send it through the collimator and dispersion paths again, this time at a slightly different elevation. To prove that imperfections in the grating did limit the resolving power, an optical flat was substituted for the grating and the central image scanned

with the instrument four passed. The test produced a central image line width only 5% greater than theoretically predicted.

In attempting accurate wavelength measurements of the HCN spectra, it became evident that the rotational motion of the grating (G_1) was not always continuous, e.g., on occasion the recorder trace of an absorption line would actually show a discontinuity. The drive chain, consisting of:

a) one of a choice of four drive motors,

b) one of a set of four interchangeable spur gear pairs,

c) a drive shaft extending through the spectrometer vacuum wall,

d) a 128:1 precision lapped worm gear,

e) a hand crafted nut and screw assembly 1-1/2" diameter 40 threads per inch 10" long and of extremely high precision,

f) a steel tape, advanced by the nut, wound about a flat faced 10" diameter ground pulley integral to the grating table, around a second identical pulley mounted on an idler shaft back onto itself,

as completely disassembled, inspected, cleaned and carefully reassembled. t was also decided to apply a 3-1/2 pound gravitational load to the grating table so that screw and nut would be held forcibly in contact, rather than relying upon friction in the tape system.

The erratic motion of the grating, thus far detectable only if it occurred while an absorption line was being traced, could only be investigated if a continuous accurate monitoring of the scan were available. To do this, a transmission grating (G_2) 1/4" x 1" with 133 lines per inch was mounted with its lines parallel to the slit in the plane of the entrance slit (after reflection from a flat mirror, M_{13}). A similar grid (G_3) this time 3" long by 1" high was mounted in a reflection (M_{14}) of the exit slit plane, and

an optically flat front surfaced mirror (M_{12}) 2-1/2" square was mounted on a swivel table attached atop the grating support. With the optical flat in proper adjustment, a high quality image of the entrance slit grid was formed by the spectrometer's collimator mirror (M_6) at the exit slit grid. This grid was then adjusted so that its lines were exactly parallel to those of the image. The light transmitted by this system with the first grid uniformly illuminated from the back was modulated in intensity by successive superposition of line upon line and line upon aperture as the grating table rotated. The output of a phototube placed to receive this radiation, when amplified, synchronously rectified and recorded, provided the desired monitoring. If the grating advanced discontinuously at <u>any</u> time during a run, the fringe record would also exhibit a discontinuity. Moreover, since many lines were being averaged in the superposition process, the grids could be considered 'perfect' and the spacing of the fringes used as a calibration device of greater reliability than the 'counter numbers' (unit rotations at the low-torque end of the drive train) usually used for this purpose. Actual fringe traces demonstrated, in addition to occasional lurches in the grating rotation, random ripple attributable to the ultimate precision of the drive mechanism. Consideration of this ripple indicated that the grating angle was determinable to 8×10^{-7} radian corresponding to a linear motion of the drive tape of $\pm 4 \times 10^{-6}$ inches, a figure in keeping with the claimed precision of the nut-screw assembly. As a check on the scanning precision, the spectrum of HCN was run in the vicinity of its ν_3 band center and a dispersion relation established using the wavelengths reported by Rank (12) which have an absolute accuracy of $\pm$ .003 cm^{-1} and a relative accuracy of $\pm$ .001 cm^{-1}. The grating drive uncertainty corresponded at

this wavelength to ± .005 cm^{-1}. A dispersion relation based upon the counter numbers did account for the observed relative line positions to within the above limits. Results of these measurements are given in Table II.

TABLE II

Comparison of the Spacing Between Rotational Lines in ν_3 HCN as Measured on the Michigan Ebert Spectrometer and as Reported by Rank et al (14)

Line	Freq (Rank)	$\Delta\nu$(Rank)	ΔCN(Rank)$_a$	ΔCN(obs)$_b$
P(8)	3287.244 cm^{-1}	-	-	-
P(7)	90.345	3.101 cm^{-1}	12.405	12.43 ± .03
P(6)	93.425	3.080	12.306	12.31
P(5)	96.484	3.059	12.194	12.19
P(4)	99.523	3.039	12.085	12.10
P(3)	3302.542	3.019	11.981	11.97
P(2)	05.540	2.998	11.874	11.88
P(1)	08.517	2.977	11.767	11.74
R(0)	14.409	5.892	23.212	23.16
R(1)	17.324	2.915	11.449	11.43
R(2)	20.217	2.893	11.348	11.37

a Based upon the grating equation $\nu = \frac{1503.53\ cm^{-1}}{\sin(0.00223744\ CN)^\circ}$

b Average of three independent runs.

Upon passing through the exit slit (S_x) the IR beam was reflected from a flat (M_9) onto a spherical mirror (M_{10}) which formed a 2X demagnified image at a hole in the vacuum enclosure. Coupled to the spectrometer at this hole via a bellows was the detector housing which contained an off-axis ellipsoidal mirror (M_{11}) which imaged at 5X demagnification upon the detector D. The recently introduced Kodak Ektron Detectors, type N-2-Gold (lead sulphide) and type P-2-Gold (plumbide), because of their ability to withstand indefinite

cycling between room temperature and liquid air temperature, made it practical to mount the detector against the cold wall of a semipermanent glass dewar as shown in Figure 4. Two different detectors were mounted in the same dewar, and could be interchanged in the optical beam without destroying the spectrometer vacuum by removing the adaptor flange screws and rotating the dewar 180° about its axis. This motion was facilitated by a shallow, well greased O-ring groove. The dewar vacuum chamber was accessible through a high-vacuum stopcock and once out-gassed held a satisfactory vacuum for ten days to two weeks. Freshly pumped, the system retained liquid nitrogen for twelve hours. Detector noise caused by bubbling of the nitrogen was eliminated by placing granular metal in the bottom of the dewar thus providing the necessary thermal mass. Care had to be taken to prevent accumulation of water within the metal ballast which could freeze, expand, and destroy the dewar, an unpleasant experience which did occur. Some difficulty was also experienced when the detector resistance gradually increased to 10^{8} ohms presumably because of out-gassing. Special precautions to eliminate pickup were necessary, shock mounting the preamplifier, and enclosing the detector dewar in aluminum foil being helpful. The detector output was amplified and synchronously rectified using lab-built electronics (11) and recorded on a Leeds and Northrup strip chart recorder. Response times of up to one minute were used to obtain the lowest noise spectra. A fourth motor had to be added to the spectrometer drive unit in order to slow the scan enough to permit use of such long time constants. Many runs were made at a rate of 1-1/2 hours per wave number (corresponding to a grating speed of 9.2 years per revolution!).

The spectrometer vacuum chamber, including the detector housing could

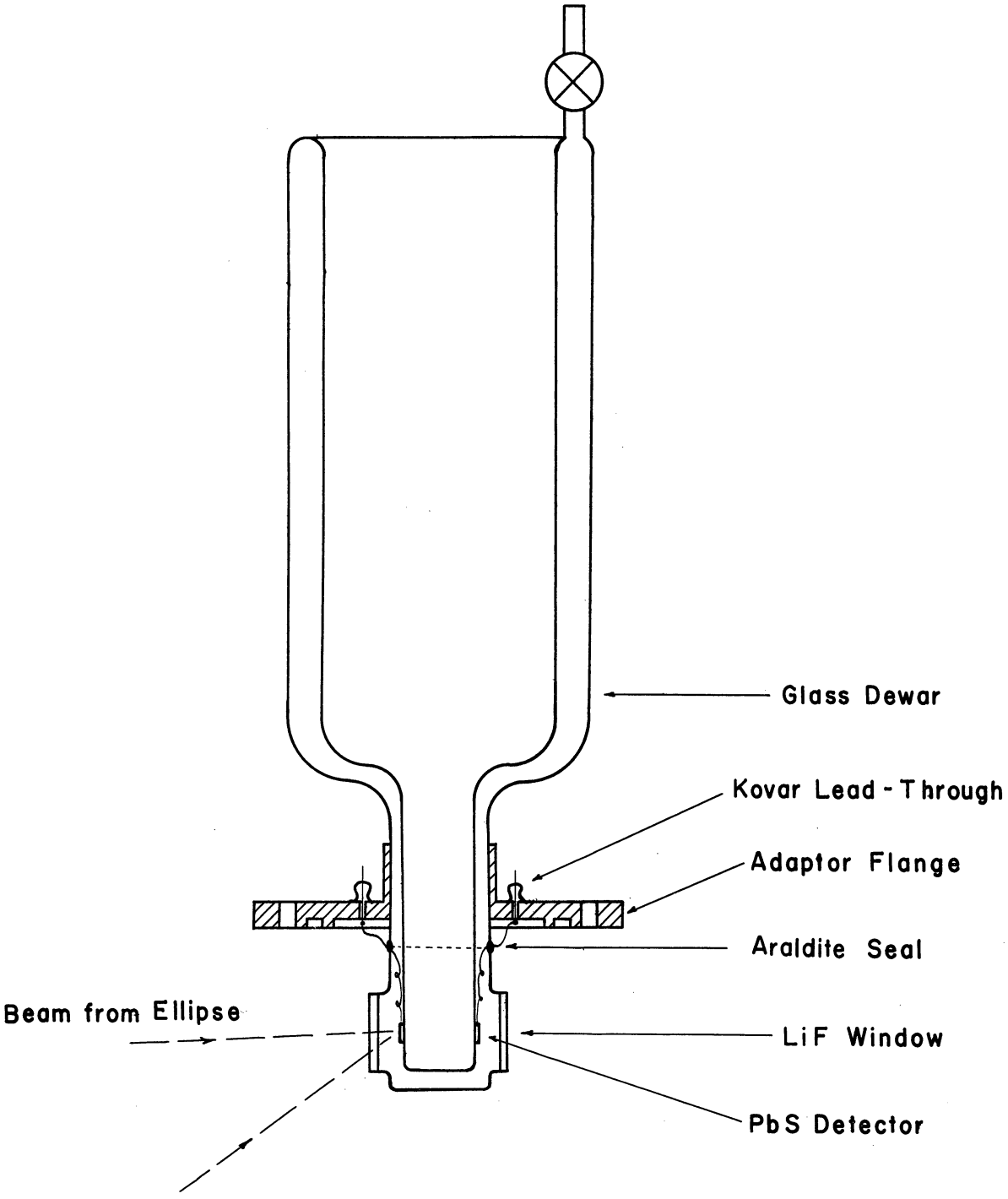

Figure 4 DUAL DETECTOR MOUNT.

be evacuated to less than one micron Hg pressure by a Kinney model DVD 8810 mechanical pump and a CVC model KS-100 four-inch booster diffusion pump. The pressure built up to about 6mm Hg overnight and the electronics were vibration sensitive enough to prohibit pumping during a run. As the optical path within the spectrometer tank was some 100 feet, difficulty in eliminating water absorption when scanning in the vicinity of a water band arose on this account.

IV. THEORY OF THE STARK EFFECT OF POLAR SYMMETRIC TOP MOLECULES

The quantum mechanical description of a rotating polar molecule in an externally applied electric field can be developed in a variety of ways. The method employed will ultimately depend upon the magnitude of the field, the molecular constants and upon the desired accuracy. The simplest approach is to assume the field small and employ conventional perturbation theory to find the corrected energy levels and wave functions. In the opposite extreme, if the field is huge, one can drop those terms in the Hamiltonian that are relatively insignificant, and attempt some sort of approximation to the resultingly simplified problem. Finally, one can attempt an exact solution of the unsimplified problem. As the first and the last of the above mentioned approaches yields results directly applicable to the explanation of observed Stark effects, they will be described in some detail. For the sake of completeness, the second method will also be outlined.

According to the prescriptions of perturbation theory, the first and second order corrections, ΔE_n^1 and ΔE_n^2, respectively, to the n^{th} energy level are given by (13)

$$\Delta E_n^1 = \langle n | \mathcal{H}^1 | n \rangle$$

$$\Delta E_n^2 = \sum_{n'}{}' \frac{|\langle n' | \mathcal{H}^1 | n \rangle|^2}{E_n^\circ - E_{n'}^\circ},$$

where $\mathcal{H}^1$ is the contribution to the exact Hamiltonian due to the perturbation. It is equal, in the present case, to the potential energy due to the applied electric field, namely $-\bar{\mu}\cdot\bar{\mathcal{E}}$ where $\bar{\mu}$ is the instantaneous molecular dipole moment and $\bar{\mathcal{E}}$ is the applied field. Similarly, the corrected wave functions $\bar{\Psi}_i$ are given in terms of the unperturbed functions ψ_i, to second order by

$$\Psi_i = \psi_i + \sum_K{}' \frac{H'_{Ki}}{E_i^\circ - E_K^\circ}\psi_K + \sum_{K,M}{}' \frac{H'_{MK} H'_{Ki}}{(E_i^\circ - E_K^\circ)(E_i^\circ - E_M^\circ)}\psi_M + \sum_M{}' \frac{H'_{Mi} H'_{ii}}{(E_i^\circ - E_M^\circ)^2}\psi_M - \frac{1}{2}\sum_K{}' \frac{|H'_{Ki}|^2}{(E_i^\circ - E_K^\circ)^2}\psi_i$$

Thus, the perturbation solution is available once the quantities

$$H'_{ij} \equiv \langle i | \mathcal{H}' | j \rangle \equiv \int d\tau\, \psi_i^* \mathcal{H}' \psi_j$$

are determined.

Let us denote the wave functions for the rigid symmetric top by $\psi_{JKM}(\psi\theta\phi)$ where ψ, θ and ϕ are the Euler angles (14), ϕ being measured about the figure axis, θ about the line of nodes and ψ about the vertical. These functions can be expressed analytically, and are given by (17)

$$\psi_{JKM}(\psi\theta\phi) = N_{JKM} \exp(iM\psi + iK\phi)\left(\sin\tfrac{\theta}{2}\right)^{|K-M|}\left(\cos\tfrac{\theta}{2}\right)^{|K+M|} {}_2F_1\left(\begin{matrix} I-J,\ I+J+1 \\ I+|K-M| \end{matrix};\ \sin^2\tfrac{\theta}{2}\right)$$

where J is a positive integer or zero and is proportional to the molecule's total angular momentum, K is an integer such that $|K| \leq J$, and represents the projection of J on the figure axis, M is an integer with $|M| \leq J$ and represents the projection of J on the vertical axis, and I equals K or M, whichever is larger. It is seen that the hypergeometric function always

terminates (as -J + I is a negative integer or zero) becoming simply a polynomial in $(\sin\frac{\theta}{2})^2$. These functions represent solutions of the Schroedinger equation

$$\left[\frac{1}{2I_{xx}}\left(\underline{P}_x^2 + \underline{P}_y^2\right) + \frac{1}{2I_{zz}}\underline{P}_z^2\right]\psi_{JKM} = E_{JKM}\psi_{JKM} =$$

$$= \left\{-B\left[\frac{\partial^2}{\partial\theta^2} + \cot\theta\frac{\partial}{\partial\theta} + \cot^2\theta\frac{\partial^2}{\partial\phi^2} + \frac{1}{\sin^2\theta}\frac{\partial^2}{\partial\chi^2} - \frac{2\cos\theta}{\sin^2\theta}\frac{\partial^2}{\partial\chi\partial\phi}\right] - A\frac{\partial^2}{\partial\phi^2}\right\}\psi_{JKM}$$

$$A \equiv \frac{\hbar^2}{2I_{zz}}, \quad B \equiv \frac{\hbar^2}{2I_{xx}}, \quad E_{JKM} = BJ(J+1) + (A-B)K^2.$$

If the applied electric field is allowed to define the vertical axis and since because of symmetry, the dipole moment of the molecule must lie along its figure axis, we see that $\bar{\mu}\cdot\bar{\mathcal{E}} = |\bar{\mu}||\mathcal{E}|\cos\angle\bar{\mu}\bar{\mathcal{E}} = \mu\mathcal{E}\cos\theta$. We are now in a position to evaluate $H'_{ij} = -\mu\mathcal{E}\int d\tau\,\psi_i^*\cos\theta\,\psi_j$, by strictly analytic means. The calculations were first made in this manner (15), but are extremely tedious and require advanced techniques in function analysis. A more modern approach, using step-up and step-down operators to derive expansions for $\cos\theta\,\psi_{JKM}$ in terms of $\psi_{J'K'M'}$ has been developed (16). The most elegant means of doing this expansion, however, is to relate $\cos\theta$ and ψ_{JKM} to the eigenfunctions of total angular momentum and utilize our knowledge of how the product of two commuting angular momentum eigenfunctions can be expressed as a sum of angular momentum eigenfunctions with appropriate coefficients, i.e., of how angular momenta add. We will develop this last method using the formalism* of Edwards (17).

Let $\underline{D}(\alpha\beta\gamma)$ denote that operator which when applied to a function of the Euler angles ψ, θ, and ϕ simply rotates the frame of reference so as to increase ψ, θ and ϕ by amounts α, β, and γ, respectively. It is well known that $\underline{L}^2$ the operation of total angular momentum, remains unchanged when the coordinate axes are rotated. Thus,

* Our choice of Euler angles and of phase factors also follow Edwards (17).

$$\underline{D}(\alpha\beta\gamma)\left\{\underline{L}^2(\psi\theta\phi)f(\psi\theta\phi)\right\} = \underline{L}^2(\psi+\alpha\ \theta+\beta\ \phi+\gamma)f(\psi+\alpha\ \theta+\beta,\ \phi+\gamma)$$
$$= (\underline{D}\,\underline{L}^2)(\underline{D}f) = \underline{L}^2\,\underline{D}f.$$

If we replace $f(\psi\theta\phi)$ by $\phi_{\ell m}(\psi\theta\phi)$, the eigenfunctions of $\underline{L}^2$ with total angular momentum ℓ and z component of angular momentum m, we get

$$\underline{L}^2\,\underline{D}\,\phi_{\ell m} = \underline{D}\,\underline{L}^2\phi_{\ell m} = \hbar^2\ell(\ell+1)\,\underline{D}\,\phi_{\ell m}.$$

Thus $\underline{D}\,\phi_{\ell m}$ is an eigenfunction of $\underline{L}$ with total angular momentum ℓ. We may, therefore, write $\underline{D}(\alpha\beta\gamma)\,\phi_{\ell m}(\psi\theta\phi) = \sum_{m'} D^{\ell}_{m'm}(\alpha\beta\gamma)\,\phi_{\ell m'}(\psi\theta\phi)$, where $D^{\ell}_{m'm}$ are the matrix elements of $\underline{D}$. Next, noting that

$$\underline{D}(\alpha\beta\gamma)\,\phi_{\ell m}(\psi\theta\phi) = \phi_{\ell m}(\psi+\alpha\ \theta+\beta\ \phi+\gamma) = \underline{D}(\psi\theta\phi)\,\phi_{\ell m}(\alpha\beta\gamma),$$

let us evaluate $\underline{L}^2$ operating on $D^{\ell}_{m'm}$.

$$\underline{L}^2(\alpha\beta\gamma)\,D^{\ell}_{m'm}(\alpha\beta\gamma) = \underline{L}^2(\alpha\beta\gamma)\int d\tau\ \phi^*_{\ell m''}(\psi\theta\phi)\,\underline{D}(\alpha\beta\gamma)\,\phi_{\ell m}(\psi\theta\phi)$$
$$= \int d\tau\ \phi^*_{\ell m'}(\psi\theta\phi)\,\underline{L}^2(\alpha\beta\gamma)\,\underline{D}(\psi\theta\phi)\,\phi_{\ell m}(\alpha\beta\gamma)$$
$$= \hbar^2\ell(\ell+1)\int d\tau\ \phi^*_{\ell m'}(\psi\theta\phi)\,\underline{D}(\alpha\beta\gamma)\,\phi_{\ell m}(\psi\theta\phi)$$
$$= \hbar^2\ell(\ell+1)\,D^{\ell}_{m'm}(\alpha\beta\gamma).$$

Thus the matrix elements of the finite rotation operator $\underline{D}$ are also eigenfunctions of total angular momentum.

We can determine the explicit dependence of $D^{\ell}_{m'm}$ on the angles ψ, θ and ϕ by first expressing $\underline{D}$, the operator of finite rotations, in terms of $\underline{L}$, the operator of infinitesimal rotations. Thus,

$$\frac{\partial}{\partial\gamma}\,\underline{D}(00\gamma)f(\psi\theta\phi) = \frac{\partial}{\partial\gamma}f(\psi\theta\ \phi+\gamma)$$
$$= \frac{\partial}{\partial\phi}f(\psi\theta\ \phi+\gamma) = \frac{\partial}{\partial\phi}\,\underline{D}(00\gamma)f(\psi\theta\phi)$$
$$= \underline{D}(00\gamma)\,\frac{i}{\hbar}\,\underline{L_z}\,f(\psi\theta\phi) = \frac{i}{\hbar}\,\underline{L_z}\,\underline{D}(00\gamma)f(\psi\theta\phi)$$

This operator equation has the solution

$$\underline{D}(00\gamma) = C' \exp\left(\frac{i}{\hbar}\gamma \underline{L_z}\right)$$

where

$$\exp\left(\frac{i}{\hbar}\gamma \underline{L_z}\right) \equiv \sum_{n=0}^{\infty} \left(\frac{i\gamma}{\hbar}\underline{L_z}\right)^n / n!$$

Similarly,

$$\frac{\partial}{\partial\beta}\underline{D}(0\beta0) f(\gamma\theta\phi) = \underline{D}(0\beta0)\frac{i}{\hbar}\underline{L_y} f(\gamma\theta\phi)$$

and

$$\underline{D}(0\beta0) = C'' \exp\left(\frac{i}{\hbar}\beta \underline{L_y}\right).$$

Also, since by the way in which $D(\alpha\beta\gamma)$ and the Euler angles were defined,

$\underline{D}(\alpha 00) = \underline{D}(00\alpha)$; we get $\underline{D}(\alpha 00) = C''' \exp\left(\frac{i}{\hbar}\alpha \underline{L_z}\right)$.

Since

$$\underline{D}(\alpha\beta\gamma) = \underline{D}(\alpha 00)\underline{D}(0\beta0)\underline{D}(00\gamma),$$

we see that

$$\underline{D}(\alpha\beta\gamma) = \exp\left(\frac{i\alpha}{\hbar}\underline{L_z}\right)\exp\left(\frac{i\beta}{\hbar}\underline{L_y}\right)\exp\left(\frac{i\gamma}{\hbar}\underline{L_z}\right),$$

where the constant multiplier is set equal to one to make $\underline{D}$ unitary. We may now partially evaluate $D^{\ell}_{m'm}(\alpha\beta\gamma)$ as

$$D^{\ell}_{m'm}(\alpha\beta\gamma) \equiv \int d\uparrow\, \phi^*_{\ell m'}\, \underline{D}(\alpha\beta\gamma)\, \phi_{\ell m}$$

$$= \int d\uparrow\, \phi^*_{\ell m'} \exp\left(\frac{i}{\hbar}\alpha \underline{L_z}\right)\exp\left(\frac{i}{\hbar}\beta \underline{L_y}\right)\exp\left(\frac{i}{\hbar}\gamma \underline{L_z}\right)\phi_{\ell m}$$

$$= \int d\uparrow \left(\exp\left\{\frac{-i}{\hbar}\alpha \underline{L_z}\right\}\phi_{\ell m'}\right)^* \exp\left(\frac{i}{\hbar}\beta \underline{L_y}\right)\left(\exp\left\{\frac{i}{\hbar}\gamma \underline{L_z}\right\}\phi_{\ell m}\right)$$

$$= e^{im'\alpha/\hbar}\, e^{im'\gamma/\hbar} \int \phi^*_{\ell m'} \exp\left(\frac{i}{\hbar}\beta \underline{L_y}\right)\phi_{\ell m}\, d\uparrow, \quad \text{or}$$

$$D^{\ell}_{m'm}(\alpha\beta\gamma) = \exp\frac{i}{\hbar}(m'\alpha + m\gamma)\; d^{\ell}_{m'm}(\beta).$$

Furthermore, we can show that ψ_{JKM} is also an eigenfunction of total angular momentum. Thus,

$$\underline{\mathcal{H}}_{ST} = \frac{1}{2I_{xx}}\left(\underline{P}_x^2 + \underline{P}_y^2\right) + \frac{1}{2I_{zz}}\underline{P}_z^2$$
$$= \frac{1}{2I_{yy}}\underline{L}^2 + \left(\frac{1}{2I_{zz}} - \frac{1}{2I_{yy}}\right)\underline{P}_z^2 .$$

But $\underline{\mathcal{H}}_{ST}\psi_{JKM} = E_{JK}\psi_{JKM} = \frac{\hbar^2}{2I_{xx}}J(J+1) + \hbar^2K^2\left(\frac{1}{2I_{zz}} - \frac{1}{2I_{xx}}\right)$ and

$\underline{P}_z^2\psi_{JKM} = \left(\frac{\hbar}{i}\right)^2\frac{\partial^2}{\partial\phi^2}\psi_{JKM} = -\hbar^2K^2\psi_{JKM}$.

Therefore, $\underline{L}^2\psi_{JKM} = 2I_{xx}\left\{\frac{\hbar^2}{2I_{xx}}J(J+1) + \hbar^2K^2\left(\frac{1}{2I_{zz}} - \frac{1}{2I_{xx}}\right)\right\}\psi_{JKM}$

$= \hbar^2J(J+1)\psi_{JKM}$.

Considering the above facts, we conclude that $\psi_{JKM} = C\,D^J_{MK}$. The constant can be determined via orthogonality relations (17)

$$\int d\tau\,\psi^*_{JKM}\psi_{JKM} = 1 = C^2\int d\Omega\,D^{J*}_{MK}D^J_{MK} = C^2\int d^{J*}_{MK}\,d^J_{MK},$$

$$1 = C^2\,8\pi^2/2J+1, \quad C = 2\pi/(J+\tfrac{1}{2})^{1/2},$$

$$\psi_{JKM} = \frac{2\pi}{\sqrt{J+1/2}}D^J_{MK}.$$

Also, since $D^J_{MK}(\psi\theta\phi)$ represents a complete set of functions in ψ, θ, and ϕ, the direction cosines of the dipole moment can be expressed as sums of D's. In particular, $\cos(\theta) = D^1_{oo}$.

Now let us expand products of the type $D^J_{MK}(\omega)\,D^{J'}_{M'K'}(\omega)$, $\omega \Longrightarrow \alpha\beta\gamma$. If $U(J_1\ M_1)\,U(J_2\ M_2)$ is the product wave function of two commuting angular momenta in a representation diagonalizing J_1, J_2, M_1 and M_2, we may transform it, using 'vector coupling coefficients' into a representation diagonalizing J_1, J_2, J, M, i.e.,

$$U(J_1M_1)\,U(J_2M_2) = \sum_{J=|J_1-J_2|}^{|J_1+J_2|} \langle JM|M_1M_2\rangle\, W(J_1\,J_2\,J\,M) \qquad M = M_1 + M_2.$$

Applying a finite rotation of the coordinate axes to the left hand side of this equation yields

$$\underline{D}\left\{U(J_1M_1)\,U(J_2M_2)\right\} = \underline{D}\,U(J_1M_1)\,\underline{D}U(J_2M_2)$$

or

$$\underline{D}\{U(J_1M_1)\,U(J_2M_2)\} = \sum_{M_1'M_2'} D^{J_1}_{M_1'M_1} D^{J_2}_{M_2'M_2}\, U(J_1M_1')\,U(J_2M_2').$$

Applying the same rotation to the right hand side gives

$$\underline{D}\sum_J \langle JM|M_1M_2\rangle W(J_1J_2JM) = \sum_{JM'} \langle JM|M_1M_2\rangle D^J_{M'M} W(J_1J_2JM')$$

$$= \sum_{JM'M_1'M_2'} \langle JM|M_1M_2\rangle D^J_{M'M} \langle M_1'M_2'|JM'\rangle U(J_1M_1')\,U(J_2M_2').$$

Equating coefficients of $U(J_1M_1)\,U(J_2M_2)$ we obtain

$$D^{J_1}_{M_1'M_1} D^{J_2}_{M_2'M_2} = \sum_J \langle JM|M_1M_2\rangle D^J_{M'M} \langle M_1'M_2'|JM'\rangle$$

where $M' = M_1' + M_2'$, $M = M_1 + M_2$, or

$$D^J_{MK}\, D^{J'}_{M'K'} = \sum_{\sigma=|J-J'|}^{|J+J'|} \langle \sigma\ K+K'|K\ K'\rangle\, D^\sigma_{M+M'\,K+K'} \langle M M'|\sigma\ M+M'\rangle.$$

The 'vector coupling' or Clebsch-Gordan coefficients $\langle JM|M_1M_2\rangle$ may be replaced by the Wigner 3-j symbols, modifications which more clearly display their functional symmetries and are defined by (17)

$$\begin{pmatrix} J_1 & J_2 & J_3 \\ M_1 & M_2 & M_3 \end{pmatrix} \equiv (-1)^{J_1-J_2-M_3} (2J_3+1)^{-\frac{1}{2}} \langle M_1M_2|J_3-M_3\rangle.$$

This then gives the relations

$$D^J_{MK}\, D^{J'}_{M'K'} = \sum_{\sigma=|J+J'|}^{|J-J'|} (-1)^{K+K'+M+M'} (2\sigma+1) \begin{pmatrix} J & J' & \sigma \\ M & M' & -M-M' \end{pmatrix} D^\sigma_{M+M'\,K+K'} \begin{pmatrix} J & J' & \sigma \\ K & K' & -K-K' \end{pmatrix}.$$

Using the relation between ψ_{JKM} and D^J_{KM} the matrix elements needed for the perturbation calculations are easily established, i.e.,

$$\cos\theta\ \psi_{JKm} = \sqrt{\frac{2J+1}{8\pi^2}}\ D^1_{00}\, D^J_{mK}$$

$$= \sqrt{\frac{2J+1}{8\pi^2}} \sum_{\sigma=J-1}^{J+1} (-)^{M+K} (2\sigma+1) \begin{pmatrix} 1 & J & \sigma \\ 0 & M & -M \end{pmatrix} D^\sigma_{MK} \begin{pmatrix} 1 & J & \sigma \\ 0 & K & -K \end{pmatrix}$$

$$= \sqrt{2J+1} \sum_{\sigma=J-1}^{J+1} (-)^{M+K} (2\sigma+1)^{\frac{1}{2}} \begin{pmatrix} 1 & J & \sigma \\ 0 & M & -M \end{pmatrix} \psi_{\sigma Km} \begin{pmatrix} 1 & J & \sigma \\ 0 & K & -K \end{pmatrix}$$

whereby

$$\int \psi^*_{J'K'm'} \cos\theta \, \psi_{JKm} \, d\tau = \sqrt{2J+1}\,(-1)^{m-K} \sum_{\sigma=J-1}^{J+1} \sqrt{2\sigma+1} \begin{pmatrix} 1 & J & \sigma \\ 0 & M-m & m \end{pmatrix} \begin{pmatrix} 1 & J & \sigma \\ 0 & K-K & K \end{pmatrix} \delta_{J'\sigma} \delta_{K'K} \delta_{m'm}$$

via the orthonormality of the ψ_{JKM}. Using the tabulated values of the 3-j symbols (17) we arrive at the final result,

$$\langle J+1\ K\ m \,|\cos\theta|\, J\ K\ m\rangle = \frac{\left[(J+1)^2-K^2\right]^{\frac{1}{2}}\left[(J+1)^2-M^2\right]^{\frac{1}{2}}}{(J+1)\left[(2J+1)(2J+3)\right]^{1/2}}$$

$$\langle J\ K\ m \,|\cos\theta|\, J\ K\ m\rangle = \frac{K m}{J(J+1)}$$

$$\langle J-1\ K\ m \,|\cos\theta|\, J\ K\ M\rangle = \frac{(J^2-K^2)^{1/2}(J^2-M^2)^{1/2}}{J(4J^2-1)^{1/2}}$$

The nonzero matrix elements of $D^1_{\pm1\ 0}$, $D^1_{\pm1\pm1}$, $D^1_{\pm1\mp1}$, and $D^1_{0\pm1}$ have also been computed and the results are given in Table III.

TABLE III

Nonvanishing Matrix Elements of $D^1_{0\ 0}$, $D^1_{\pm1\ 0}$, $D^1_{\pm1\pm1}$, $D^1_{\pm1\mp1}$.

$$\langle J+1\ K\ M \mid D^1_{0\ 0} \mid J\ K\ M\rangle = \left[\frac{\{(J+1)^2-M^2\}\{(J+1)^2-K^2\}}{(J+1)^2(2J+1)(2J+3)}\right]^{1/2}$$

$$\langle J\ K\ M \mid D^1_{0\ 0} \mid J\ K\ M\rangle = \frac{KM}{J(J+1)}$$

$$\langle J-1\ K\ M \mid D^1_{0\ 0} \mid J\ K\ M\rangle = \left[\frac{(J^2-M^2)(J^2-K^2)}{J^2(4J^2-1)}\right]^{1/2}$$

$$\langle J+1\ K\ M\pm1 \mid D^1_{\pm1\ 0} \mid J\ K\ M\rangle = \left[\frac{\{(J+1)^2-K^2\}\{J\pm M+1\}\{J\pm M+2\}}{2(J+1)^2(2J+1)(2J+3)}\right]^{1/2}$$

$$\langle J\ K\ M\pm1 \mid D^1_{\pm1\ 0} \mid J\ K\ M\rangle = \frac{\mp K\left(\frac{1}{2}\{J\mp M\}\{J\pm M+1\}\right)^{1/2}}{J(J+1)}$$

$$\langle J-1\ K\ M\pm1 \mid D^1_{\pm1\ 0} \mid J\ K\ M\rangle = -\left[\frac{(J^2-K^2)(J\mp M)(J\mp M-1)}{2J^2(2J-1)(2J+1)}\right]^{1/2}$$

$$\langle J+1\ K\pm1\ M \mid D^1_{0\pm1} \mid J\ K\ M\rangle = \left[\frac{\{J\pm K+1\}\{J\pm K+2\}\{(J+1)^2-M^2\}}{2(J+1)^2(2J+1)(2J+3)}\right]^{1/2}$$

$$\langle J\ K\pm1\ M \mid D^1_{0\pm1} \mid J\ K\ M\rangle = \frac{\mp M\{\frac{1}{2}(J\mp K)(J\pm K+1)\}^{1/2}}{J(J+1)}$$

$$\langle J-1\ K\pm1\ M \mid D^1_{0\pm1} \mid J\ K\ M\rangle = -\left[\frac{(J\mp K)(J\mp K-1)(J^2-M^2)}{2J^2(2J-1)(2J+1)}\right]^{1/2}$$

$$\langle J+1\ K\pm1\ M\pm1 \mid D^1_{\pm1\pm1} \mid J\ K\ M\rangle = \left[\frac{(J\pm K+1)(J\pm K+2)(J\pm M+1)(J\pm M+2)}{4(J+1)^2(2J+1)(2J+3)}\right]^{1/2}$$

$$\langle J\ K\pm1\ M\pm1 \mid D^1_{\pm1\pm1} \mid J\ K\ M\rangle = \frac{\{(J\mp K)(J\pm K+1)(J\mp M)(J\pm M+1)\}^{1/2}}{2J(J+1)}$$

$$\langle J-1\ K\pm1\ M\pm1 \mid D^1_{\pm1\pm1} \mid J\ K\ M\rangle = \left[\frac{(J\mp K)(J\mp K-1)(J\mp M)(J\mp M-1)}{4J^2(2J-1)(2J+1)}\right]^{1/2}$$

$$\langle J+1\ K\mp1\ M\pm1 \mid D_{\pm1\mp1} \mid J\ K\ M\rangle = \left[\frac{(J\mp K+1)(J\mp K+2)(J\pm M+1)(J\pm M+2)}{4(J+1)^2(2J+1)(2J+3)}\right]^{1/2}$$

$$\langle J\ K\mp1\ M\pm1 \mid D^1_{\pm1\mp1} \mid J\ K\ M\rangle = -\frac{\{(J\pm K)(J\mp K+1)(J\mp M)(J\pm M+1)\}^{1/2}}{2J(J+1)}$$

$$\langle J-1\ K\mp1\ M\pm1 \mid D^1_{\pm1\mp1} \mid J\ K\ M\rangle = \left[\frac{(J\pm K)(J\pm K-1)(J\mp M)(J\mp M-1)}{4J^2(2J-1)(2J+1)}\right]^{1/2}$$

Upper (lower) signs must be used consistently

The following Relations Prevail:

$$\cos(z\,\bar{z}) = D^1_{0\ 0}$$

$$\cos(x\,\bar{z}) = \frac{1}{\sqrt{2}}(D^1_{1\ 0} - D^1_{-1\ 0}) \qquad \cos(z\,\bar{x}) = \frac{1}{\sqrt{2}}(D^1_{0\ 1} - D^1_{0-1})$$

$$\cos(y\,\bar{z}) = -\frac{i}{\sqrt{2}}\left(D^1_{1\,0}+D^1_{-1\,0}\right) \qquad \cos\,(z\,\bar{y}) = \frac{i}{\sqrt{2}}\left(D^1_{0\,1}+D^1_{0-1}\right)$$

$$\cos\,(x\,\bar{x}) = \frac{1}{2}\left(D^1_{1\,1}+D^1_{-1-1}-D^1_{1-1}-D^1_{-1\,1}\right)$$

$$\cos\,(y\,\bar{y}) = \frac{1}{2}\left(D^1_{1\,1}+D^1_{-1-1}+D^1_{1-1}+D^1_{-1\,1}\right)$$

$$\cos\,(x\,\bar{y}) = \frac{i}{2}\left(D^1_{1\,1}-D^1_{-1-1}+D^1_{1-1}-D^1_{-1\,1}\right)$$

$$\cos\,(y\,\bar{x}) = -\frac{i}{2}\left(D^1_{1\,1}-D^1_{-1-1}-D^1_{1-1}+D^1_{-11}\right)$$

Knowing the matrix elements, the first and second order corrections to the energy levels can be computed and are given by

$$\Delta E^1_{JKM} = -\mu\mathcal{E}\frac{KM}{J(J+1)}$$

$$\Delta E^2_{JKM} = \frac{\mu^2\mathcal{E}^2}{2B}\left[\frac{(J^2-M^2)(J^2-K^2)}{J^3(4J^2-1)} - \frac{[(J+1)^2-M^2][(J+1)^2-K^2]}{(J+1)^3(2J+1)(2J+3)}\right]$$

The corrected wave functions are also readily calculated and the perturbation calculation is complete. For the case of linear molecules, we may put K = 0 getting only a second order effect; namely,

$$\Delta E^2_{JM} = \frac{\mu^2\mathcal{E}^2}{2B}\left[\frac{J^2-M^2}{J(4J^2-1)} - \frac{(J+1)^2-M^2}{(J+1)(2J+1)(2J+3)}\right].$$

Special care is needed in handling the case J = M = 0. The result obtained by first putting M = J and J = 0 may be shown to be correct, i.e.,

$$\Delta E^2_{00} = -\frac{\mu^2\mathcal{E}^2}{6B}$$

Of course, higher order corrections may be calculated according to standard techniques (13), but they will depend upon nothing more than the maxtrix elements already computed and thus are essentially solved for. It will be noted

that the energy levels now depend upon $|M|$ and what was a single absorption line without an applied field will now appear as a series of lines, one corresponding to each allowed M transition.

This solution is applicable only when the perturbing Hamiltonian is 'small' compared to the unperturbed Hamiltonian; i.e., when the computed corrections of higher and higher order get progressively smaller and samller. It will be seen that, aside from factors of order unity in the limit $J \to \infty$, which depend upon the quantum numbers, successive approximations based on perturbation theory are proportional to $\frac{\mu\mathcal{E}}{JB}$. Let us compute this 'smallness parameter' for HCN. Since $\mu \cong 3$ debye, $B \cong 1.5$ cm^{-1} and $\mu\mathcal{E} = 0.016803$ cm^{-1}/debye-kV/cm. For a field E = 50 kV/cm we find that

$$\mu\mathcal{E}/JB = 1.68/J$$

Thus only for $J > 10$ can the perturbation theory be expected to account satisfactorily for the observed shifts. Moreover, for fields small enough to allow perturbation theory to hold, the frequency shifts are smaller than the available spectral resolution (0.04 cm^{-1}). For instance, if $\mu\mathcal{E}/B = 0.1$, $\mathcal{E} \cong 3$kV/cm and the ground state ($J = 0$) shifts by only $\frac{\mu^2\mathcal{E}^2}{6B} \cong .025$ cm^{-1}. It is of interest to compute the correction to the energy of the ground state for some typical linear and symmetric top molecules. Table IV gives the results for $\mathcal{E} = 50{,}000$ V/cm together with the largest spectral shift calculated on the basis of second order perturbation theory. Note that HCN because of its favorable dipole moment, is somewhat unique in that it is the only linear molecule showing spectral shifts appreciably greater than the available spectrometer resolution, even at the highest fields attainable.

To account for the Stark effects seen in HCN, a solution applicable for all field strengths must be found. Since $\frac{\mu\mathcal{E}}{JB} \not\ll 1$, we cannot expect

TABLE IV

Summary of Molecular Constants Pertinent to a Perturbation Calculation of the Stark Effect

Molecule	μ_o	B_o	$\frac{\mu_o \mathcal{E}}{B_o}$ [a]	Perturbation Correction to Ground Rot. State [a]	Largest Spectral Shift [a,b]
HF	1.9 debye	$20.94 cm^{-1}$	.048	$-.0081 cm^{-1}$	$+.026 cm^{-1}$
HCl^{35}	1.03	10.59	.081	- .0118	+ .038
HBr^{79}	0.78	8.47	.077	- .0083	+ .027
HI	0.38	6.55	.049	- .0026	+ .008
HCN	2.98	1.48	1.690	- .711	+2.27
CO	0.10	1.96	.043	- .0006	+ .0019
CH_3F	1.79	.850	1.76	- .439	- .626
CH_3Cl^{35}	1.87	.443	3.62	- .967	- .650
CH_3Br^{79}	1.80	.316	4.78	-1.205	- .630
CH_3I	1.65	.250	5.56	-1.289	- .576
CH_3CN	3.92	.307	10.71	-5.870	-1.37
CF_3H	1.64	.345	4.00	- .921	- .575
$CCl_3^{35}H$	1.2	.110	9.17	-1.541	- .420

a for $\mathcal{E}$ = 50,000 V/cm

b $J'M' = 1,0$ $J''M'' = 0,0$ for linear molecules
$J'K'M' = 210$ $J''K''M'' = 11\text{-}1$ for symmetric top molecules

that a high-field approximation would be helpful, although this calculation will be made later. Instead, the total Hamiltonian must be attacked. An exact solution is available, although it is not of a closed form.

Including the Stark energy in the symmetric top Hamiltonian does not alter the Hamiltonian's cyclic dependence upon the variables and ϕ, and K and M remain good quantum numbers. Also, although J is no longer a good quantum number, the levels of given K and M are unambiguously labeled by specifying

their J value in the limit of zero electric field. The wave functions in the exact case, ψ^e_{JKM}, may be expressed in terms of the unperturbed wave functions, ψ_{JKM}, by

$$\psi^e_{JKM} = \sum_{J'=I}^{\infty} A^{KM}_{J'J}\, \psi_{J'KM}.$$

The sum is taken from I = |M| or |K|, whichever is larger. $A^{KM}_{J'J}$ are expansion coefficients which we must determine. If $\underline{\mathcal{H}} = \underline{\mathcal{H}}_0 + \underline{\mathcal{H}}_1$, where $\underline{\mathcal{H}}_0$ is the unperturbed symmetric top Hamiltonian with energy E_{JK}, and $\underline{\mathcal{H}}_1 = -\mu\mathcal{E}\cos\theta$, we have to solve the equation:

$$\underline{\mathcal{H}}\,\psi^e_{JKM} = E^e_{JKM}\,\psi^e_{JKM},$$

or

$$(\underline{\mathcal{H}}_0 + \underline{\mathcal{H}}_1)\sum_{J'=I}^{\infty} A^{KM}_{J'J}\,\psi_{J'KM} = E^e_{JKM}\sum_{J''=I}^{\infty} A^{KM}_{J''J}\,\psi_{J''KM},$$

or

$$\sum_{J'=I}^{\infty}\left\{E_{J'K}\psi_{J'KM} + \sum_{J''=I}^{\infty}\langle J''|\underline{\mathcal{H}}_1|J'\rangle\psi_{J''KM} - E^e_{JKM}\psi_{J'KM}\right\}A^{KM}_{J'J} = 0.$$

Defining $H_{J''J'} = \langle J''|\underline{\mathcal{H}}_1|J'\rangle$, we have seen that $H_{J''J'} = 0$ unless $J'' = J'+1$ J' or $J'-1$. Thus

$$\sum_{J'=I}^{\infty} A^{KM}_{J'J}\left\{E_{J'K} - E^e_{JKM} + H_{J'J}\right\}\psi_{J'KM} + \sum_{J'=I}^{\infty} A^{KM}_{J'J}\,H_{J'+1,J'}\,\psi_{J'+1KM} + \sum_{J'=I}^{\infty} A^{KM}_{J'J}\,H_{J'-1\,J}\,\psi_{J'-1KM} = 0,$$

shifting index,

$$\sum_{J'=I}^{\infty} A^{KM}_{J'J}\left\{E_{J'K} - E^e_{JKM} + H_{J'J}\right\}\psi_{J'KM} + \sum_{J'=I+1}^{\infty} A^{KM}_{J'-1\,J}\,H_{J'\,J'-1}\,\psi_{J'KM} + \sum_{J'=I-1}^{\infty} A^{KM}_{J'+1\,J}\,H_{J'\,J'+1}\,\psi_{J'KM} = 0$$

The first term of the third sum being identically zero because $J < I$, we get upon grouping the coefficients of $\psi_{J'KM}$,

$$\sum_{J'=I+1}^{\infty}\left[A^{KM}_{J'-1\,J}\,H_{J'\,J'-1} + A^{KM}_{J'J}\left\{E_{J'K} - E^e_{JKM} + H_{J'J'}\right\} + A^{KM}_{J'+1\,J}\,H_{J'+1\,J'}\right]\psi_{J'KM} +$$
$$+\left[A^{KM}_{IJ}\left\{E_{IK} - E^e_{JKM} + H_{II}\right\} + A^{KM}_{I+1\,J}\,H_{I\,I+1}\right]\psi_{IKM} = 0.$$

As the ψ_{JKM} are orthonormal and complete, the coefficients must each be zero. Therefore, $A^{KM}_{J'-1\,J}\,H_{J'J'-1} + A^{KM}_{J'J}\left\{E_{J'K} - E^e_{JKM} + H_{J'J}\right\} + A^{KM}_{J'+1\,J}\,H_{J'+1\,J'} = 0$ and

$$A^{KM}_{IJ}\left\{E_{IK} - E^e_{JKM} + H_{II}\right\} + A^{KM}_{I+1\,J}\,H_{I+1\,I} = 0.$$

Letting $U^{KM}_{J'J} \equiv A^{KM}_{J'-1,J}/A^{KM}_{J'J}$, we see from the second equation that

$$U^{KM}_{I+1\,J} = H_{I+1\,I} \Big/ E^{e}_{JKM} - E_{IK} - H_{II},$$

and from the first that $U^{KM}_{J'J} H_{J'J'-1} + \left\{E_{J'K} - E^{e}_{JKM} + H_{J'J}\right\} + \dfrac{H_{J'+1\,J'}}{U^{KM}_{J'+1\,J}} = 0.$

Let us define

$$B\,C^{KM}_{J'} \equiv H_{J'J'-1} \equiv H_{J'-1\,J'}$$

and

$$B\,B^{KM}_{J'} \equiv E^{e}_{JKM} - E_{J'K} - H_{J'J'}$$

or

$$C^{KM}_{J'} = -\frac{\mu\mathcal{E}}{B} \frac{(J'^2-M^2)^{1/2}(J'^2-K^2)^{1/2}}{J'(4J'^2-1)^{1/2}}$$

$$B^{KM}_{J'} = \frac{E^{e}_{JKM}}{B} - J'(J'+1) + \left(1-\frac{A}{B}\right)K^2 + \frac{\mu\mathcal{E}}{B}\frac{KM}{J'(J'+1)}.$$

With these abbreviations

$$U^{KM}_{J'J}\,C^{KM}_{J'} = B^{KM}_{J'} - \frac{C^{KM}_{J'+1}}{U^{KM}_{J'+1\,J}} = B^{KM}_{J'} - \frac{\left(C^{KM}_{J'+1}\right)^2}{U^{KM}_{J'+1\,J}\,C^{KM}_{J'+1}} = B^{KM}_{J'} - \frac{\left(C^{KM}_{J'+1}\right)^2}{B^{KM}_{J'+1} - C^{KM}_{J'+2}/U^{KM}_{J'+2\,J}}$$

Continuing the expansion, we get

$$U^{KM}_{J'J}\,C^{KM}_{J'} = B^{KM}_{J'} - \cfrac{\left(C^{KM}_{J'+1}\right)^2}{B^{KM}_{J'+1} - \cfrac{\left(C^{KM}_{J'+2}\right)^2}{B^{KM}_{J'+2} - \cfrac{\left(C^{KM}_{J'+3}\right)^2}{B^{KM}_{J'+3} - \cfrac{\left(C^{KM}_{J'+4}\right)^2}{B^{KM}_{J'+4} - \cdots}}}}$$

Using the fact that

$$U^{KM}_{I+1\,J} = H_{I+1\,I} \Big/ E^{e}_{JKM} - E_{IK} - H_{II} = C^{KM}_{I+1} \Big/ B^{KM}_{I},$$

we obtain a continued fraction relation independent of $U^{KM}_{J'J}$, namely

$$\left(C^{KM}_{I+1}\right)^2 \Big/ B^{KM}_{I} = B^{KM}_{I+1} - \cfrac{\left(C^{KM}_{I+2}\right)^2}{B^{KM}_{I+2} - \cfrac{\left(C^{KM}_{I+3}\right)^2}{B^{KM}_{I+3} - \cfrac{\left(C^{KM}_{I+4}\right)^2}{B^{KM}_{I+4} - \cfrac{\left(C^{KM}_{I+5}\right)^2}{\cdots}}}}$$

Inverting both sides, this becomes

$$0 = B_I^{KM} - \cfrac{\left(C_{I+1}^{KM}\right)^2}{B_{I+1}^{KM} - \cfrac{\left(C_{I+2}^{KM}\right)^2}{B_{I+2}^{KM} - \cfrac{\left(C_{I+3}^{KM}\right)^2}{B_{I+3}^{KM} - \left(C_{I+4}^{KM}\right)^2}}}$$

$$\cdots$$

In terms of molecular parameters and the electric field as defined by

$$\lambda \equiv \frac{\mu \mathcal{E}}{B}, \quad \epsilon_{JKM} \equiv \frac{E^e_{JKM}}{B} \quad \text{and} \quad R = \left(1 - A/B\right),$$

we get

$$0 = \epsilon_{JKM} - I(I+1) + RK^2 + \frac{KM}{I(I+1)}\lambda - \cfrac{\dfrac{[(I+1)^2 - M^2][(I+1)^2 - K^2]}{(I+1)^2(2I+1)(2I+3)}\lambda^2}{\epsilon_{JKM} - (I+1)(I+2) + RK^2 + \dfrac{KM\lambda}{(I+1)(I+2)} - \xi}$$

$$\xi = \cfrac{\dfrac{[(I+2)^2 - M^2][(I+2)^2 - K^2]\lambda^2}{(I+2)^2(2I+3)(2I+5)}}{\epsilon_{JKM} - (I+2)(I+3) + RK^2 + \dfrac{KM\lambda}{(I+2)(I+3)} - \dfrac{[(I+3)^2 - M^2][(I+3)^2 - K^2]}{(I+3)^2(2I+5)(2I+7)}}$$

$$\cdots$$

This infinite continued fraction, corresponding to fixed K and M, may be inverted an infinite number of times to yield a polynomial of infinite degree in the unknown $\epsilon_{JKM} = \frac{E^e_{JKM}}{B}$. The smallest root will correspond to the J = I state, the next smallest to J = I+1, etc. This fact is assured because wave functions adjacent in energy have connecting matrix elements, and hence their energy levels may never cross.

The continued fraction may be broken off after N terms by neglecting the term $(C_{N+I}^{KM})^2/B_{N+I}^{KM}$ compared to B_{N+I-1}^{KM}. If I is considered fixed, then

for large N $(C^{KM}_{N+I})^2 \sim \frac{\mu^2\mathcal{E}^2}{4B^2}$ and $B^{KM}_{N+I} \sim N^2$ so that $(C^{KM}_{N+I})^2/B^{KM}_{N+I} \sim \frac{\mu^2\mathcal{E}^2}{4B^2N^2}$ and the neglected term compares to the retained term as $(1/N)^4$. Thus, the fraction submits readily to numerical solution. Indeed, using the continued fraction, Shirley (18) has recently machine calculated the symmetric top Stark energy levels for all states with $J \leq 4$ and for fields up to $\lambda = 20$. Schlier (19) has also given curves for the Stark energies of symmetric top molecules for states up to $J \leqslant 2$. Kusch and Hughes (20) have carried out similar calculations for the case of a linear molecule for all states with $J \leqslant 4$. A plot of their data is shown in Figure 5, and as a careful interpolation of their data for $J \leq 2$ was found necessary in treating the observed effects in HCN, coefficients in the expansions

$$\epsilon_{Jm} = a_0 + (\lambda-2)a_1 + (\lambda-2)^2 a_2 + (\lambda-2)^3 a_3 + \cdots,$$
$$\epsilon_{Jm} = b_0 + (\lambda-3)b_1 + (\lambda-3)^2 b_2 + (\lambda-3)^3 b_3 + \cdots,$$

were evaluated and are listed in Table V.

As pointed out by Professor K. Hecht, use may be made of this continued fraction to compute higher order corrections to the Stark energies for the case of small λ. The fraction may be rearranged by successive inversions to give

$$B_{I+1} = \frac{C_I^2}{B_I} + \frac{C_{I+1}^2}{B_{I+2} - \frac{C_{I+2}^2}{\cdots}},$$

$$B_{I+2} = \frac{C_{I+1}^2}{B_{I+1} - \frac{C_I^2}{B_I}} + \frac{C_{I+2}^2}{B_{I+3} - \frac{C_{I+3}^2}{\cdots}},$$

$$\vdots$$

$$B_J = \frac{C_{J-1}^2}{B_{J-1} - \frac{C_{J-2}^2}{\cdots}} + \frac{C_J^2}{B_{J+1} - \frac{C_{J+1}^2}{\cdots}}$$

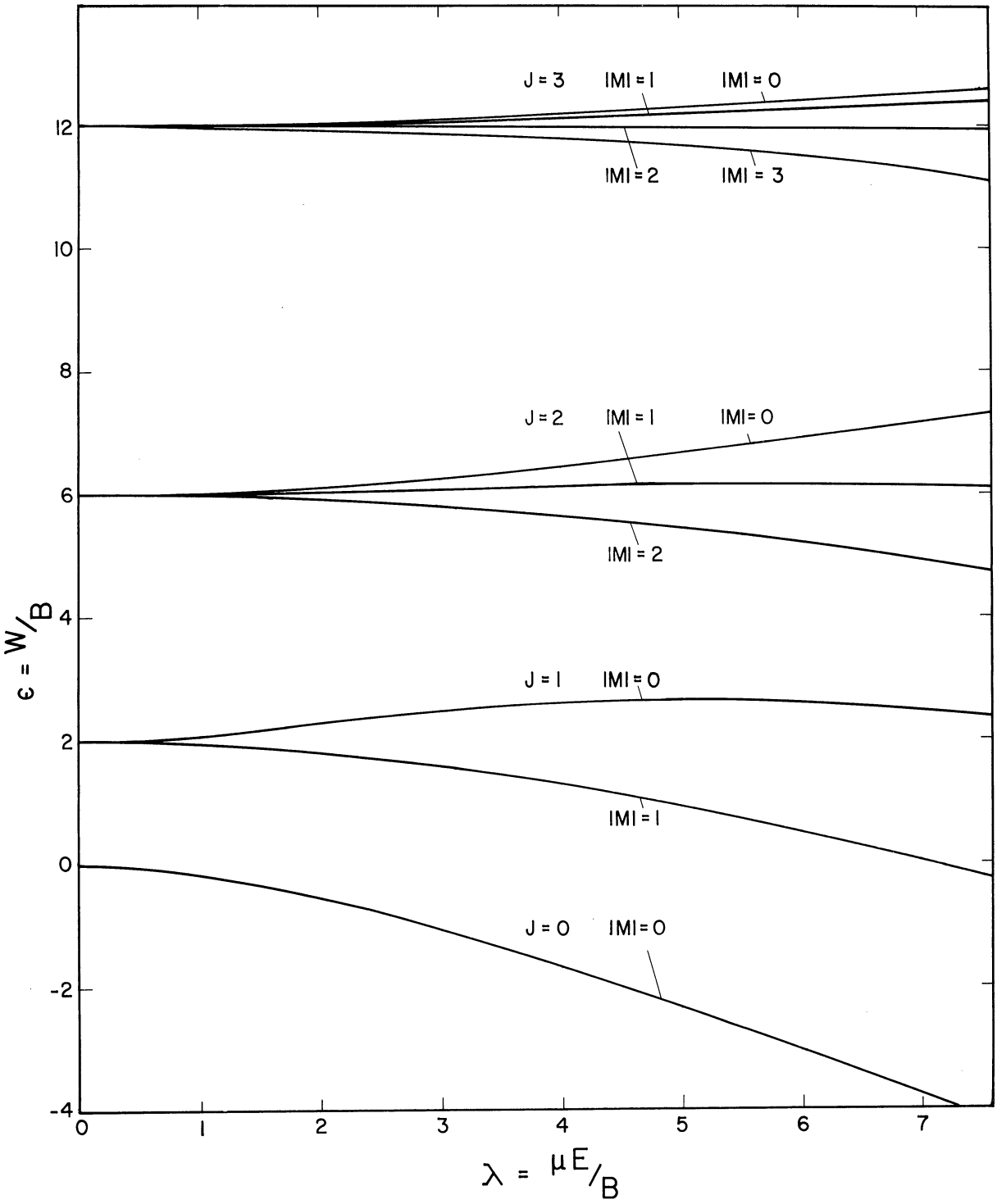

Figure 5 Energies (W) of a Linear Molecule (rotational constant B, dipole moment μ) in an Electric Field (E), from tables by Kusch and Hughes, Handbuch der Physik XXXVII/1, 141.

TABLE V

Polynomial Expansions for $\epsilon_{JM}(\lambda)$ to fit Data of Kusch and Hughes (21)

Let $\epsilon_{JM}(\lambda) = a_o + a_1(\lambda-2) + a_2(\lambda-2)^2 + a_3(\lambda-2)^3 + a_4(\lambda-2)^4 =$

$b_o + b_1(\lambda-3) + b_2(\lambda-3)^2 + b_3(\lambda-3)^3 + b_4(\lambda-3)^4.$

	a_o	a_1	a_2	a_3	a_4
ϵ_{00}	- .5573	- .4813	- .0659	.0138	- .0020
ϵ_{10}	2.2872	.2079	- .0005	- .0144	.0002
ϵ_{11}	1.8051	- .1900	- .0430	.0018	.0001
ϵ_{20}	6.0984	.1016	.0443	.0004	- .0002
ϵ_{21}	6.0426	.0378	.0051	.0010	- .0001
ϵ_{22}	5.9054	- .0939	- .0149	.0000	.0000

	b_o	b_1	b_2	b_3	b_4
ϵ_{00}	-1.9027	- .5813	- .0795	.0073	- .0014
ϵ_{10}	2.4780	.1643	- .0352	- .0068	.0017
ϵ_{11}	1.5741	- .2696	- .0365	.0021	.0000
ϵ_{20}	6.2278	.1582	+ .0324	- .0007	- .0003
ϵ_{21}	6.0837	.0468	.0052	- .0036	- .0016
ϵ_{22}	5.7890	- .1383	.0221	.0003	.0001

where we have dropped the superscripts K and M for the sake of neatness.

Here $$B_J = \frac{E_J^e}{B} - J(J+1) + \left(1 - \frac{A}{B}\right)K^2 + \lambda \frac{KM}{J(J+1)}$$

$$C_{J-1}^2 = \lambda^2 \frac{(J^2-M^2)(J^2-K^2)}{J^2(4J^2-1)} .$$

Let us expand E^e/B as a series in λ, i.e., let

$$E^e/B = W_0 + \lambda W_1 + \lambda^2 W_2 + \lambda^3 W_3 + \cdots .$$

To the third order of approximation, for example, W_0, W_1, W_2 and W_3 are retained on the left hand side of the continued fraction while since $C^2 \sim \lambda^2$, the denominators of the right hand side need only be evaluated to the first order. Thus

$$W_0 + \lambda W_1 + \lambda^2 W_2 + \lambda^3 W_3 - J(J+1) + (1 - A/B)K^2 + \lambda KM/J(J+1) =$$

$$= \lambda^2 \frac{(J^2-M^2)(J^2-K^2)/J^2(4J^2-1)}{W_0 + \lambda W_1 - J(J-1) + (1-A/B)K^2 + \lambda KM/J(J+1)} +$$

$$+ \lambda^2 \frac{[(J+1)^2-M^2][(J+1)^2-K^2]/(J+1)^2(2J+1)(2J+3)}{W_0 + \lambda W_1 - (J+1)(J+2) + (1-A/B)K^2 + \lambda KM/(J+1)(J+2)} .$$

Since the right hand side of this expression is of order two and higher, we obtain an expression good to first order by neglecting it altogether, along with the terms W_2 and W_3, giving

$$W_0 = J(J+1) - (1 - A/B)K^2$$

$$W_1 = -\frac{KM}{J(J+1)} .$$

Using these values for W_0 and W_1, we obtain

$$\lambda^2 W_2 + \lambda^3 W_3 = \lambda^2 \frac{(J^2-M^2)(J^2-K^2)/J^2(4J^2-1)}{2J(1 + \lambda KM/J^2(J^2-1))} - \lambda^2 \frac{[(J+1)^2-M^2][(J+1)^2-K^2]/(J+1)^2(2J+1)(2J+3)}{2(J+1)(1+\lambda KM/(J+1)^2(J^2+2J))}$$

$$= \lambda^2 \left[\frac{(J^2-M^2)(J^2-K^2)}{2J^3(4J^2-1)}\left\{1 - \lambda \frac{KM}{J^2(J^2-1)}\right\}\right] - \lambda^2 \left[\frac{\{(J+1)^2-M^2\}\{(J+1)^2-K^2\}}{2(J+1)^3(2J+1)(2J+3)}\left\{1 - \lambda \frac{KM}{(J+1)^2(J^2+2J)}\right\}\right] .$$

Equating coefficients of λ^2 we get $W_2 = \frac{(J^2-M^2)(J^2-K^2)}{2J^3(4J^2-1)} - \frac{\{(J+1)^2-M^2\}\{(J+1)^2-K^2\}}{2(J+1)^3(2J+1)(2J+3)}$.

Equating coefficients of λ^3 gives $W_3 = \frac{KM\{(J+1)^2-M^2\}\{(J+1)^2-K^2\}}{2J(J+1)^5(J+2)(2J+1)(2J+3)} - \frac{KM(J^2-M^2)(J^2-K^2)}{2(J^2-1)J^5(4J^2-1)}$.

The expressions for the first and second order terms agree precisely with those previously calculated via the usual perturbation scheme. The fourth order term has also been worked out, together with the special cases J = M = K = 0 and J = |M| = |K| = 1. Table VI summarizes these results.

As stated earlier, an approximation may also be made for the limiting case $\lambda \rightarrow \infty$. E. B. Wilson, as quoted in reference 30, gives for the case of a linear rotor in this limit

$$W = -\mu\mathcal{E} + (2J - |M| + 1)(2\mu\mathcal{E}B)^{1/2}.$$

This result may be derived by expanding the Hamiltonian including the Stark energy about $\theta = 0$, since for large λ the potential energy $-\mu\mathcal{E}\cos\theta$ has a deep minima very near $\theta = 0$. The resulting Schroedinger equation may then be solved by expanding the wave functions as power series in θ, the eigenvalues being obtained by requiring the solutions to be polynomials multiplied by their appropriate $\theta \rightarrow 0$ and $\theta \rightarrow \infty$ limits. A somewhat more accurate formula can be derived in a simpler manner by expanding the effective potential energy, after one-dimensionalizing the Hamiltonian, about its minimum rather than about $\theta = 0$, and approximating it by a parabola. The problem is then that of a harmonic oscillator, the energies being given by

$$E = (n+1/2)\hbar\omega + V(\theta_e)$$

where

$$\omega = \sqrt{k/m} = \sqrt{\frac{1}{m}\left.\frac{\partial^2 V_{eff}}{\partial\theta^2}\right|_{\theta_e}}$$

The exact Hamiltonian is, for the case of a linear rotor,

$$-\hbar^2/2I_0\left\{\frac{d^2}{d\theta^2} + \cot\theta\frac{d}{d\theta} - \frac{M^2}{\sin^2\theta}\right\}\psi - \mu\mathcal{E}\cos\theta\,\psi = E\psi.$$

Since the normalization integral is $\int\psi^*\psi\sin\theta\,d\theta$ we may one-dimensionalize the problem, thereby eliminating first derivative terms in the

TABLE VI

Perturbation Calculation to Fourth Order for the Stark Effect of a Symmetric Top Molecule

$$\epsilon = J(J+1) + \left(\frac{A}{B} - 1\right)K^2$$

$$+ \lambda\left[-\frac{KM}{J(J+1)}\right] + \lambda^2\left[\frac{J^3(J+1)^3 - 3(M^2+K^2)J^2(J+1)^2 + M^2K^2\{5J(J+1)+3\}}{2J^3(J+1)^3(2J-1)(2J+3)}\right]$$

$$+ \lambda^3(-KM)\left[\frac{\begin{array}{l}5J^4(J+1)^4 - (M^2+K^2)J^2(J+1)^2(7J^2+7J+6) \\ + M^2K^2(9J^4+18J^3+28J^2+19J+6)\end{array}}{2J^5(J+1)^5(J-1)(J+2)(2J-1)(2J+3)}\right] + \lambda^4\left[\text{Fourth order Coef.}\right]$$

$$\left[\text{Fourth Order Coefficient}\right] \times \left[8(2J-1)^3(2J-3)(2J+3)^3(2J+5)\right] =$$

$$20J^2 + 20J + 33 - \frac{18(M^2+K^2)(28J^2+28J-5)}{J(J+1)} + \frac{9(M^2+K^2)^2(68J^4+136J^3+125J^2+57J-45)}{J^3(J+1)^3}$$

$$+ \frac{1}{(J-1)(J+2)J^3(J+1)^3}\left[\begin{array}{l} 2M^2K^2\left[\begin{array}{l}2052J^6 + 6156J^5 + 4885J^4 - 490J^3 \\ - 4292J^2 - 3021J + 1710\end{array}\right] \\ - \frac{2M^2K^2(M^2+K^2)}{J^2(J+1)^2}\left[\begin{array}{l}2860J^8 + 11440J^7 + 19539J^6 \\ + 18577J^5 - 92J^4 - 17799J^3 \\ - 9522J^2 + 576J + 2430\end{array}\right] \\ + \frac{M^4K^4}{J^4(J+1)^4(J+2)}\left[\begin{array}{l}5876J^{11} + 41132J^{10} + 134009J^9 \\ + 275214J^8 + 355474J^7 + 217100J^6 \\ - 58250J^5 - 194746J^4 - 125274J^3 \\ - 8775J^2 + 22140J + 8100\end{array}\right]\end{array}\right]$$

Except when:

$$J = K = M = 0,\ \epsilon = -\lambda^2\frac{1}{6} + \lambda^4\frac{11}{1080} - \lambda^6\frac{1}{725},$$

$$J = |K| = |M| = 1,\ \epsilon = 1 + \frac{C}{A} - \lambda\frac{KM}{2} - \lambda^2\frac{3}{80} + \lambda^3\frac{KM}{320} - \lambda^4\frac{89}{2,688,000}.$$

Hamiltonian, by substituting $\psi_1 = \psi\sqrt{\sin\theta}$. Making this substitution, one gets

$$\frac{1}{2I_B}\left(\frac{\hbar}{i}\frac{d}{d\theta}\right)^2\psi_1 + \frac{\hbar^2}{2I_B}\left[\frac{m^2-1/4}{\sin^2\theta} - \lambda\cos\theta\right]\psi_1 = \left[E+\frac{B}{4}\right]\psi_1,$$

which may be likened to

$$\frac{p^2}{2m}\psi + V\psi = E\psi$$

where if

$$V = \tfrac{1}{2}Kx^2, \text{ then } E = (n+1/2)\hbar\sqrt{K/m} = (n+1/2)\hbar\sqrt{\frac{1}{m}\frac{d^2V}{dx^2}}.$$

In our case, $V_{eff} = \frac{\hbar^2}{2I_b}\left[\frac{m^2-1/4}{\sin^2\theta} - \lambda\cos\theta\right]$ must first be expanded about its minimum. θ_e is determined by setting the first derivative of V_{eff} equal to zero. Thus

$$\left.\frac{dV_{eff}}{d\theta}\right|_{\theta_e} = 0 = \frac{-2\left[m^2-1/4\right]\cos\theta_e}{\sin^4\theta_e} + \lambda\sin\theta_e,$$

$$\sin^4\theta_e = \frac{2\left[m^2-1/4\right]}{\lambda}\cos\theta_e.$$

Since λ is very large, we make the approximation $\theta_e \ll 1$ and

$$\theta_e^4 = \frac{2}{\lambda}\left(m^2-1/4\right).$$

Evaluating the second derivative of V_{eff}, we get

$$\frac{d^2V_{eff}}{d\theta^2} = \frac{\hbar^2}{2I_b}\left[2\left(m^2-1/4\right)\frac{1+2\cos^2\theta}{\sin^4\theta} + \lambda\cos\theta\right]$$

and

$$\left.\frac{d^2V_{eff}}{d\theta^2}\right|_{\theta_e} \cong \frac{\hbar^2}{2I_b}\left[\left(m^2-1/4\right)\frac{6}{\theta_e^4} + \lambda\right] = \frac{2\hbar^2}{I_b}\lambda$$

Also

$$V_{eff}|_{\theta_e} \cong \frac{\hbar^2}{2I_B}\left[\frac{m^2-1/4}{\theta_e^2} - \lambda\left(1-\frac{\theta_e^2}{2}\right)\right]$$

$$= \frac{\hbar^2}{2I_b}\left[\sqrt{\frac{\lambda}{2}\left(m^2-1/4\right)} - \lambda\left(1-\tfrac{1}{2}\sqrt{\frac{2}{\lambda}\left(m^2-1/4\right)}\right)\right]$$

$$= \frac{\hbar^2}{2I_b}\left[-\lambda + 2\sqrt{\lambda}\sqrt{m^2-1/4}\right] = -m\mathcal{E} + \sqrt{2m\mathcal{E}B}\sqrt{m^2-1/4}.$$

Thus, the energy is given by

$$E = -\mu\mathcal{E} - B/4 + \left(2n+1+\sqrt{M^2-1/4}\right)\sqrt{2\mu\mathcal{E}B}\,.$$

Also, the state J with zero field corresponds uniquely to the state n = J - |M| with large field. This is true since for fixed M, adjacent J states have connecting matrix elements and hence cannot cross as the field increases. Thus, as the states are ordered by the integers J - |M| for zero field and by the integers n for large field, the correspondence $n \blacktriangleright J - |M|$ must hold. Thus in our approximation,

$$E = -\mu\mathcal{E} - \frac{B}{4} + \left(2J - 2|M| + \sqrt{M^2-1/4} + 1\right)\sqrt{2\mu\mathcal{E}B}$$

This formula differs from the one given by Wilson, except for an additive constant, only to the extent of the term 1/4 indicated by the arrow. Our derivation, it must be pointed out, is not valid for the case M = 0. At M = 0, the expansion must be made about $\Theta = 0$ since V_{eff} has no minimum for this value of M. A high field expansion has also been developed by Peter and Strandberg (21b).

The same calculations may be carried out for the case of a symmetric rotor, the result being given by

$$E = -\mu\mathcal{E} + (A-B)K^2 - B/4 + \left[2J - 2I + 1 + \sqrt{(M-K)^2 - 1/4}\right]\sqrt{2\mu\mathcal{E}B}\,,$$

where I = |M| or |K|, whichever is the larger. Again, the case M = K must be treated separately by an expansion about $\Theta = 0$ which yields

$$E = -\mu\mathcal{E} + (A-B)K^2 - B/4 + \left[2J - 2|M| + 1\right]\sqrt{2\mu\mathcal{E}B}\,.$$

Once the energy levels are known, the wave functions can be obtained, for we saw that if $\psi^e_{JKM} = \sum_{J'=I}^{\infty} A^{KM}_{J'J}\,\psi_{JKM'}$ then

$$A^{KM}_{J'-1\,J}\,H_{J'J'-1} + A^{KM}_{J'J}\left\{E_{J'K} - E^e_{JKM} + H_{J'J'}\right\} + A^{KM}_{J'+1\,J}\,H_{J'+1\,J'} \equiv 0$$

and that

$$A^{KM}_{IJ}\left\{E_{IK} - E^e_{JKM} + H_{II}\right\} + A^{KM}_{I+1\,J}\,H_{I+1\,I} = 0$$

For a linear molecule this reduces to

$$A^{M}_{J'J} = \sqrt{\frac{4J'^2-1}{J'^2-M^2}}\ \frac{J'(J'-1) - \epsilon_{JM}}{\lambda} A^{M}_{J'-1\,J} - \sqrt{\frac{[(J'-1)^2-M^2][2J'+1]}{(J'^2-M^2)(2J'-3)}}\ A^{M}_{J'-2\,J}$$

for $J' \geq |M| + 1$.

This relation has been employed to determine exact wave functions for all the M sublevels for J up to two at fields corresponding to λ = 1, 2, 3, and 6. The results appear in Table VII. Calculation of the expansion coefficients is a self-checking process as well as being an excellent test of the accuracy of the published energy values, for unless every detail of the calculation is absolutely correct the magnitude of successive coefficients, instead of tending uniformly to zero, will explode violently.

The intensities of the Stark absorptions may also be calculated. If only the relative strengths of M components resulting from transitions between the same two 'J' states are desired it suffices to consider only the ratios of the squared matrix elements of the dipole moment between the states involved. The dependence of the absorption strengths of these components upon population and frequency differences will be negligible in view of the accuracy of any intensity determinations.

Choosing axes as in Figure 6 where the applied field defines the $\vec{Z}$ direction, perpendicular to the Poynting vector $\vec{S}$ of the infrared radiation which in turn makes an angle α with the space fixed $\vec{Y}$ axis. Let $\vec{n}$ denote the direction perpendicular to both $\vec{Z}$ and $\vec{S}$. The infrared beam is then to be thought

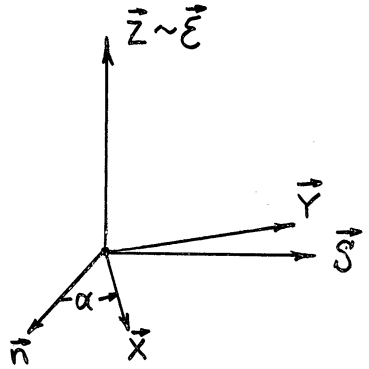

Fig. 6. Orientation of Poynting Vector $\vec{S}$ Relative to the Space-Fixed Axes.

TABLE VII

Wave Functions for a Linear Molecule in an Electric Field

$$\text{Exact } JM = \sum_{J'} A^{M}_{J'J} \; JM$$

J M λ	A^{M}_{0J}	A^{M}_{1J}	A^{M}_{2J}	A^{M}_{3J}	A^{M}_{4J}	A^{M}_{5J}
0 0 0	1.000	0	0	0	0	0
1	.964	.263	.022	.001	.000	.000
2	.898	.434	.069	.006	.000	.000
3	.840	.530	.118	.013	.001	.000
6	.726	.642	.235	.011	.001	.000
1 0 0	0	1.000	0	0	0	0
1	- .264	.956	.127	.007	.000	.000
2	- .436	.865	.248	.026	.002	.000
3	- .533	.763	.361	.059	.005	.002
6	- .617	.463	.601	.203	.024	.008
1 1 0	0	1.000	0	0	0	0
1	0	.994	.111	.007	.000	.000
2	0	.977	.213	.020	.001	.000
3	0	.952	.302	.042	.002	.000
6	0	.865	.486	.125	.011	.000
2 0 0	0	0	1.000	0	0	0
1	.012	- .128	.988	.084	.003	.000
2	.048	- .253	.952	.166	.012	.000
3	.102	- .369	.891	.242	.027	.002
6	.298	- .596	.611	.425	.104	.025
2 1 0	0	0	1.000	0	0	0
1	0	- .110	.991	.079	.003	.000
2	0	- .213	.964	.157	.011	.000
3	0	- .304	.925	.230	.024	.002
6	0	- .490	.758	.417	.090	.008
2 2 0	0	0	1.000	0	0	0
1	0	0	.998	.063	.002	.000
2	0	0	.992	.124	.008	.000
3	0	0	.983	.183	.016	.000
6	0	0	.940	.336	.060	.003

of as composed of one component polarized in the $\vec{Z}$ direction and one in the $\vec{n}$ direction. Absorption of the $\vec{Z}$ polarization will be proportional to I_Z where

$$I_z = \left| \int \psi^{e*}_{J'K'M'} \mu_z \psi^{e}_{JKM} \, d\tau \right|^2,$$

while absorption of $\vec{n}$ polarization is proportional to I_n where

$$I_n = \left| \int \psi^{e*}_{J'K'M'} (\mu_x \cos\alpha - \mu_y \sin\alpha) \psi^{e}_{JKM} \, d\tau \right|^2$$

We see that

$$\mu_z = \mu_0 \cos(z\vec{z}) = \mu_0 \cos\theta = \mu_0 D^1_{00},$$
$$\mu_x = \mu_0 \cos(x\vec{z}) = \mu_0 \cos\phi \sin\theta = \mu_0 (D^1_{10} - D^1_{-10})/\sqrt{2},$$
$$\mu_y = \mu_0 \cos(y\vec{z}) = \mu_0 \sin\phi \sin\theta = -i\mu_0 (D^1_{10} + D^1_{-10})/\sqrt{2}$$
$$\mu_x \cos\alpha - \mu_y \sin\alpha = \mu_0 (e^{i\alpha} D^1_{10} - e^{-i\alpha} D^1_{-10})/\sqrt{2}.$$

Thus

$$I_z = \mu_0^2 \left| \int \psi^{e*}_{J'K'M'} D^1_{00} \psi^{e}_{JKM} \, d\tau \right|^2$$

$$I_n = \frac{\mu_0^2}{2} \left| e^{i\alpha} \int \psi^{e*}_{J'K'M'} D^1_{10} \psi^{e}_{JKM} \, d\tau - e^{-i\alpha} \int \psi^{e*}_{J'K'M'} D^1_{-10} \psi^{e}_{JKM} \, d\tau \right|^2$$

Expanding the exact wave functions in terms of the symmetric top functions, we get

$$I_z = \mu_0^2 \left| \sum_{\sigma'\sigma} A^{K'M'}_{\sigma'J'} A^{KM}_{\sigma J} \int \psi^{*}_{\sigma'K'M'} D^1_{00} \psi_{\sigma KM} \, d\tau \right|^2$$

and

$$I_n = \frac{\mu_0^2}{2} \left| \sum_{\sigma'\sigma} A^{K'M'}_{\sigma'J'} A^{KM}_{\sigma J} \left(e^{i\alpha} \int \psi^{*}_{\sigma'K'M'} D^1_{10} \psi_{\sigma KM} \, d\tau \right.\right.$$
$$\left.\left. - e^{-i\alpha} \int \psi^{*}_{\sigma'K'M'} D^1_{-10} \psi_{\sigma KM} \, d\tau \right) \right|^2.$$

The matrix elements of $D^1_{0\,0}$, $D^1_{1\,0}$ and $D^1_{-1\,0}$ have been computed and are given in Table III. It is seen that for transitions involving $\Delta M = 0$, only $D^1_{0\,0}$ has nonzero matrix elements and for $\Delta M = \pm 1$ only $D^1_{\pm 1\,0}$ contributes. Thus a $\Delta M = 0$ line will be polarized in the $\vec{z}$ direction and have an intensity proportional to I_0 where

$$I_0 = \mu_0^2 \left| \sum_{\sigma\sigma'} A^{K'M}_{\sigma'J'} A^{KM}_{\sigma J} \int \psi^*_{\sigma' K' M'} D'_{00} \psi_{\sigma K M}\, d\tau \right|^2 .$$

A $\Delta M = \pm 1$ line will be polarized in the $\vec{n}$ direction and have an intensity proportional to $I_{\pm 1}$ where

$$I_{\pm 1} = \mu_0^2/2 \left| \sum_{\sigma\sigma} A^{K'M\pm 1}_{\sigma'J'} A^{KM}_{\sigma J} \int \psi^*_{\sigma' K' M\pm 1} D'_{\pm 10} \psi_{\sigma K M}\, d\tau \right|^2 .$$

The lengthy sums necessary for the computation of actual intensities have been carried out for certain field strengths for low J lines of a linear molecule. The results are tabulated in Table VIII.

The most striking feature of the calculated intensity tables, perhaps is the appearance of weak Q ($\Delta J=0$), O ($\Delta J=-2$), and S ($\Delta J=+2$) branches. Actually, since the exact wave functions are composed of symmetric top functions of many different total angular momenta, nonzero intensities will exist for transitions of arbitrary ΔJ. This is simply a statement of the fact that in the presence of an applied field the total angular momentum is no longer a constant of the motion and that J is therefore not a 'good' quantum number. These 'field induced' transitions for $\Delta J \geq 2$ are too weak to be detected in the present experiment but the Q branch is observed.

V. OBSERVED STARK EFFECTS AND THEIR INTERPRETATION

5.1 Hydrogen Cyanide

Figure 7 shows the observed electric field effects in HCN near the band center of ν_3 (the C-H stretching vibration). The normal absorption spectrum

TABLE VIII

Relative Intensities of the Stark-Shifted 'M'-Components of a Linear Molecule

Branch	Transition		Relative Intensity $I^{\dagger}_{0,\pm1}$ (a)				
	$J'\|M\|'$	$J''\|M\|''$	$\lambda = 0$	$\lambda = 1$	$\lambda = 2$	$\lambda = 3$	$\lambda = 6$
Q(0)	00	00	0.000	0.088	0.232	0.336	0.484
Q(1)	10	10	0.000	0.027	0.043	0.027	0.008
	11	10	0.000	0.019	0.051	0.077	0.153
	11	11	0.000	0.020	0.072	0.114	0.292
Q(2)	20	20	0.000	0.002	0.010	0.025	0.073
	21	20	0.000	0.000	0.002	0.006	0.038
	21	21	0.000	0.001	0.003	0.003	0.000
	22	21	0.000	0.002	0.009	0.018	0.047
	22	22	0.000	0.004	0.018	0.038	0.132
P(1) or R(0)	10	00	0.333	0.270	0.182	0.128	0.062
	11	00	0.333	0.327	0.281	0.255	0.212
P(2) or R(1)	20	10	0.267	0.266	0.265	0.263	0.213
	21	10	0.200	0.199	0.201	0.208	0.300
	20	11	0.067	0.064	0.058	0.042	0.022
	21	11	0.400	0.391	0.363	0.328	0.227
	22	11	0.400	0.399	0.389	0.377	0.328
O(0) or S(0)	20	00	0.000	0.004	0.008	0.009	0.002
	21	00	0.000	0.003	0.007	0.008	0.006

(a) $I^{\dagger}_{0,\pm1} = a\, I_{0,\pm1}$ where $I_{0,\pm1}$ is defined on Page 48 and a = 1 if M' and M'' are both zero and a = 2 otherwise

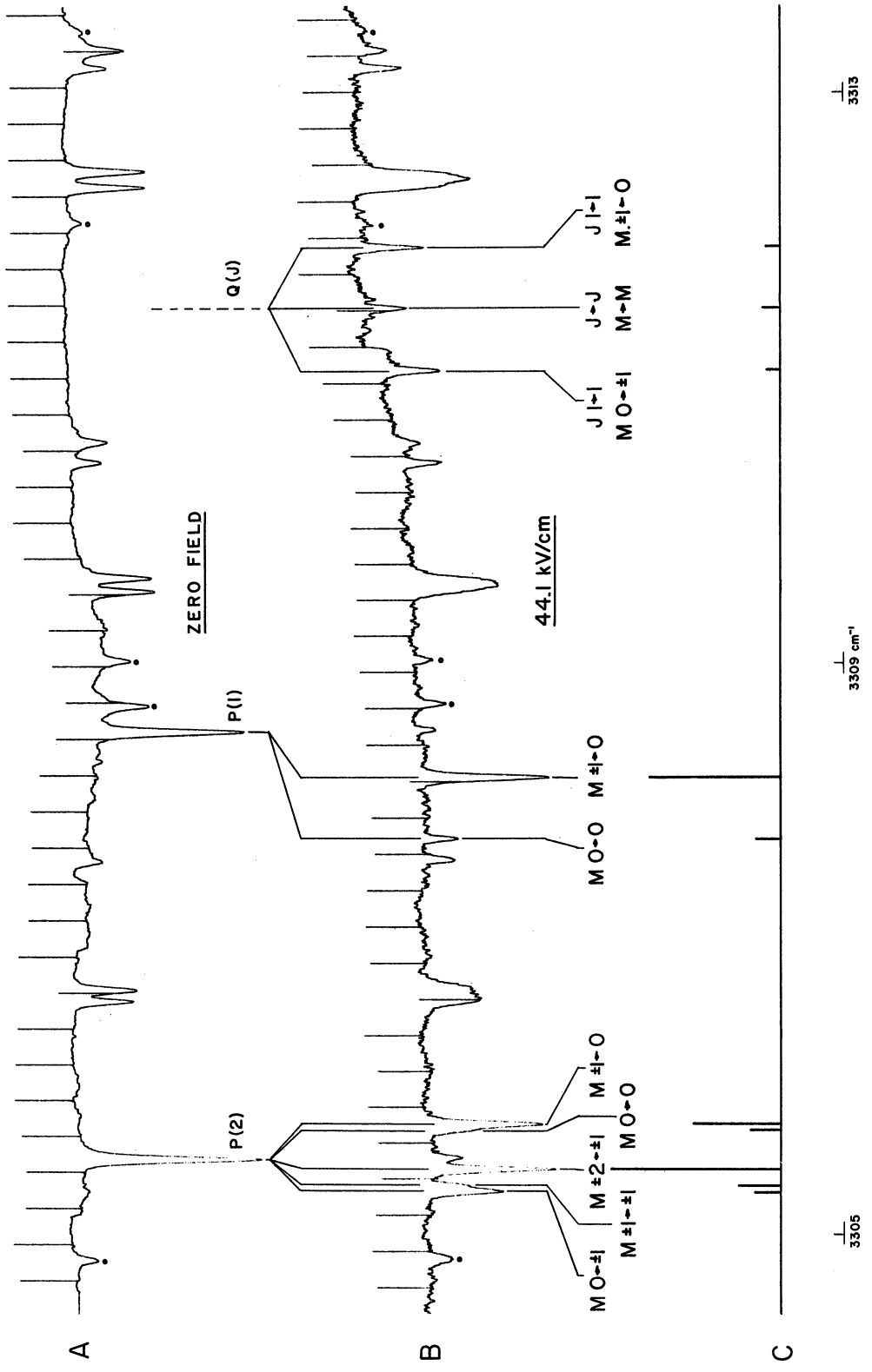

Figure 7 STARK EFFECTS NEAR THE ν_3 BAND CENTER OF HYDROGEN CYANIDE.

A. Normal spectrum. B. Spectrum with 44.1 kv/cm DC electric field. C. Predicted spectrum.

is at the top and the spectrum with an applied D.C. electric field corresponding to $\lambda = 1.5$, together with the theoretically predicted spectrum, below. $\Delta M = 0$ transitions only absorb radiation polarized in the $\bar{z}$ direction parallel to the electric field; $\Delta M = \pm 1$ transitions only absorb the perpendicular polarization. The transmission of the perpendicular polarization through the Stark cell was nearly three times greater than that for the parallel polarization. This factor has been included in the predicted spectrum.

The induced absorption of the Q branch is apparent in Figure 7, with the stronger members labeled. The M components of lines P(1) and P(2) are partially resolved and are labeled. Lines marked with dots appearing in both spectra are due to small amounts of water vapor in the sample. The series of doublets in the normal trace which show Stark effects in the electric field trace are members of the combination band $\nu_3 + \nu_2 - \nu_2$. Also present but barely discernible at the present sample pressure is the ν_3 fundamental of $HC^{13}N$. Though the $\nu_3 + \nu_2 - \nu_2$ band shows modest electric field effects in the trace of Figure 7, and would seem an interesting example of the Stark effect in a band having λ-type doubling, the weak intensities of the low-J lines prohibit their measurement.

Figure 8 is a section of a trace at a field of 120,000 volts/cm ($\lambda \sim 4$) showing the 'lines' R(2), R(3) and R(4). In order to obtain this extreme field, a cell with a gap of 0.2mm was used. Transmission of the perpendicular polarization in this case was less than 10%, while that of the parallel polarization was practically zero. Thus, only the $\Delta M = \pm 1$ transitions can contribute to the spectrum. The M components of the 'line' R(2) are completely resolved. The R(3) and R(4) 'lines' show incomplete splitting

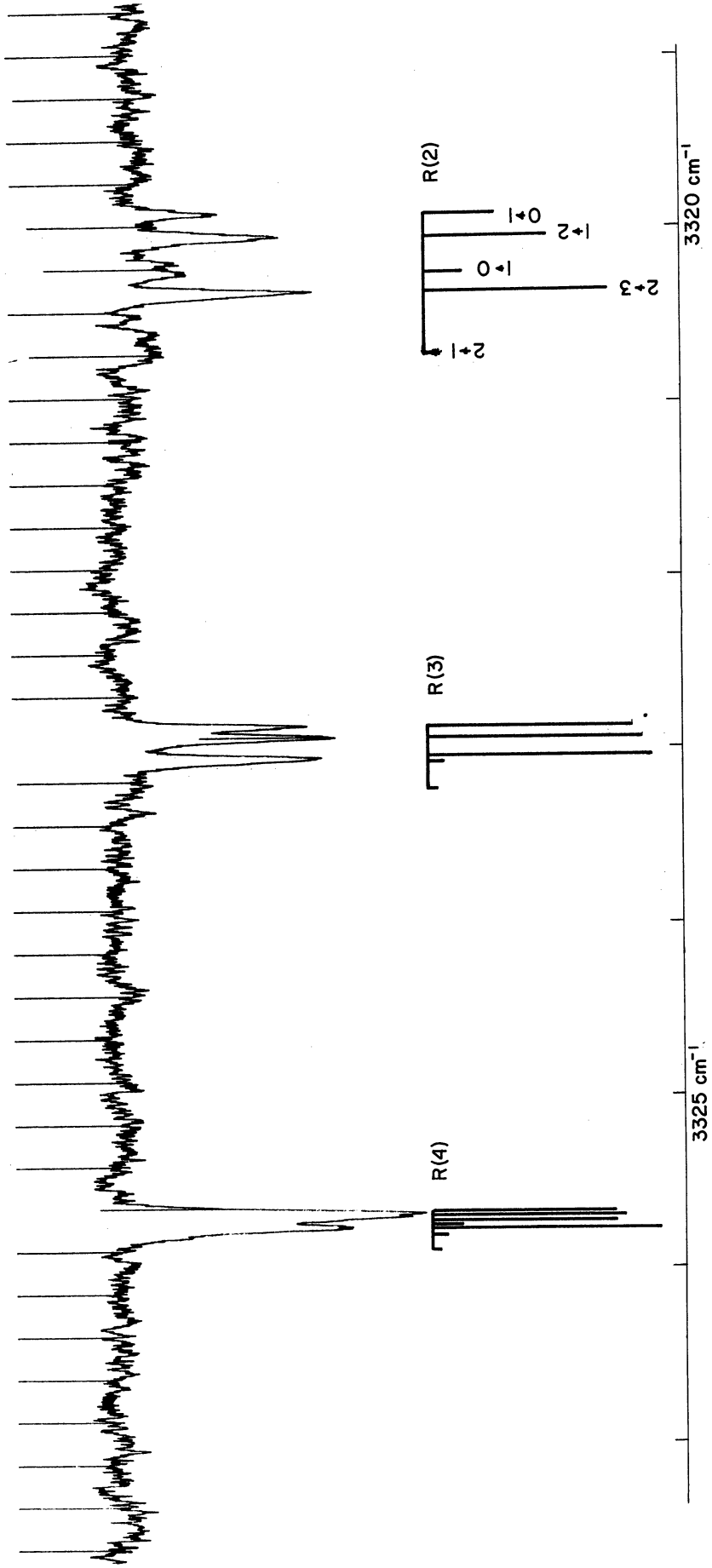

Figure 8 HIGH FIELD STARK EFFECTS IN HYDROGEN CYANIDE

above = recorder trace of Stark spectrum with $\mathcal{E}$ = 125,000 volts/cm, p = 1/3 mm hg.

below = predicted spectrum assuming complete attenuation of the parallel ($\Delta m = 0$) polarization, m assignments given for R(2) only.

even at this maximum field.

The polarization dependence of the M components is verified by the spectra of Figure 9. Here the region of ν_3 P(1) with unpolarized radiation and zero field is shown in Figure 9a. The spectrum was then run with a field corresponding to $\lambda \doteq 1$, using polarized radiation. Figure 9b is the result for the parallel polarization, Figure 9c for the perpendicular. It is seen that the spectrum is completely polarized, as predicted. In order to insert the silver chloride polarizer, a section of the brass tubing enclosing the beam had to be removed and the dry nitrogen flush of the foreoptics discontinued. The line marked (o) appearing in all three traces is due to atmospheric water vapor.

An expanded, low noise, high resolution scan of the P(1) region of HCN, ν_3, at a field of $\lambda = 2$ is shown in Figure 10. The trace required six hours running time and represents the best resolution and signal to noise attained. The observed frequency splittings and intensities for this case are shown on line one of Table IX. The values calculated from ground state molecular data given on line two of Table IX are only in fair agreement with observation, and indicate that the effects of the excited state upon the molecular constants must be considered. Thus, the Stark spectrum is correctly predicted only by determining the rotational energy levels of each vibrational state separately, using the molecular constants of that state. For the fundamental vibrational state of HCN, the reciprocal moment of inertia is 1.467799 cm^{-1}(12), as compared to 1.478219 cm^{-1}(21) in the ground state (B_1 and B_0, respectively). However, only the ground state dipole moment μ_0 has been measured, the most recent determination being 2.985 ±.005 debye, from the microwave Stark effect (22).

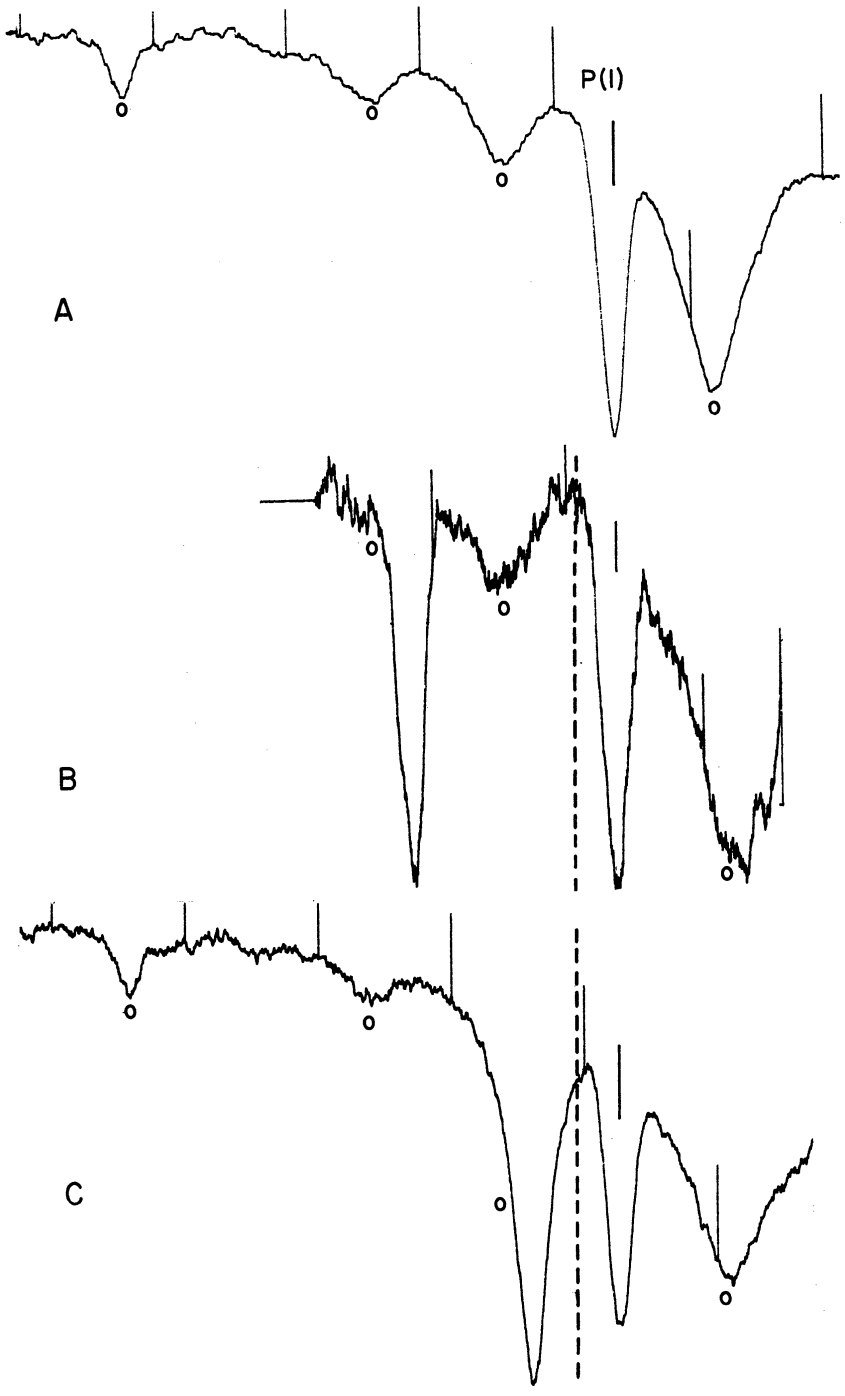

Figure 9 STARK EFFECT OF P(I) HCN USING POLARIZED RADIATION.

A. unpolarized, $\mathcal{E} = 0$

B. polarized $\bar{E}_{rad.} \parallel \bar{\mathcal{E}}_{stark}$, $\bar{\mathcal{E}} = 0$ to the right of the dashed line, $\mathcal{E} = 30$ kV/cm to the left of the dashed line.

C. polarized $\bar{E} \perp \bar{\mathcal{E}}$, $\mathcal{E} = 0$ on right, $\mathcal{E} = 30$ kV/cm on left.

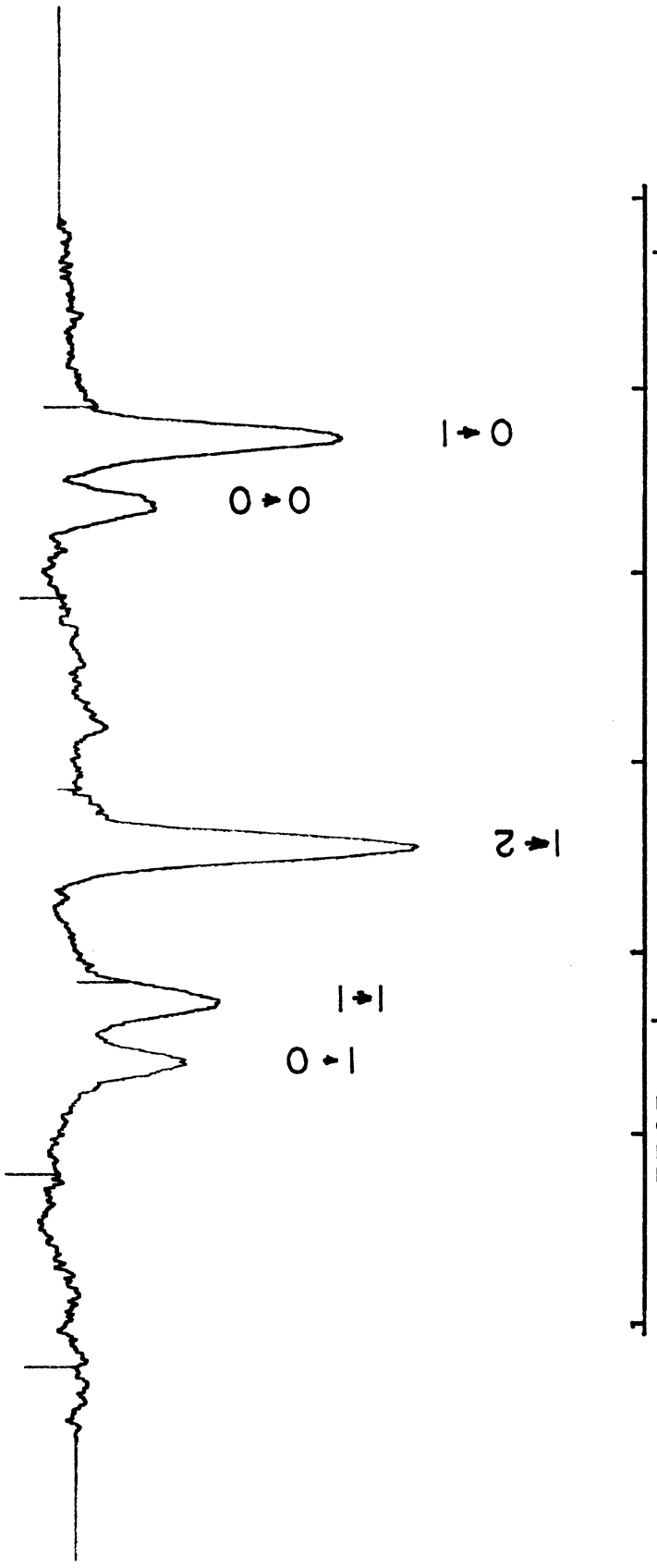

Figure 10 HIGH DISPERSION TRACE OF THE P(2) LINE IN THE ν_3 FUNDAMENTAL OF HYDROGEN CYANIDE SHOWING COMPLETE ISOLATION AND IDENTIFICATION OF ALL FIVE 'M' COMPONENTS

ϵ = 60 kV/cm p = 1/4 mm hg

TABLE IX

Summary of Observed and Calculated Splittings and Intensities for the P(1) Line of the ν_3 HCN Fundamental with an Electric Field Strength Near 60 kV/cm

	Relative Position of the $M' \leftarrow M''$ Component				
	0←0	1←0	0←1	1←1	1←2
Observed	-.086 cm^{-1}	-.825	0	-.743	-.538
Calculated$_A$	-.083	-.802	0	-.716	-.513
Calculated$_B$	-.083	-.831	0	-.748	-.540

	Relative Intensity of the$_C$ $M' \leftarrow M''$ Component				
	0←0	1←0	0←1	1←1	1←2
Observed	.26	.21	.70	.32	1.00
Calculated$_A$	.25	.20	.70	.33	1.35
Calculated$_B$	--	--	--	--	--

A Using $\lambda = 2.01 = \lambda_0 = \lambda_1$

B Using $\lambda_0 = 2.01$; $\lambda_1 = 2.06$

C Assuming $T'/T'' = 3.68$

The predicted spectrum of Table IX line 3 was obtained using $\mu_1 = 3.04$ debye and the above values for B_0, B_1 and μ_0; it differs from the observed spectrum by less than the experimental error.

Since it is necessary to include the effects of a changed excited state dipole moment to account for the observed spectrum, this change must be evaluated as carefully as possible. Moreover, the change is of fundamental interest, never before having been measured. There are many means of reducing the available data to determine μ_1; two of the most direct methods will be described.

Let $W_{JM'}(\lambda_1) = B_1 \epsilon_{J'M'}(\lambda_1)$ be the rotational energy of the excited vibrational state and $W_{J''M''}(\lambda_0)$ that of the ground vibrational state. Since $\lambda \equiv \mu\mathcal{E}/B$, $\mu_1/\mu_0 \simeq 1$ and $B_1/B_0 \simeq 1$, then $\Delta\lambda = \lambda_1 - \lambda_0 = \Delta\frac{\mu\mathcal{E}}{B} \simeq \lambda_0\left(\frac{\Delta\mu}{\mu_0} - \frac{\Delta B}{B_0}\right)$ and $\epsilon_{JM}(\lambda_1) \simeq \epsilon_{JM}(\lambda_0) + \left.\frac{d\epsilon_{JM}}{d\lambda}\right|_{\lambda_0} \Delta\lambda$. To a good approximation, we see that

$$W_{J'M'}(\lambda_1) = (B_0 + \Delta B)\left[\epsilon_{J'M'}(\lambda_0) + \left.\frac{d\epsilon_{J'M'}}{d\lambda}\right|_{\lambda_0}\left(\frac{\Delta\mu}{\mu_0} - \frac{\Delta B}{B_0}\right)\lambda_0\right]$$

and

$$\nu_{J'M' \leftarrow J''M''} = \nu_{VIB.} + B_0\left[\epsilon_{J'M'}(\lambda_0) - \epsilon_{J''M''}(\lambda_0)\right] + \Delta B\,\epsilon_{J'M'}(\lambda_0) + \lambda_0(B_0 + \Delta B)\left(\frac{\Delta\mu}{\mu_0} - \frac{\Delta B}{B_0}\right)\left.\frac{d\epsilon_{J'M'}}{d\lambda}\right|_{\lambda_0}.$$

The same transition with zero field falls at

$$\nu_{J'M' \leftarrow J''M''} = \nu_{VIB} + (B_0 + \Delta B)\epsilon_{J'M'}(0) - B_0\epsilon_{J''M''}(0) = \nu_{VIB} + J'(J'+1)(B_0 + \Delta B) - J''(J''+1)B_0.$$

The Stark shift accordingly is given by

$$\Delta\nu_{J'M' \leftarrow J''M''} = B_0\left[\epsilon_{J'M'}(\lambda_0) - J'(J'+1) - \epsilon_{J''M''}(\lambda_0) + J''(J''+1)\right] + \Delta B\left[\epsilon_{J'M'}(\lambda_0) - J'(J'+1)\right] + \lambda_0 B_1\left(\frac{\Delta\mu}{\mu_0} - \frac{\Delta B}{B_0}\right)\left(\left.\frac{d\epsilon_{J'M'}}{d\lambda}\right|_{\lambda_0}\right).$$

The Stark shift of the transition which proceeds between the same two rotational levels, but now from J'M' in the ground vibrational state to J''M'' in the excited state is similarly given by

$$\Delta\nu_{J''M''\leftarrow J'M'} = B_0\left[\epsilon_{J''M''}(\lambda_0) - J''(J''+1) - \epsilon_{J'M'}(\lambda_0) + J'(J'+1)\right]$$
$$+ \Delta B\left[\epsilon_{J''M''}(\lambda_0) - J''(J''+1)\right] + \lambda_0 B_1\left(\frac{\Delta\mu}{\mu_0} - \frac{\Delta B}{B_0}\right)\left(\frac{d\epsilon_{J''M''}}{d\lambda}\bigg|_{\lambda_0}\right).$$

Adding these two frequency shifts yields

$$\Delta\nu_{J'M'\leftarrow J''M''} + \Delta\nu_{J''M''\leftarrow J'M'} = \Delta B\left[\epsilon_{J'M'}(\lambda_0) + \epsilon_{J''M''}(\lambda_0) - J'(J'+1) - J''(J''+1)\right.$$
$$\left. + \lambda_0 B_1\left[\frac{\Delta\mu}{\mu_0} - \frac{\Delta B}{B_0}\right]\left[\frac{d}{d\lambda}\left\{\epsilon_{J'M'}(\lambda) + \epsilon_{J''M''}(\lambda)\right\}\right]_{\lambda_0}\right.$$

Table VI may be used to obtain expressions for $\epsilon_{J'M'} + \epsilon_{J''M''}$ for all levels up to J = 2 as polynomials in (λ - a) for a = 2 or 3. These expansions may be differentiated and the results used in the above equation to determine the only unknown $\Delta\mu$. To achieve the greatest accuracy in the determination of $\Delta\mu$ those levels most sensitive to changes in λ should be measured at the highest possible field. Thus the levels J = 0, M = 0 and J = 1, M = 1 were employed and the following expressions developed:

$$\epsilon_{11} + \epsilon_{00} = 1.2478 - 0.6712(\lambda-2) - 0.1089(\lambda-2)^2 + 0.0156(\lambda-2)^3 - 0.0019(\lambda-2)^4,$$

$$\epsilon_{11} + \epsilon_{00} = 0.4814 - 0.8508(\lambda-3) - 0.0738(\lambda-3)^2 + 0.0093(\lambda-3)^3 - 0.0013(\lambda-3)^4.$$

Differentiating:

$$\frac{d}{d\lambda}(\epsilon_{11} + \epsilon_{00}) = -0.6712 - 0.2178(\lambda-2) + 0.0468(\lambda-2)^2 - 0.0076(\lambda-2)^3,$$

$$\frac{d}{d\lambda}(\epsilon_{11} + \epsilon_{00}) = -0.8508 - 0.1976(\lambda-3) + 0.0279(\lambda-3)^2 - 0.0052(\lambda-3)^3.$$

As a check on the range over which these expansions may be safely used, $\frac{d}{d\lambda}(\epsilon_{11}+\epsilon_{00})\Big|_{2.5}$ was evaluated using the first and then the second relations, yielding -0.7693 and -0.7694, respectively. It was concluded that the expansions were valid over the small regions encountered in the calculations ($1.85 < \lambda < 2.15$). Thus, for example, with λ = 2.00, we get

$$\frac{\Delta\mu}{\mu_o} = \frac{\Delta\lambda}{\lambda_o} + \frac{\Delta B}{B_o} = -0.003258 - 0.4756\left[\Delta\nu_{11\leftarrow 00} + \Delta\nu_{00\leftarrow 11}\right].$$

Many independent determinations of $\Delta\lambda/\lambda$ were made for fields very close to $\lambda = 2.0$. The experimental procedure finally adopted involved scanning the spectrometer slowly through the line $P(1)_{0\leftarrow 1}$, with a D.C. voltage applied to the Stark cell. Then both electrodes of the Stark cell were grounded and the scan continued without interruption through the zero-field position of P(1). The spectrometer was then advanced by hand to within thirty minutes running time of the unshifted R(0) line and it was scanned. The electric field was re-established and the scan continued without stop through $R(0)_{1\leftarrow 0}$. The two splittings were then added algebraically (their magnitudes subtracted since $\Delta\nu_{00\leftarrow 11}$ is already negative). The results of seven runs are listed in Table X and a typical trace is shown in Figure 11. Also shown in Figure 11 is a recording of the fringes, mentioned earlier. Their lack of smoothness is attributed solely to erratic rotation of the grating. Drive train slack is responsible for the delay of the first fringes and necessitates a twenty to thirty minute 'running in' prior to each scan. The precision of the measurements is obviously poor, being limited by the drive mechanism to about ± 0.005 cm^{-1} on a single run. The final value obtained for $\frac{\Delta\lambda}{\lambda}$ was 0.0126 ± 0.0017, corresponding to $\Delta\mu = +(0.0055 \pm 0.0017)\mu_o$, and $\mu_1 = 3.001 \pm .001$ debye.

The above method affords a determination of the dipole moment change between ground and excited vibrational states and thus will provide a more precise value for $\Delta\mu$ than would a scheme of data reduction leading directly

TABLE X

Summary of Data Used in Calculation of μ_1, HCN

Run	λ	$\Delta R(0)_{\pm 1\ 0}$	$\Delta P(1)_{0\ \pm 1}$	$\Delta\lambda/\lambda$ [a]
1	1.87	0.484 cm^{-1}	-0.496 cm^{-1}	0.0109
2	1.94	.521	- .542	.0150
3	1.94	.524	- .551	.0182
4	2.01	.549	- .563	.0112
5	2.06	.547	- .594	.0265
6	2.07	.581	- .600	.0133
7	2.07	.509	- .519	.0086

$\frac{\Delta\lambda}{\lambda} = 0.0126 \pm .0017$ (Neglecting Run #5)

$\frac{\Delta\mu}{\mu} = 0.0055 \pm .0017$

a Using relation given on Page 59.

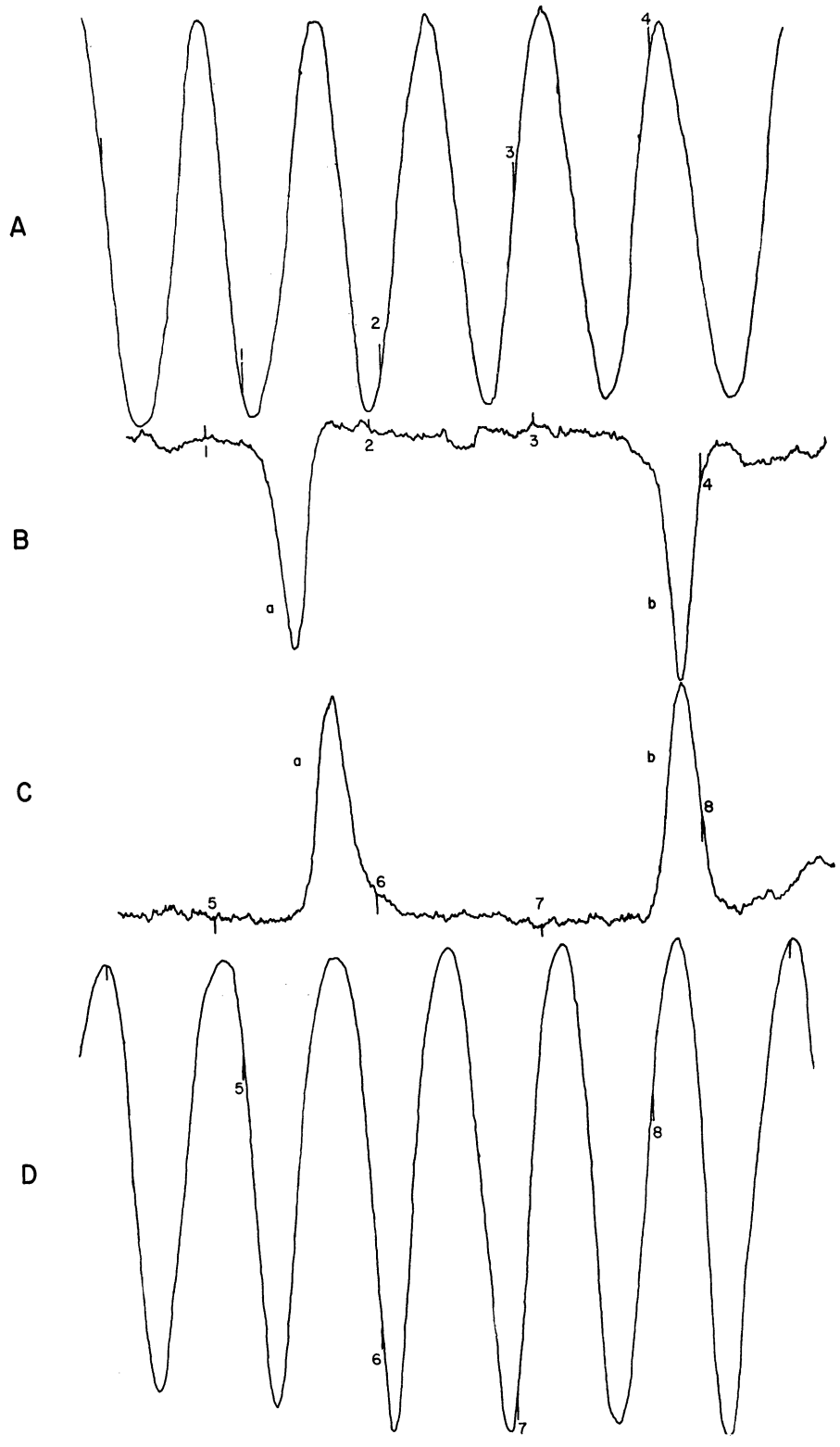

Figure 11 SPECTRA USED TO COMPUTE THE DIPOLE MOMENT OF HCN IN ITS ν_3 VIBRATIONAL STATE.

A. FRINGE TRACE ACCOMPANYING B.
B. P(1) a: ZERO FIELD b: λ = 2.06 (≈ 60 kV/cm) $\Delta M = 0$ COMPONENT.
C. R(0) a: ZERO FIELD b: λ = 2.06, $\Delta M = 0$.
D. FRINGE TRACE ACCOMPANYING C.
LIKE NUMERALS DESIGNATE CORRESPONDING FIDUCIAL MARKS

to a value for μ_1. Such a method, somewhat simpler than the one just described, is to measure the difference of the splittings of two lines having one rotation-vibration level in common. The result will depend only upon the molecular constants of the second vibrational state. Thus,

$$\nu_{J'''m''' \leftarrow J'm'} - \nu_{J''m'' \leftarrow J'm'} = B_1\left[\epsilon_{J''m''}(\lambda_1) - \epsilon_{J'''m'''}(\lambda_1)\right],$$

and

$$\nu_{J'm' \leftarrow J'''m'''} - \nu_{J'm' \leftarrow J''m''} = B_0\left[\epsilon_{J''m''}(\lambda_0) - \epsilon_{J'''m'''}(\lambda_0)\right].$$

The above relations can be used to calculate the field by determining λ_0, and with the known values for μ_0 and B_0, then $\mathcal{E} = \frac{B_0\lambda_0}{\mu_0}$. Conversely, the field, either as known from voltage and cell gap measurements, or as determined from a measurement of λ_0, may be considered as a known quantity and μ_1 evaluated. For this purpose, the following relation was derived from the data of Kusch and Hughes (21):

$$\lambda = 9.634\,\Delta^{1/2} - 0.2035\,\Delta + 0.0922\,\Delta^2, \quad \Delta \equiv \frac{\nu_{20 \leftarrow 11} - \nu_{22 \leftarrow 11}}{B_1} \text{ OR } \frac{\nu_{11 \leftarrow 22} - \nu_{11 \leftarrow 20}}{B_0}.$$

This expression proves to be accurate to ±0.1% and, therefore, allows a determination of μ to the precision with which the field is known or to the precision of the wavelength measurements, whichever is larger. Using this method of measurement, λ_1 was evaluated with $\lambda_0 \simeq 2 \cdot \mu_1$ was thus determined to be $(1.018 \pm .015)\mu_0$, consistent in value with the previous result. The method can also be used to obtain μ_0. The value from the present work is $\mu_0 = 2.96 \pm .04$ debye, in agreement with the microwave determination.

The possible influence of polarization effects of the electric field on the molecule has not been considered. Although no data are available on the polarizability components for HCN, they are typically of the order of 10^{-24} esu (11). Thus, the induced dipole would be of the order of $\mathcal{E} \times 10^{-24}$; at maximum field strength about $120{,}000/300 \times 10^{-24}$ or 0.0004 debye.

This is negligible in comparison to the permanent dipole moment of HCN of 3 debye and the barely discernible change of dipole moment between ground and first excited vibrational state of 0.0165 debye. Consequently, one would not expect to see any such influences with the present apparatus.

5.2 Methyl Fluoride, CH_3F.

Only symmetric top molecules will in general show linear Stark effects. Methyl fluoride was selected for study as a representative case because of its following properties:

a. No isotopic species of fluorine to complicate its spectrum.

b. Fundamental vibrational frequencies within the wavelength range of good detectivity (23).

c. Large dipole moment, 1.79 debye (24).

d. Large value for B and (A-B) (25).

Unfortunately, in none of its absorption bands does methyl fluoride absorb as strongly as does hydrogen cyanide in its ν_3 fundamental. Furthermore, the low J lines, which have the fewest M components and greatest M splitting in the presence of a field, are weaker in intensity relative to the strongest lines in the band for methyl fluoride than for hydrogen cyanide because of methyl fluoride's lower B value. In order to obtain sufficient percentage absorptions for these low J lines high sample pressures were needed, and only moderate electric field strengths could be used. Quantitatively measureable Stark patterns thus were difficult to produce. Even though chosen for its large B value and consequent widely spaced rotational structure, the great number of absorption lines in the methyl fluoride spectrum invariably afforded camouflage for the M components produced by the field. All attempts to identify Stark fine structure patterns in methyl fluoride were unsuccessful.

A number of interesting effects were noticed in the Stark spectra of methyl fluoride, however, particularly when using a modulated electric field. Since the frequency splittings for weak fields are comparable to the original line width (determined primarily by pressure broadening) the over-all effect of the electric field is to somewhat broaden the absorption line. If the difference between absorption with field on and field off is recorded, with phase-sensitive electronics, a spectrum as illustrated in Figure 13c will result. The magnitude of the difference signal is determined by the amount of the line broadening together with the zero-field line strength; the spectra recorded in this manner show an intensity pattern markedly different from that of the normal trace.

The calculation of the line broadening by the electric field for arbitrary values of J, K and M is laborious because of the large number of components and the integration over the line widths of the numerous transitions. By first order perturbation theory (Chapter IV), the components are shifted by an amount

$$\Delta\nu_{J+\Delta J,\,K+\Delta K\;M+\Delta M \leftarrow JKM} = \mu\mathcal{E}\left[\frac{(2J+1+\Delta J)KM - J(J+1)(K\Delta M + M\Delta K + \Delta K\Delta M)}{J(J+1)(J+\Delta J)(J+1+\Delta J)}\right],$$

or

$$\Delta\nu_{J'K'M' \leftarrow J''K''M''} = \mu\mathcal{E}\left[\frac{M'\{J'(J'+1)K'' + J''(J''+1)K'\} - J'(J'+1)K''\Delta M}{J'(J'+1)J''(J''+1)}\right].$$

From the first expression, the broadening is seen to be symmetric about the parent line. It is also observed, by inspection of the second expression for the shifts, that for certain values of K'', K' and J, the coefficient of M' vanishes. Thus for $\Delta J = +1$, $\Delta K = +1(-1)$, $K' = \frac{J'}{2}(-\frac{J'}{2})$ (and for $\Delta J = -1$, $\Delta K = -1(+1)$, $K' = \frac{J+1}{2}$ $(-\frac{J+1}{2})$) corresponding to the line ${}^{R}R(J)_{\frac{J}{2}}$ $({}^{P}P(J)_{\frac{J+1}{2}})$, the M-splitting depends not upon M but only upon ΔM. The Stark

spectrum of these lines will consist of only three components. Under these circumstances, the first order line shifts are given by

$$\Delta\nu_{J'K'M' \leftarrow J''K''M''} = -\mu\mathcal{E}\frac{K''\Delta M}{J''(J''+1)} .$$

For example, the line $^{R}R(6)_3$ in the ν_4 fundamental of methyl fluoride, at a field of 15 kV/cm, is made up of a component shifted -0.0317 cm^{-1} with a relative intensity of 1.0 corresponding to $\Delta K = +1(-1)$, $\Delta M = +1(-1)$, a second corresponding to $\Delta K = +1(-1)$ $\Delta M = -1(+1)$ of the same intensity shifted by +0.0317 cm^{-1}, and a third unshifted component of intensity 2.0 corresponding to $\Delta M = 0$. In computing these relative intensities, the wave functions with field are assumed identical to those without field (consistent with first order perturbation theory). The observed and calculated spectra are shown in Figures 12a and 12b. The discrepancy between them is probably due to the the fact that the naturally occurring line $^{R}R(6)_3$ is strong enough to be in the nonlinear absorption region. Satisfactory agreement can be obtained as shown in Figure 12c, by assuming a 68% absorption for the zero field line (which is close to the measured value).

As a further example, the Stark spectrum of the line $^{Q}R(3)_2$ for $2\nu_5$ of methyl fluoride at a field of 10 kV/cm has been calculated, as in Figure 13. The fine structure could only be resolved with a resolution of 0.01 cm^{-1}; only a broadened line will result with the actual resolution of 0.03 cm^{-1}.

For an arbitrary line of high J value, the Stark broadening will vary roughly as K/J^2. Therefore, the intensities of the rotational lines observed by using Stark difference-signal techniques will be modulated by this factor in addition to those present with no field. This accentuation of the high K, low J lines can be employed to great advantage in the analysis of the rotational structure of an absorption band. The technique has been applied

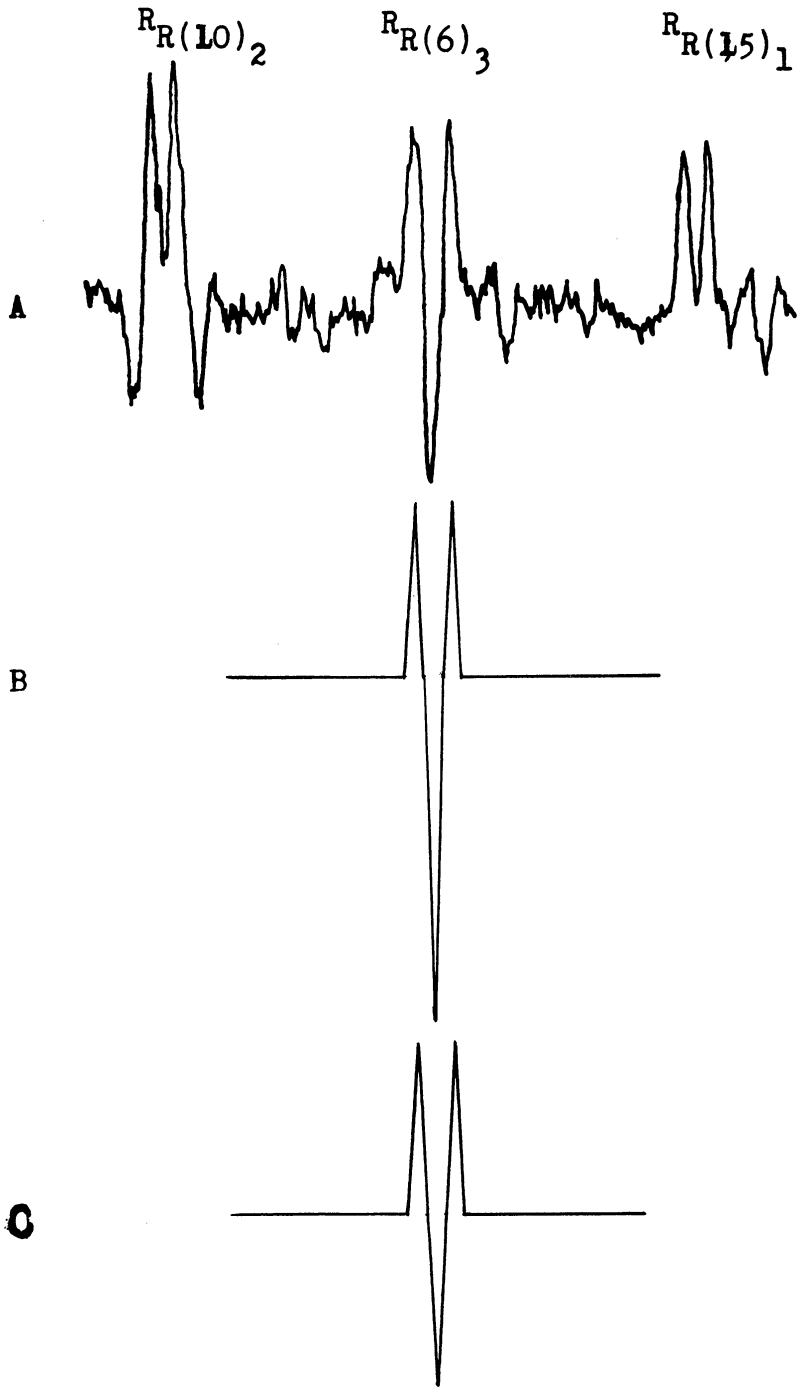

Figure 12 OBSERVED AND CALCULATED $R_{R(6)_3}$ IN THE ν_4 BAND OF METHYL FLUORIDE

A. Observed difference signal, 15kV/cm, 0.03 cm^{-1} resolution. Positive signal implies greater absorption with field on.

B. Calculated spectrum assuming linear absorption.

C. Calculated spectrum assuming exponential absorption and 68% absorption for the zero field line.

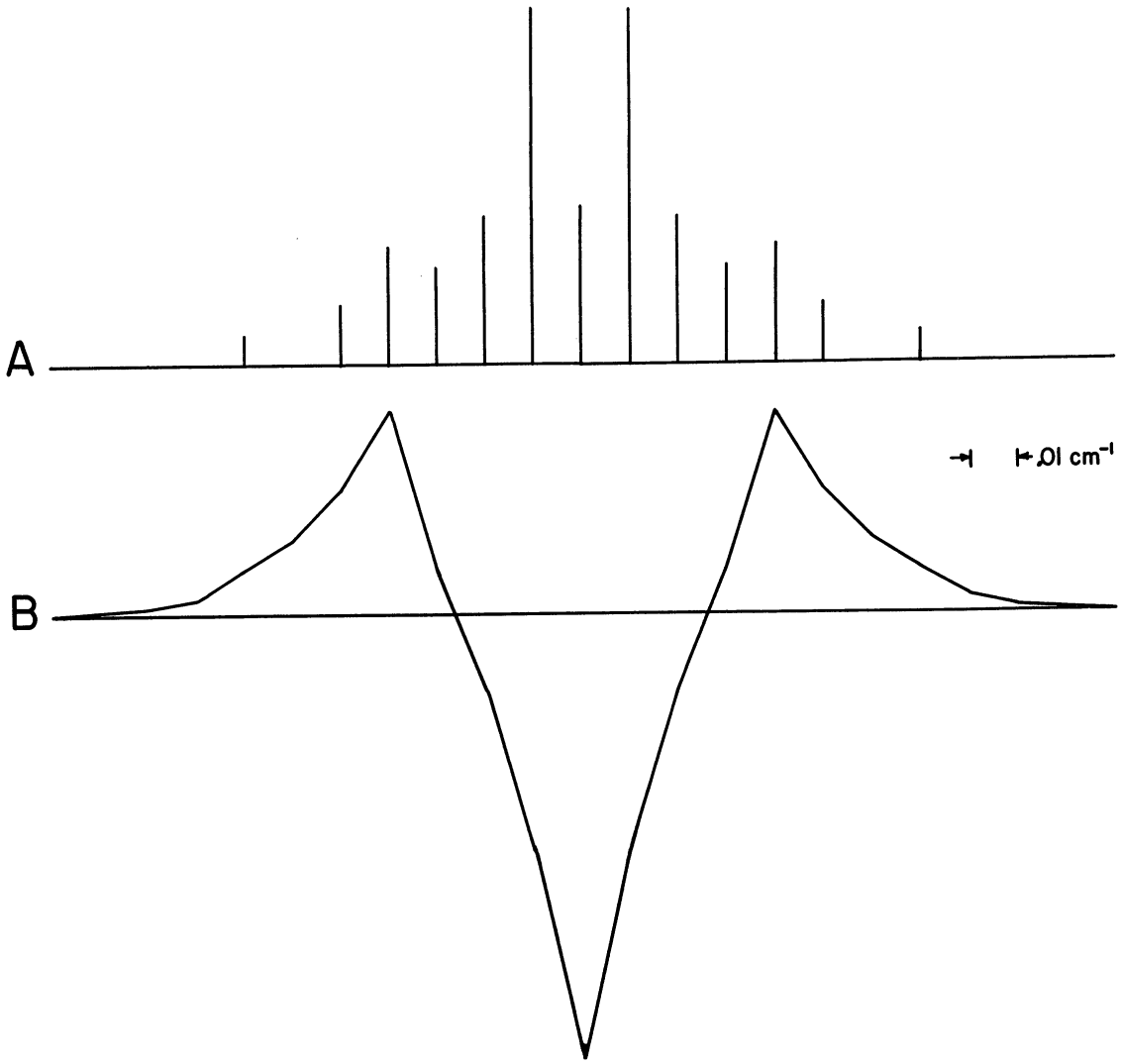

Figure 13 PREDICTED SPLITTING AND DIFFERENCE SPECTRUM OF THE LINE $^{Q}R(3)_2$ IN THE $2\nu_5$ BAND OF METHYL FLUORIDE.

A. Splittings and Relative Intensities Calculated to First Order for $\mathcal{E}$ = 10kV/cm

B. Difference Spectrum with a Spectral Resolution of 0.03 cm^{-1}

extensively, and successfully, to the ν_4 fundamental of methyl fluoride and several of the results will be presented.

In Figure 14 we see the region of the band center. As ν_4 derives its infrared activity from a dipole moment change perpendicular to the figure axis, the selection rule in K is $\Delta K = \pm 1$. Following the usual conventions, this change in K is denoted by a left superscript P ($\Delta|K| = -1$) or R ($\Delta|K| = +1$) while the ground vibrational state $|K|$ value is denoted by a right subscript. The J states involved are as usual denoted by P, Q, or R followed in parenthesis by the J value of the lower state. Thus, ${}^{R}Q(7)_5$ labels the transition $J'' = 7$, $J' = 7$, $K'' = 5$ and $K' = 6$. Returning to the figure, a normal spectrum of the region is shown above and no distinguishing structure is noted. Only careful measurements and a trained eye can establish the location of ${}^{R}R(0)_0$, and positive identification of Q branches (only ${}^{R}Q(J)_0$ and ${}^{R}Q(J)_1$ are shown here) is difficult. The fact that for $K = 3n$, $n = 0, 1, 2\ldots$ the Q-branch strength is greater because of nuclear statistics is of course helpful but three choices for the band center will remain, since ${}^{P}Q(J)_3$, ${}^{R}Q(J)_0$ and ${}^{R}Q(J)_3$ are approximately equal in strength. A quick glance at the Stark difference signal, shown in the lower half of Figure 14, is enough to convince one of its value. Here the entire sub-branch ${}^{R}R(J)_0$ can immediately be identified, the fact that the first line of the sub-branch occurs just 2B cm^{-1} from the associated Q branch (where 2B is not calculated but simply measured as the distance between the successive rotational lines of what surely is a sub-band) proving the correctness of the assignment of ${}^{R}Q(J)_0$. The first three members of the sub-branch ${}^{R}P(J)_0$ are identified, this assignment being somewhat more difficult since the sub-branches ${}^{R}P(J)_K$

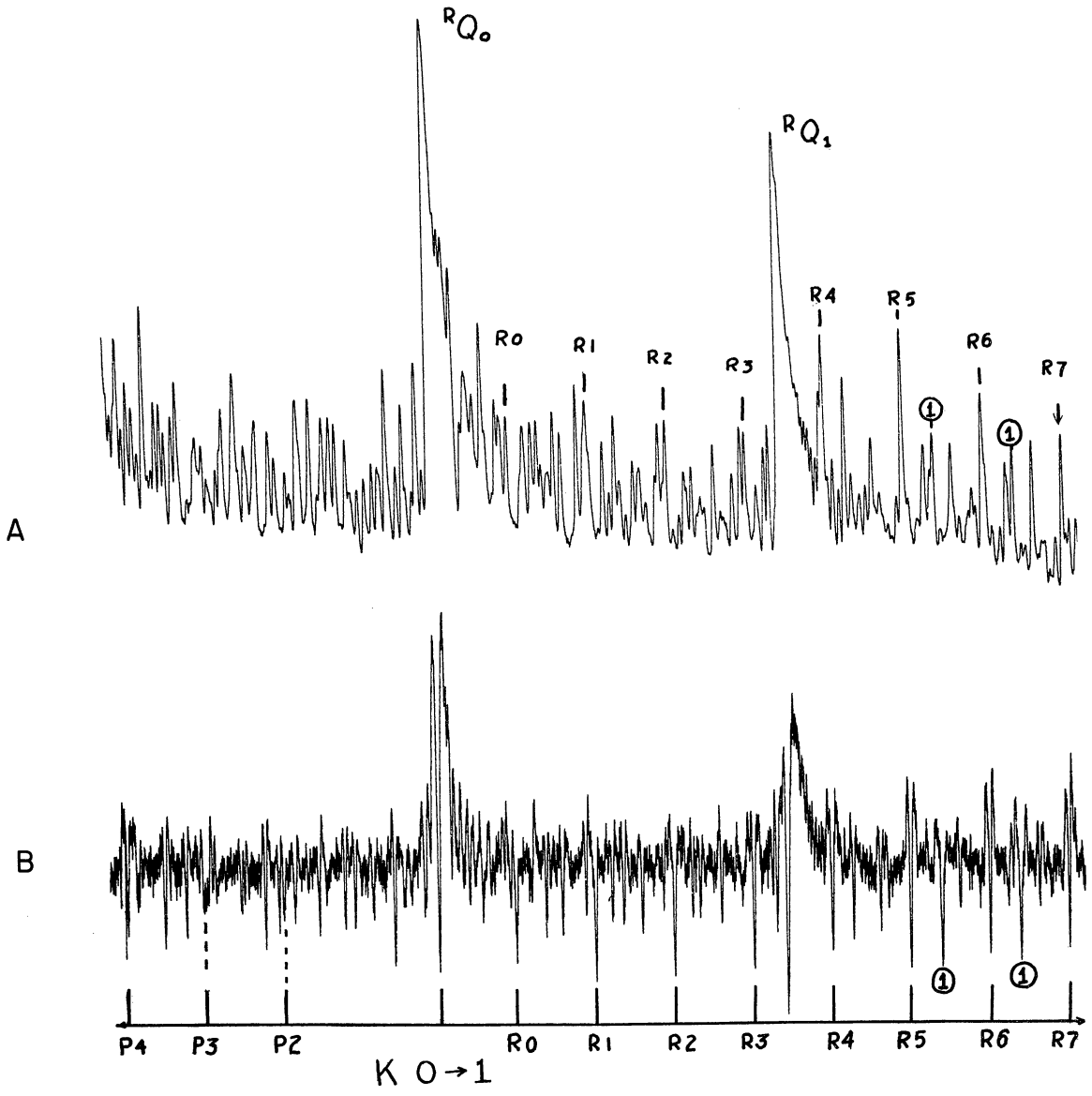

Figure 14 STARK EFFECTS NEAR $^{R}Q(J)_0$ OF THE ν_4 FUNDAMENTAL OF METHYL FLUORIDE.

A. Normal Spectrum. The R(J) subbranch of $^{R}Q_0$ is designated.

B. Stark Difference Signal Spectrum. $\mathcal{E} = 12$ kV/cm. Positive signal implies greater absorpton with field on.

and ${}^{P}R(J)_{K}$ are much weaker in intensity than are ${}^{P}P$ and ${}^{R}R$ sub-branches (26). The first two lines of ${}^{R}R(J)_{1}$ are also shown, where, as to be expected ${}^{R}R(0)_{1}$ is missing (because J must be greater than or equal to $|K|$). That quantitative measurements of the Stark effect are hindered by the multitude of absorption lines is well illustrated by this spectrum. Although at 12 kV/cm (the field used for this run) the M components of ${}^{R}R(1)_{0}$ are all certainly resolved, one from another, they are overlapped by other, stronger, transitions. The Stark spectrum here has been taken with the infrared signal and the electric field modulation phased so that absorption with no field is recorded down scale while absorption with field is recorded up scale. The net signal above the zero line indicates that the absorptions with zero field are of a nonlinear type as explained previously.

Figure 15 shows the region from ${}^{R}Q(J)_{2}$ to ${}^{R}Q(J)_{7}$ of ν_4 methyl fluoride, an extension of Figure 14. Again the sub-branches may be readily identifield with the help of the Stark spectrum of the lower half of the figure. Each line so identified has been labeled with its K" value. It is seen that the strong lines of the normal spectrum, aside from those of the Q branch, have all been assigned. The remaining weak lines may be either members of ${}^{P}R$ sub-branches or belong to 'hot' bands. An interesting phenomena is seen to occur at ${}^{R}Q(J)_{4}$. This Q branch is extremely broad compared to ${}^{R}Q(J)_{3}$ and for ${}^{R}Q(J)_{5}$ and higher the Q branches are not split at all. The exact explanation of this anomaly is not proffered but it has been suggested (27) that it arises from a Coriolis resonance between the K = 5 levels of ν_4 and ν_1. Associated with this disturbance is an increase of the effective B value of the sub-branch ${}^{R}R(J)_{4}$, an unmistakable fact in view of the Stark effect spectrum where no ambiguities exist in making the assignments. The lines

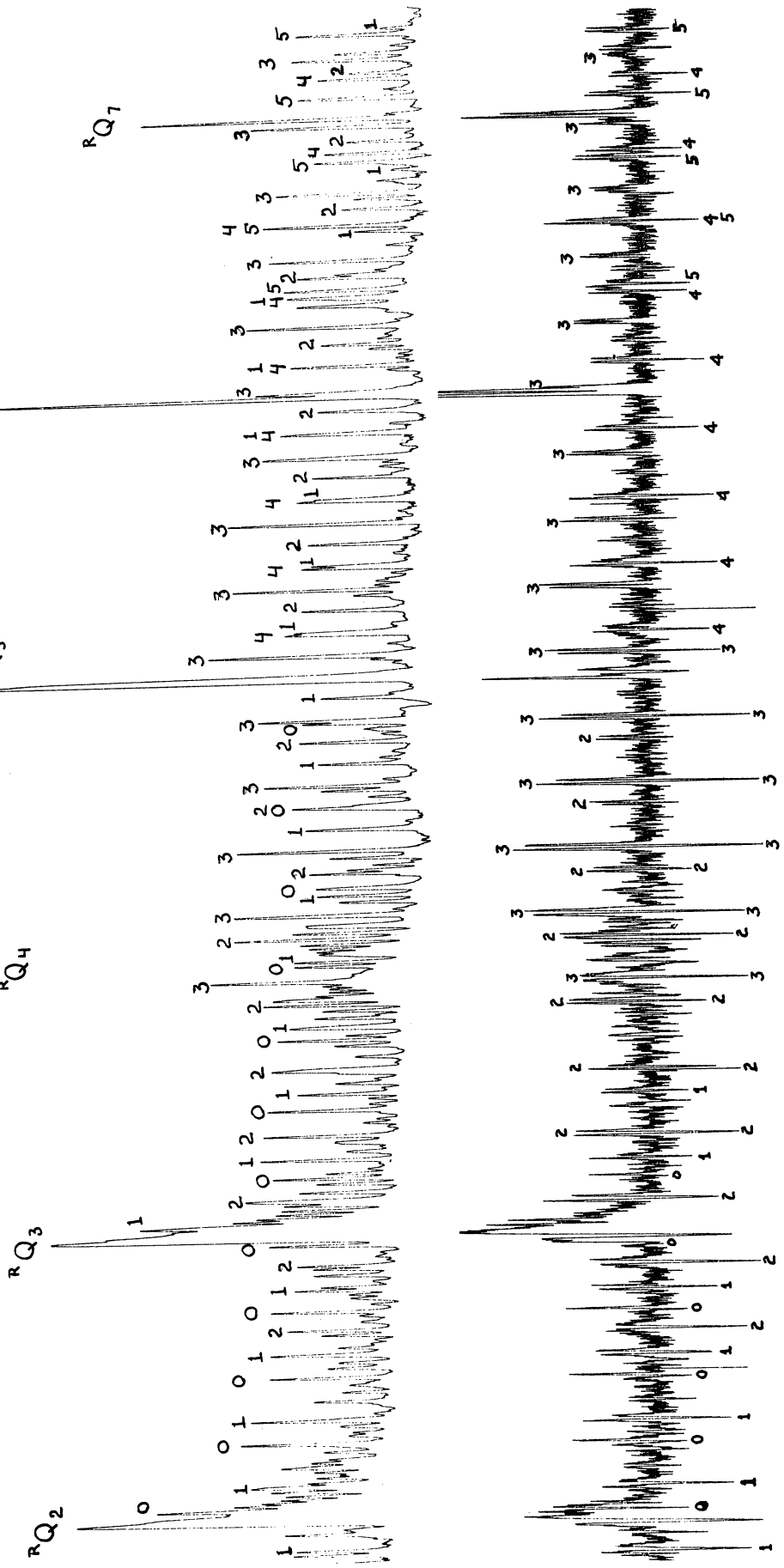

Figure 15 STARK EFFECTS IN THE ν_4 FUNDAMENTAL OF METHYL FLUORIDE FROM $^RQ(J)_2$ TO $^RQ(J)_7$.

Above: Normal spectrum. Below: Stark difference signal. 12 kV/cm. Positive signal implies greater absorption with field on.

Numerals designate the K value of $^RR(J)_K$ subbranch members.

$^{R}R(10)_4$ and $^{R}R(6)_5$ fall on top of one another while $^{R}R(9)_4$ is to the left of $^{R}R(5)_5$ and $^{R}R(11)_4$ is to the right of $^{R}R(7)_5$. Unraveling this sort of snarl would be quite a tedious task, whereas a positive identification of the lines can be made almost immediately via the Stark effect.

Figure 16 shows the Stark difference spectrum of ν_4 of methyl fluoride from $^{R}Q(J)_7$ to $^{R}Q(J)_{13}$ a further extension of Figures 14 and 15. The ability of the Stark effect to modulate the intensity pattern of the zero field spectrum is perhaps best illustrated here. The region of $^{R}Q(J)_{12}$ is dense with lines in the normal spectrum, whereas only the members of the sub-branch $^{R}R(J)_9$ appear in the Stark modulated spectrum. The abrupt termination of this branch near 3091 cm^{-1} in the Stark effect mode is unmistakable, and simple measurements indicate that 9 x (2B) to the left brings us exactly to $^{R}Q(J)_9$. The sub-branches $^{R}R(J)_7$ and $^{R}R(J)_9$ are indicated, and little effort is required to identify several more. In this figure we note the complete lack of negative going signals, indicating that, at the pressures employed, the normal absorptions approached 100% so that a negligible decrease in the maximum absorption occurred when the line was broadened by the Stark field.

Figure 17 shows sections of a high-resolution, slow speed scan of ν_4 methyl fluoride in which as many assignments as possible have been made with the Stark effect. Some twenty five members of the $^{R}Q(J)_3$ branch are indicated on the normal spectrum, but the Stark effect provides no clue to their assignment. The region of $^{R}Q(J)_4$ is also shown where the complete disruption of the usually intense Q branch has already been noted. The change in spacing in the corresponding sub-branch is also illustrated by the section showing the crossing at $^{R}R(10)_4$ of the $^{R}R(J)_4$ and $^{R}R(J)_5$ sub-branches.

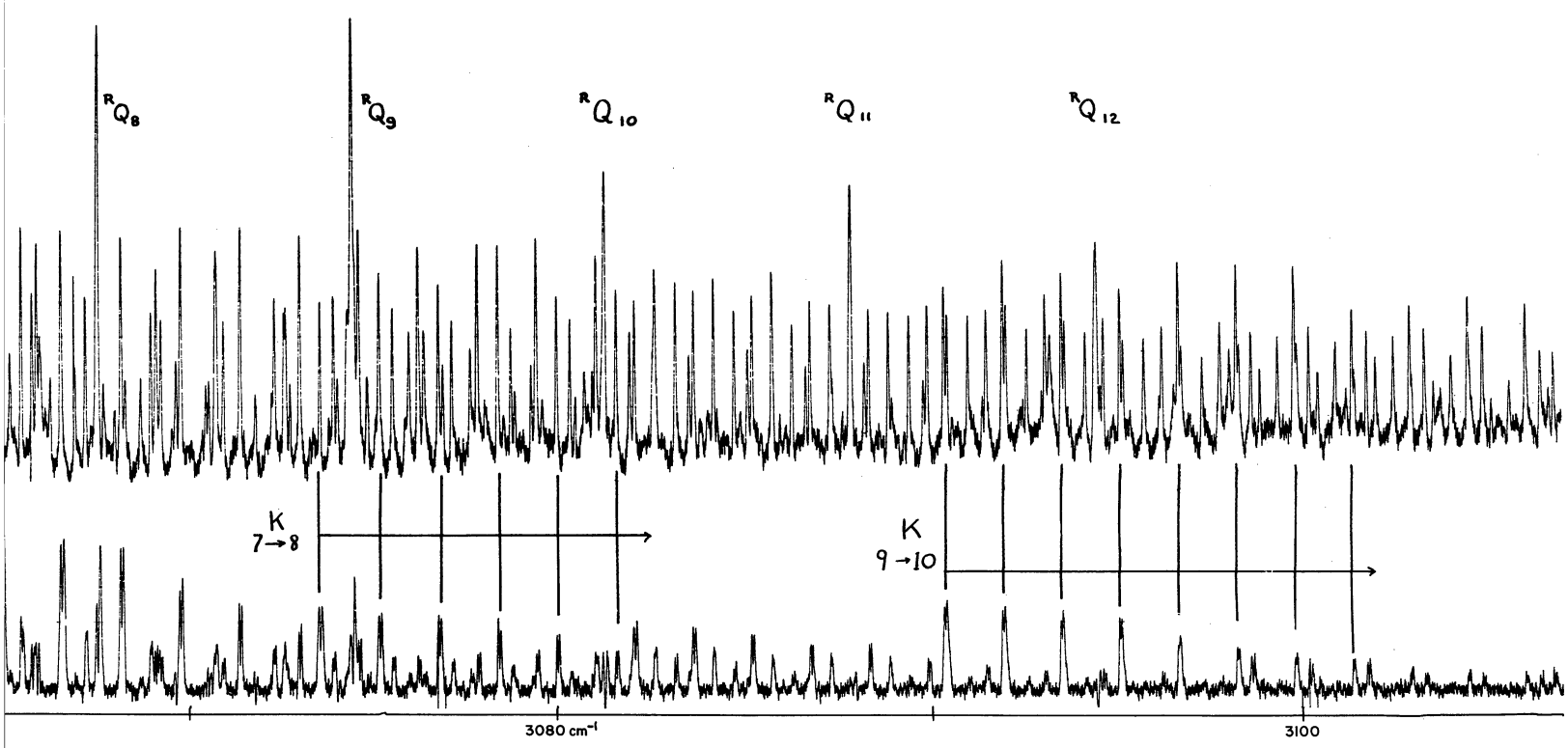

EFFECTS IN THE ν_4 FUNDAMENTAL OF METHYL FLUORIDE FROM $^{R}Q(J)_7$ TO $^{R}Q(J)_{13}$.

ectrum. Below: Stark difference signal spectrum. $\mathcal{E}$ = 18 kV/cm. Positive signal implies greater absorption with field on. Members of the $^{R}R(J)_7$ and $^{R}R(J)_9$ subbranches are indicated.

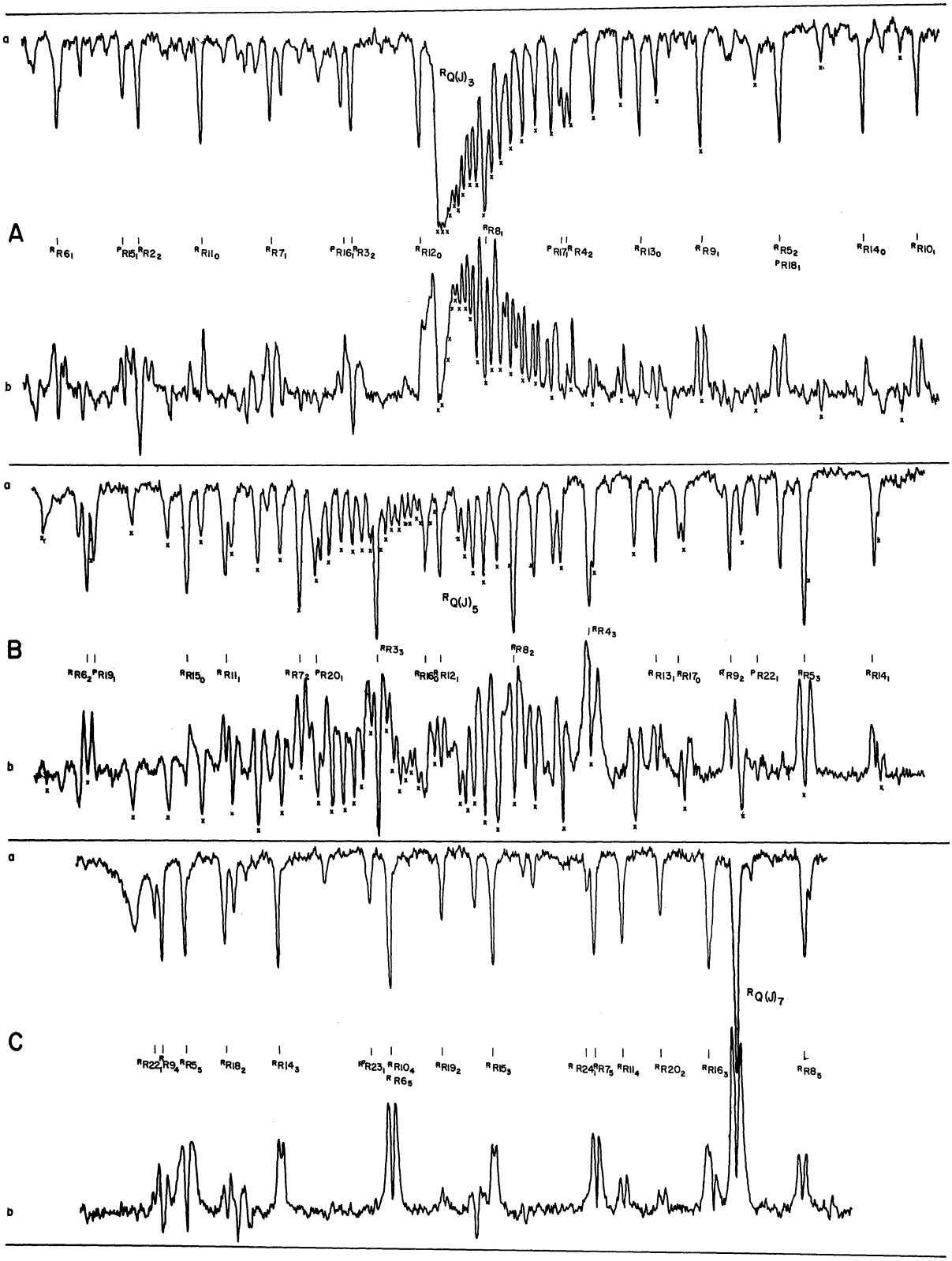

Figure 17 STARK EFFECTS IN THE ν_4 FUNDAMENTAL OF METHYL FLUORIDE UNDER HIGH RESOLUTION.

A. Illustration of the $^{R}Q(J)_3$ region. Successive members of the Q branch are marked by 'x'.

B. The $^{R}Q(J)4$ region showing the degeneration of the Q branch. Successive members of both wings are marked by 'x'.

C. The region of $^{R}R(10)4$ and $^{R}R(6)5$ illustrating the increased effective 'B' value in the $^{R}R(J)4$ subranch.

a. Normal spectrum. 0.03 cm^{-1} spectral slit width.

b. Stark difference signal. 15 kV/cm field. Positive signal implies greater absorption with field on.

5.3 Methyl Iodide, CH_3I

To further illustrate the value of the Stark difference signal as a tool in unraveling the rotational structure of complex bands, a molecule having very closely spaced lines was sought. Methyl iodide was chosen as it has a single isotope, a fundamental vibration within range of lead sulfide detectors, sufficient vapor pressure, and a B-value of only 0.25 cm^{-1} (23). As in methyl fluoride, it was found that high sample pressures were needed for sufficient absorption so that fields of only about 10 kV/cm could be applied without breakdown. No quantitative measurements were attempted.

Figure 18 shows the normal and Stark difference spectra of the ν_4 fundamental band center. The only recognizable features of the zero field trace are the strong Q branches identified as $^{R}Q(J)_0$ and $^{P}Q(J)_1$. The Stark difference signal trace, on the other hand, shows beautifully developed $^{R}R(J)_0$ and $^{R}P(J)_0$ sub-branches, as identified by 0's on the figure. It is seen that the sub-branch lines reach maximum intensity for $J \cong 30$ in the normal spectrum, but for $J \cong 5$ in the Stark spectrum. Thus the Stark difference signal eliminates most of the high J transitions.

This fact is strikingly demonstrated in Figure 19 which again compares normal and Stark spectra, this time in the region of $^{R}Q(J)_3$. Here a monotone of weak, unresolved, unassignable lines is found between the Q branches of the normal spectrum. In the Stark spectrum, only a half-dozen or so single, completely resolved lines appear, identified as the 3rd through 9th members of the sub-branch $^{R}R(J)_3$ (lettered 'J') and the fourth through seventh members of $^{R}R(J)_2$.

A further effect which proved useful in making assignments in parallel

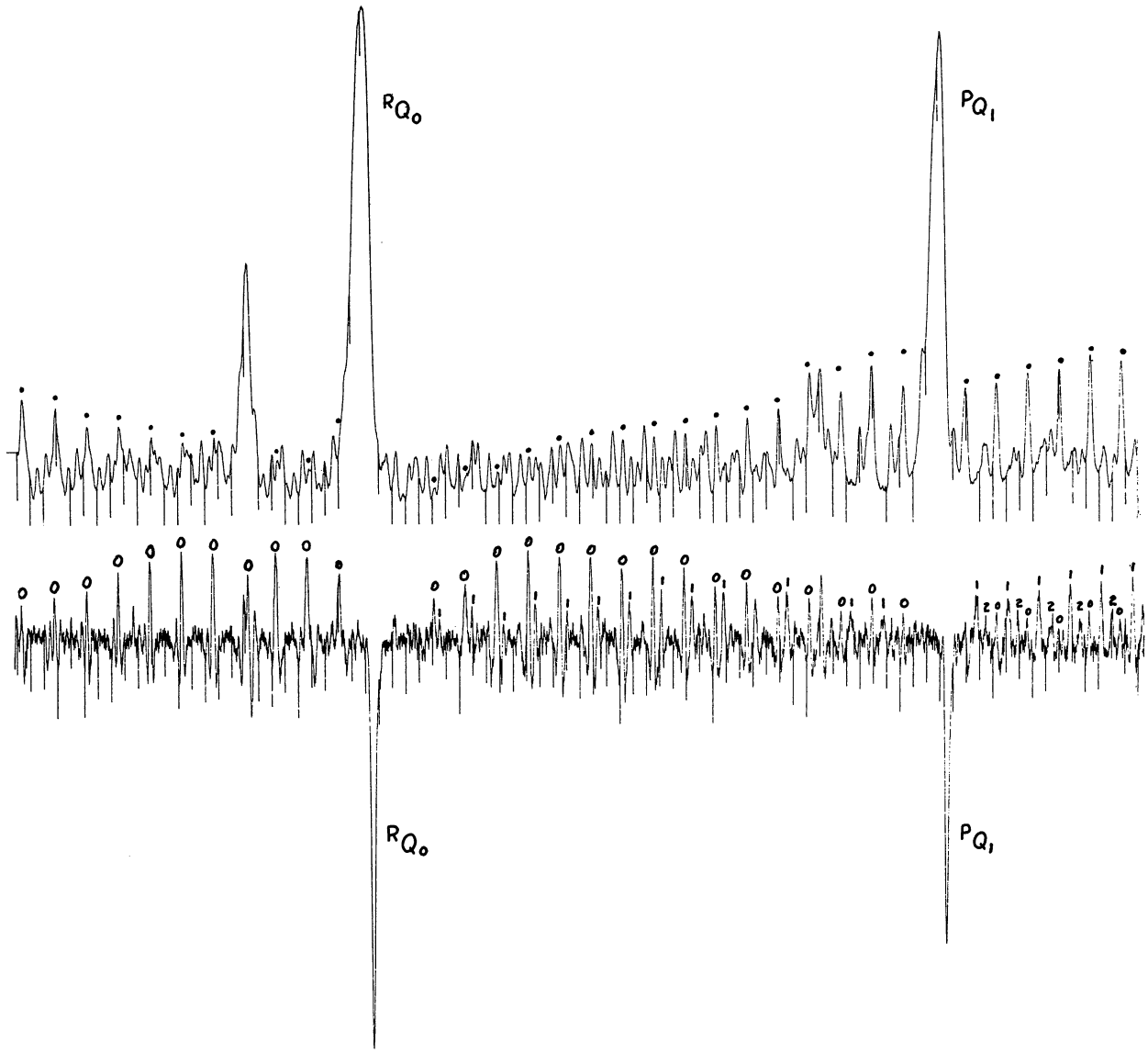

Figure 18 STARK EFFECTS NEAR $^{R}Q(J)_0$ OF THE ν_4 FUNDAMENTAL OF METHYL IODIDE.

Above: Normal spectrum. Members of $^{R}R(J)_0$ and $^{R}P(J)_0$ are dotted.

Below: Stark difference signal spectrum. $\mathcal{E}$=10 kV/cm. Numerals indicate the K value of members of $^{R}R(J)_K$ subbranches. $^{R}P(J)_0$ is also indicated.

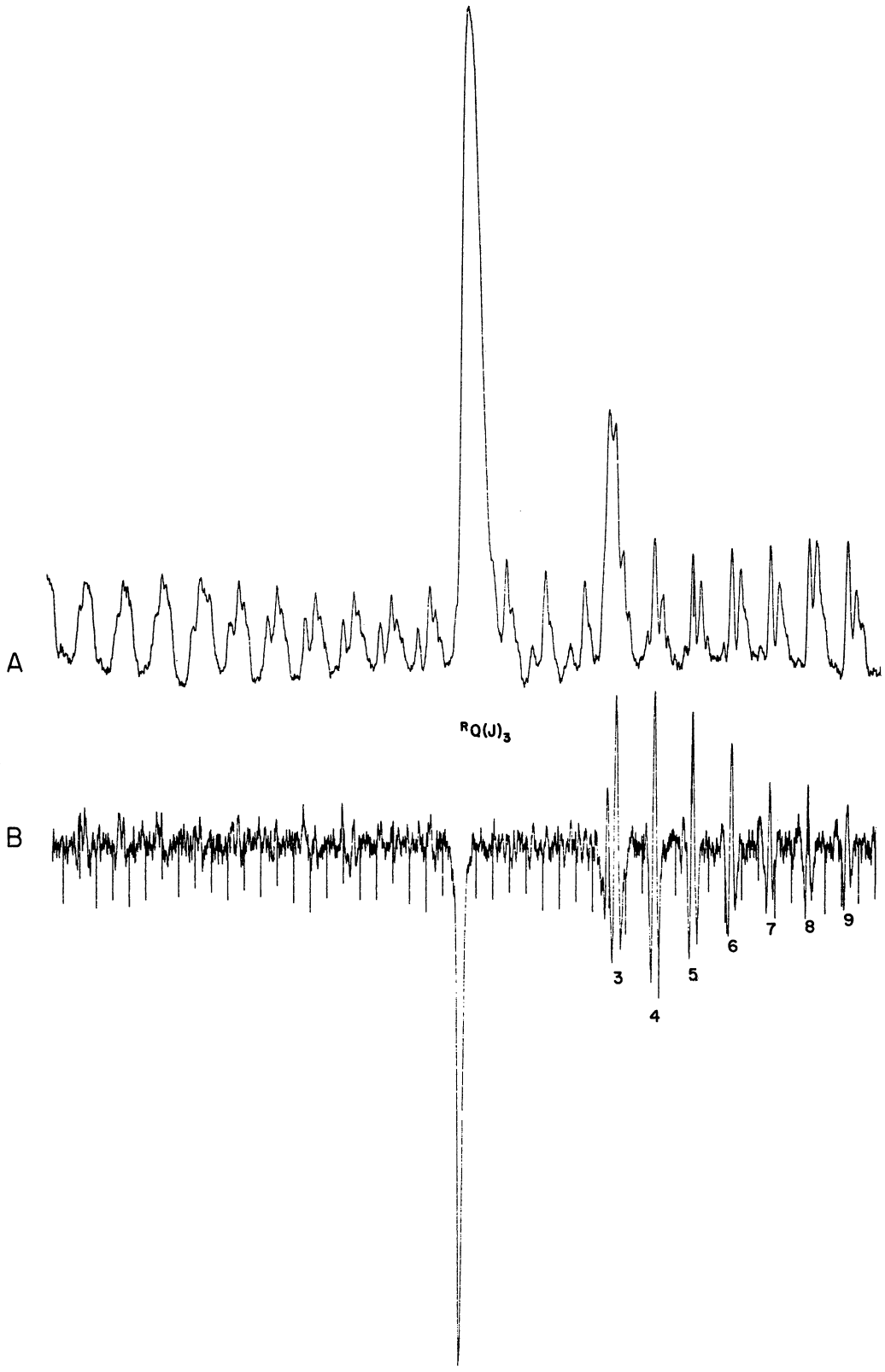

Figure 19 STARK EFFECTS IN METHYL IODIDE NEAR $^{R}Q(J)_3$ OF THE ν_4 FUNDAMENTAL.

A. Normal spectrum.

B. Stark difference spectrum; 15 kV/cm, negative signal implies greater absorption with field on, members of the $^{R}R(J)_3$ subbranch are labeled by their 'J' value.

type bands (ones involved a vibrational dipole moment change parallel to the figure axis of the molecule and therefore requiring $\Delta K = 0$) can also be demonstrated in methyl iodide. For low fields the first order perturbation treatment can be expect to apply; and since $\Delta K = 0$,

$$\Delta\nu_{J'K''M \leftarrow J''K''M''} = \mu\mathcal{E}K''\left[\frac{M''}{J''(J''+1)} - \frac{M'}{J'(J'+1)}\right].$$

For the case $K'' = 0$, no shifts occur. The spectrum of a parallel type band is complicated in general by the 'K' splitting of the individual ${}^{Q}R(J)_K$ and ${}^{Q}P(J)_K$ lines. Thus each ${}^{Q}R(J)_K$ 'line' has J components (one for each value of $|K|$). Ideally, these components are degenerate, but centrifugal distortion and vibration-rotation interaction terms cause them to split somewhat, giving rise to structures varying from slightly broadened lines to actual 'sub-branches.' The ν_1 vibration of methyl iodide at 2970 cm^{-1} is such a parallel band having rather large 'K' splitting, as indicated in Figure 20. Here the assignments may be given to some extent by observation, a few being labeled. On applying a D.C. Stark field, the K components suffer symmetric Stark broadening which simply 'washes out' their intensity the net result being destruction of the 'line' spectrum. This does not occur, however, for K = 0, since there is no Stark shift for these lines. Figure 21 demonstrates this effect where we see the normal and Stark spectra (with a D.C. field of 10 kV/cm) and observe that only three 'lines' persist in the R branch and must correspond to ${}^{Q}R(0)_0$, ${}^{Q}R(1)_0$, and ${}^{Q}R(2)_0$. With this help, the K components of the normal spectrum can be assigned with certainty.

5.4 Ammonia, NH_3.

It is well known that the ammonia molecule, shaped as a pyramid, may suffer an inversion, the nitrogen atom crossing through the triangle formed

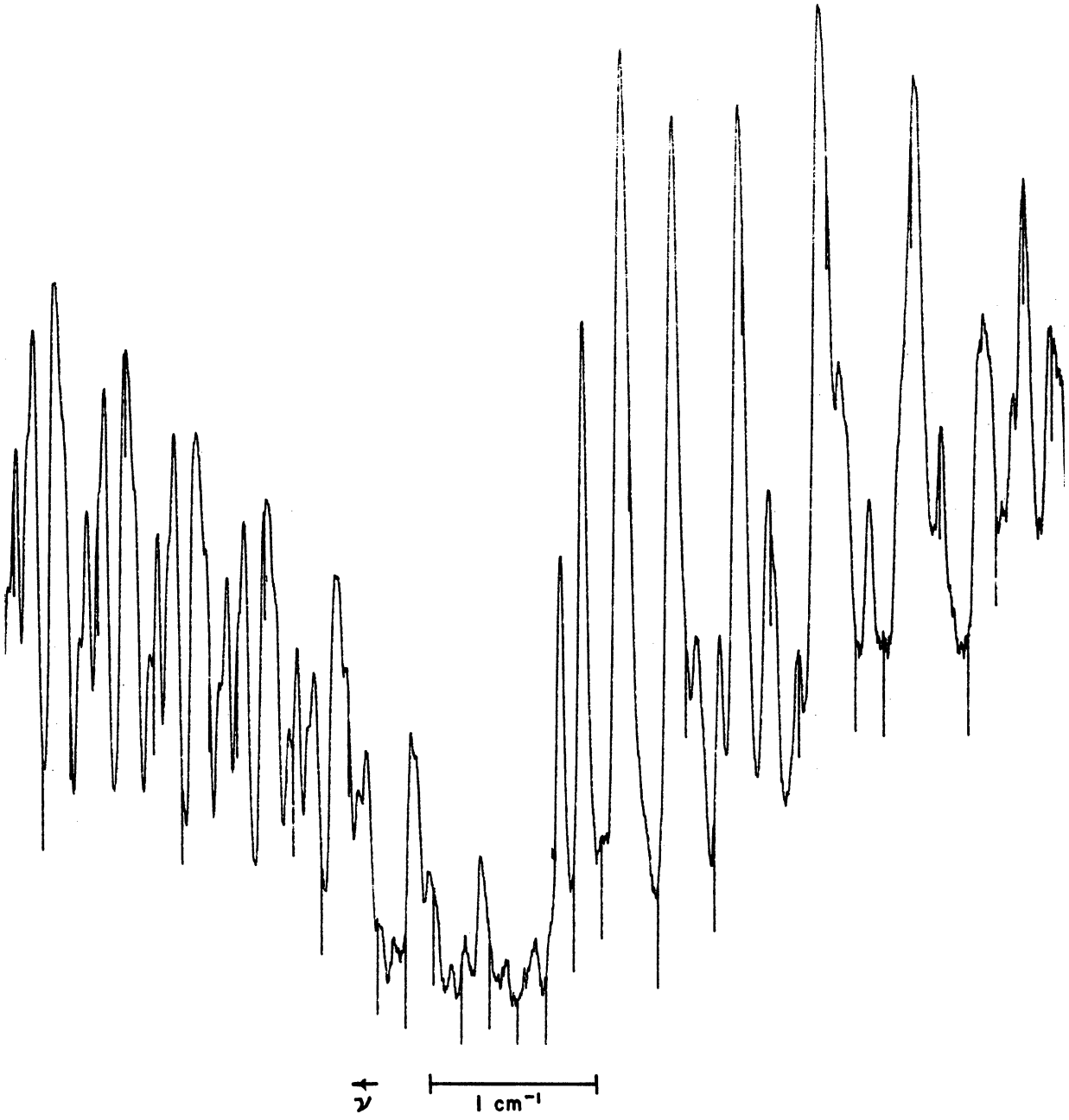

Figure 20 METHYL IODIDE ν_1 BAND CENTER NEAR 2970 cm^{-1}.

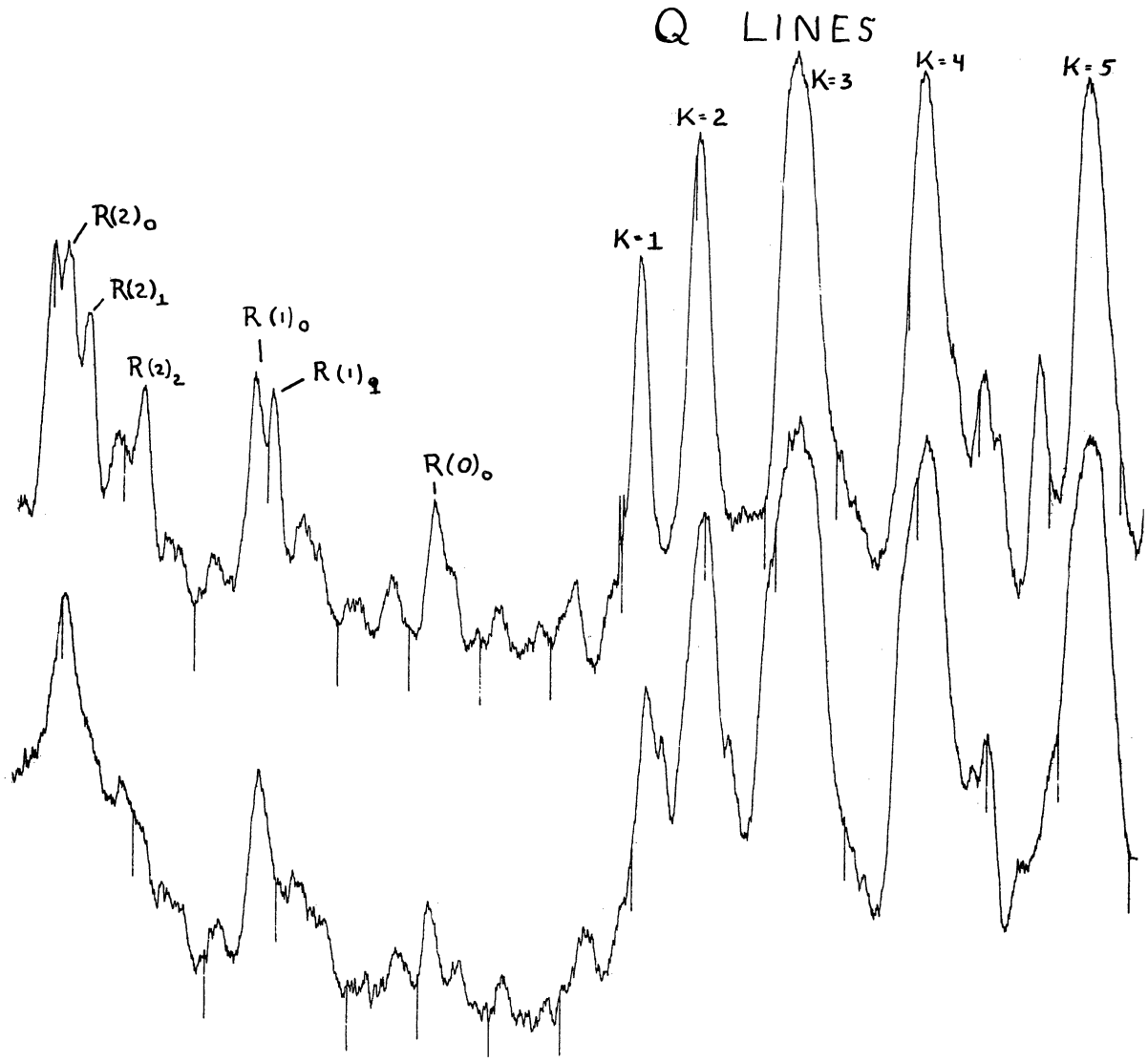

Figure 21 DC FIELD STARK EFFECTS IN THE ν_1 FUNDAMENTAL OF METHYL IODIDE

Above: Normal Spectrum. Below: Spectrum with 10 kV/cm DC Electric Field.

by the three hydrogens at the rate of about 24 KMC (28). This phenomena leads to a doubling of all otherwise single rotational states. The energy separation of these inversion doublets is of the order of one wave number for the vibrational modes encountered in the present work. Adjacent inversion states have a connecting dipole moment matrix element. Since the next nearest interacting state is $2(J+1)B = 20(J+1)$ cm^{-1} away, to a good approximation the inversion pair may be considered doubly degenerate and the presence of the other rotational states may be ignored.

The wave functions properly describing inversion states change sign under an inversion of the molecule through its center of mass. The molecular dipole moment, behaving as a vector, also changes sign under this operation. Thus first order contributions of the electric field to the energy are zero, for:

$$\underline{I}_{cm} \langle J K M P_{cm} | \vec{\mu}\cdot\vec{\mathcal{E}} | J K M P_{cm} \rangle = - \langle J K M P_{cm} | \vec{\mu}\cdot\vec{\mathcal{E}} | J K M P_{cm} \rangle ,$$

and the energy must be invariant with respect to symmetry operations.

Second order effects do occur, however, and nonvanishing matrix elements for this case (developed in Chapter IV) and their corresponding energy denominators are:

$$\langle J+1\, K M - P_{cm} | -\bar{\mu}\cdot\bar{\mathcal{E}} | J K M P_{cm} \rangle = -\mu_0 \mathcal{E} \left\{ \left[(J+1)^2 - K^2 \right] \left[(J+1)^2 - M^2 \right] / (J+1)^2 (2J+1)(2J+3) \right\}^{1/2} ; \quad -2B(J+1) - (-1)^K P_{cm} \Delta ,$$

$$\langle J K M - P_{cm} | -\bar{\mu}\cdot\bar{\mathcal{E}} | J K M P_{cm} \rangle = -\mu_0 \mathcal{E}\, KM / J(J+1) ; \quad (-1)^{K+1} P_{cm} \Delta ,$$

$$\langle J-1\, K M - P_{cm} | -\bar{\mu}\cdot\bar{\mathcal{E}} | J K M P_{cm} \rangle = -\mu_0 \mathcal{E} \left\{ (J^2 - K^2)(J^2 - M^2) / J^2 (4J^2 - 1) \right\}^{1/2} ; \quad +2BJ - (-1)^K P_{cm} \Delta$$

Here, Δ is the energy separation of inversion doublets. The choice of sign $(-1)^{K+1} P_{cm}$, for the inversion contribution to the energy differences is not

arbitrary but depends upon the fact that the lowest level of an inversion doublet will have positive symmetry under $\underline{R}_{xy}$ (a reflection in the plane through the center of mass and perpendicular to the figure axis). Since

$$\underline{R}_{xy} = \underline{I}_{cm} \cdot \underline{C}_2^z \quad \text{and} \quad \underline{C}_2^z \psi_{JKMP_{cm}} = (-1)^K \psi_{JKMP_{cm}},$$

$$\underline{R}_{xy} \psi_{JKMP_{cm}} = (-1)^K P_{cm} \psi_{JKMP_{cm}}.$$

The second order corrections to the energy are then

$$\Delta W_{JKMP_{cm}} = \mu_0^2 \mathcal{E} \left[\frac{[(J+1)^2-K^2][(J+1)^2-M^2]}{(J+1)^2(2J+1)(2J+3)} \times \frac{1}{-2B(J+1)-(-1)^K P_{cm}\Delta} + \frac{K^2M^2}{J^2(J+1)^2} \times \frac{1}{(-1)^{K+1} P_{cm}\Delta} + \frac{(J^2-K^2)(J^2-M^2)}{J^2(4J^2-1)} \times \frac{1}{2BJ-(-1)^K P_{cm}\Delta} \right],$$

where

$$\mu_0 \equiv \int \psi^{VIB*}_{-P_{cm}} \mu_z \psi^{VIB}_{P_{cm}} \, d\tau.$$

The energy denominators in this expression for ΔW are approximately $2BJ \pm \Delta$ for the first the third terms, but only Δ for the second term. Hence the second term will usually be dominant. (In certain vibrational modes involving ν_2, Δ can become large and the relative importance of the three terms will change. For example when $(\nu_1\nu_2\nu_3{}^{\ell_3}\nu_4{}^{\ell_4}) = (011^10^0)$, $\Delta = 18.5$ cm^{-1} (29) and $2B = 19.88$ cm^{-1} so that $2BJ-\Delta\big|_{J=1} = 1.43$ cm^{-1}.)

The exact solution to the problem of two interacting states is available (2) and may be given as:

$$E_1 = E_0 - \frac{\Delta}{2}(1+\xi^2)^{1/2}, \qquad E_2 = E_0 + \frac{\Delta}{2}(1+\xi^2)^{1/2},$$

$$\psi_1 = \frac{1}{\sqrt{2}}(1+\xi^2)^{-1/4}\left[(1+\sqrt{1+\xi^2})^{1/2}\psi_{JKMP} - (1-\sqrt{1+\xi^2})^{1/2}\psi_{JKM-P}\right],$$

$$\psi_2 = \frac{1}{\sqrt{2}}(1+\xi^2)^{-1/4}\left[(1-\sqrt{1+\xi^2})^{1/2}\psi_{JKMP} + (1+\sqrt{1+\xi^2})^{1/2}\psi_{JKM-P}\right],$$

where $\zeta \equiv \frac{2\mu_0 \mathcal{E}}{\Delta} \frac{KM}{J(J+1)}$ and ψ_1 is the state of lower energy.

As in the case of the symmetric top molecules studied, many millimeters pressure of ammonia had to be used to produce reasonable absorption strengths for the low J (simple Stark pattern) lines. Consequently, fields were limited to the order of 30-50 kV/cm. For example, the state (JKMPcm) = (222 +) shifts by -0.117 cm^{-1} under an applied field of 10,000 volts/cm. The change of frequency of a transition involving this state will be the difference between its shift and that of the other participant state, and will be equal to or greater than this amount. In spite of these large displacements, identification of individual Stark patterns was not possible with available resolution simply because of the great number of components which arose when a field was applied.

Ordinarily the selection rule $P'_{cm} \longleftrightarrow -P''_{cm}$, $P'_{cm} \not\longleftrightarrow +P''_{cm}$ holds for the parallel vibrations of ammonia. We have seen, however, that application of a Stark field mixes states of different P_{cm} and this rule is vitiated to the extent of the mixing. Figure 22 is a schematic level diagram illustrating the splitting of the J=1 level of the ground vibrational state and the J=2 level of the ν_1 fundamental vibrational state with a field of 20 kV/cm. The M splittings caused by application of the field and the inversion splitting are drawn to the same scale as indicated in the figure. Figure 23 shows a trace run under these conditions, using the modulated field technique, together with the regular spectrum and that predicted on the basis of the above theory, including the difference in transmission of the cell for the two polarizations. This last factor effectively eliminated radiation polarized parallel to the field so that only transitions involving $\Delta|M|=\pm 1$ were observed. The two weak absorption peaks located symmetrically about

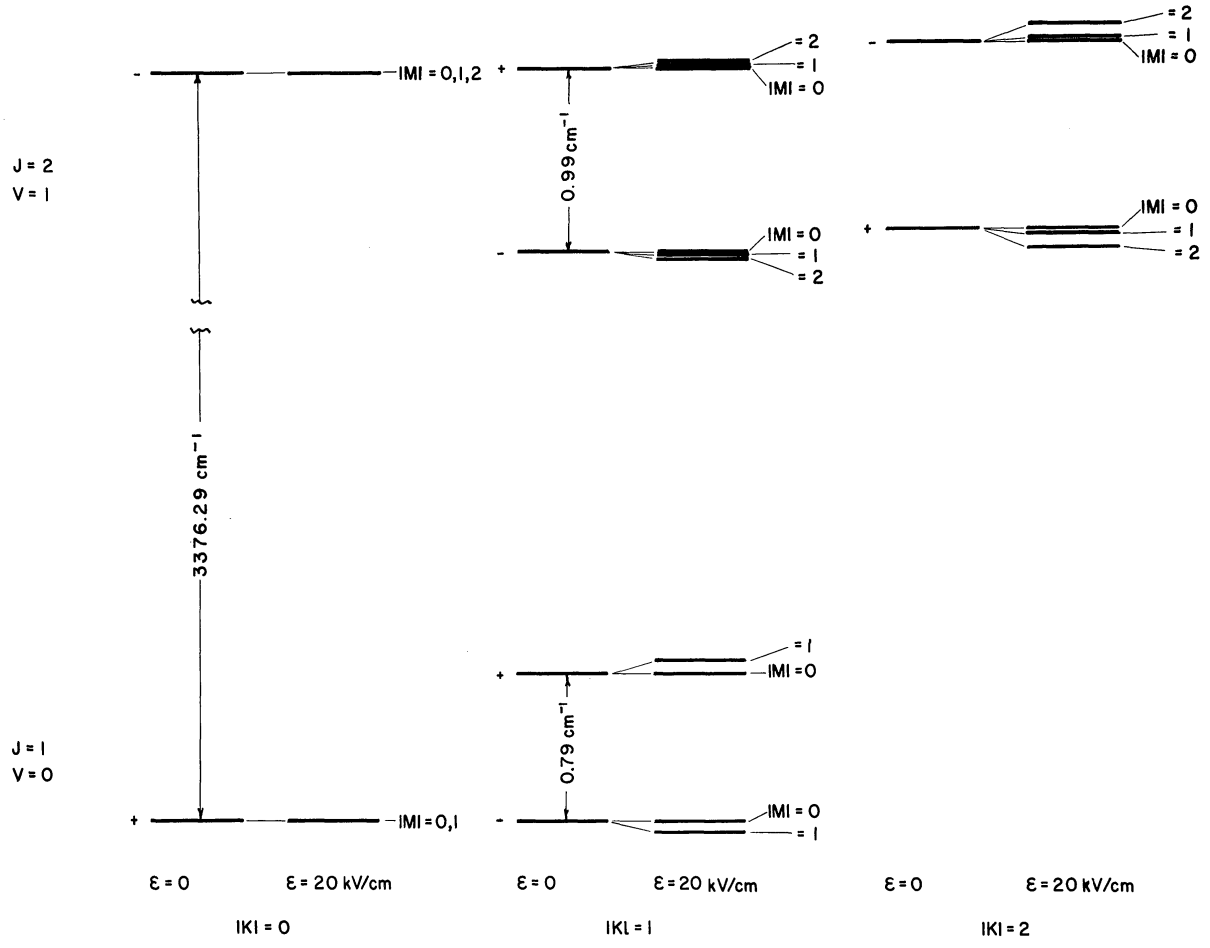

Figure 22 ENERGY LEVEL DIAGRAM FOR THE R(1) TRANSITIONS IN THE ν_1 FUNDAMENAL OF AMMONIA, WITH AND WITHOUT AN EXTERNALLY APPLIED ELECTRIC FIELD.

Selection rules for allowed transitions:
with field, $\Delta K = 0$, $\Delta M = 0, \pm 1$, $+ \leftrightarrow -$, $+ \leftrightarrow +$, $- \leftrightarrow -$.
without field, $\Delta K = 0$, $\Delta M = 0, \pm 1$, $+ \leftrightarrow -$,

The K dependence of the energy is suppressed, only the difference term between states of the same K being retained.

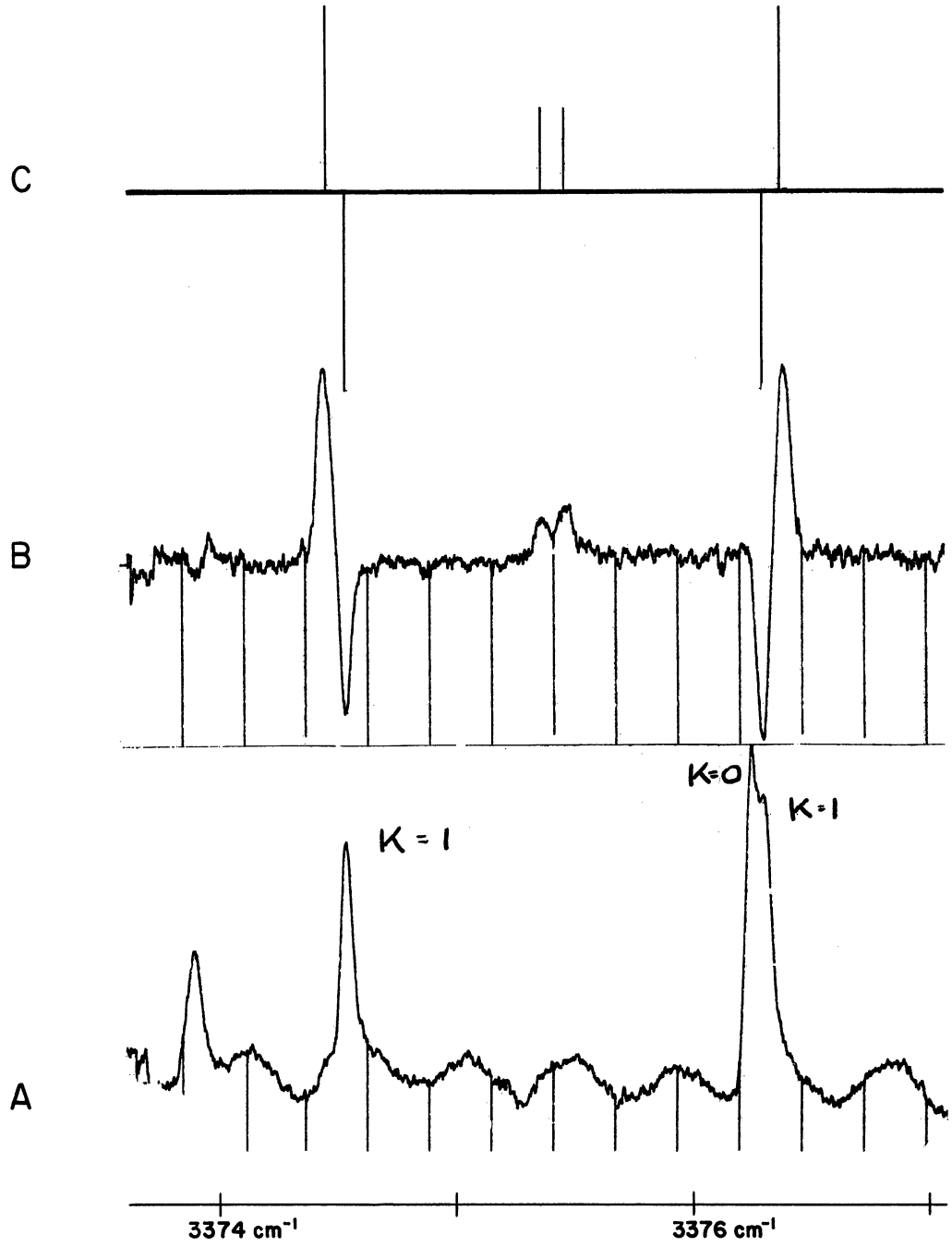

Figure 23 STARK EFFECTS OF R(1) IN THE ν_1 FUNDAMENTAL OF AMMONIA

A. Normal absorption spectrum.

B. Stark difference signal spectrum, 15 kV/cm.

C. Predicted spectrum.

the center of gravity of the inversion doublet are the 'induced' transitions resulting from the mixing of the wave functions by the field. Although in principle there are eight such induced absorptions, only two have appreciable intensity, namely the $|M| = 1$ to $|M| = 2$ transitions. (Two of the others are weak due to the polarization effects of the Stark cell. The remaining four transitions involve $M = 0$ states which remain 'pure' in the presence of a field and hence are not strongly 'induced.') The frequency separation of this pair is dependent upon the field strength. On extrapolation of this separation to zero field (where the line intensities are zero), one obtains directly the frequency difference between the inversion splitting in the ground and excited vibrational states. Since the sum of these inversion splittings may be obtained directly from the frequency interval between the members of the normally active doublet, the individual splittings may be determined. These inversion splittings have been thoroughly investigated in ammonia (29, 30, 31, 32). However, the spectra of the mixed isotopes NH_2D and NHD_2 (which are asymmetric tops) are difficult to analyze by conventional methods, and it would appear that the Stark difference signal would be of aid in identifying the doublets and in determining their inversion splittings.

Figure 24 shows the R(3) region of the ν_1 fundamental of ammonia with and without an A.C. field of 20 kV/cm. Identification of Stark components was hindered by the presence of small water vapor absorptions (marked with dots) which also showed Stark effects. In a supreme effort, and at the cost of one burned out Stark cell, the same region was run at a D.C. field of 50 kV/cm. Figure 25 is a level diagram for these conditions, the displacements being drawn to scale. The allowed transitions have not been indicated as there are 133 obeying the $P'_{cm} \leftrightarrow -P''_{cm}$ and 132 more, weaker ones, in

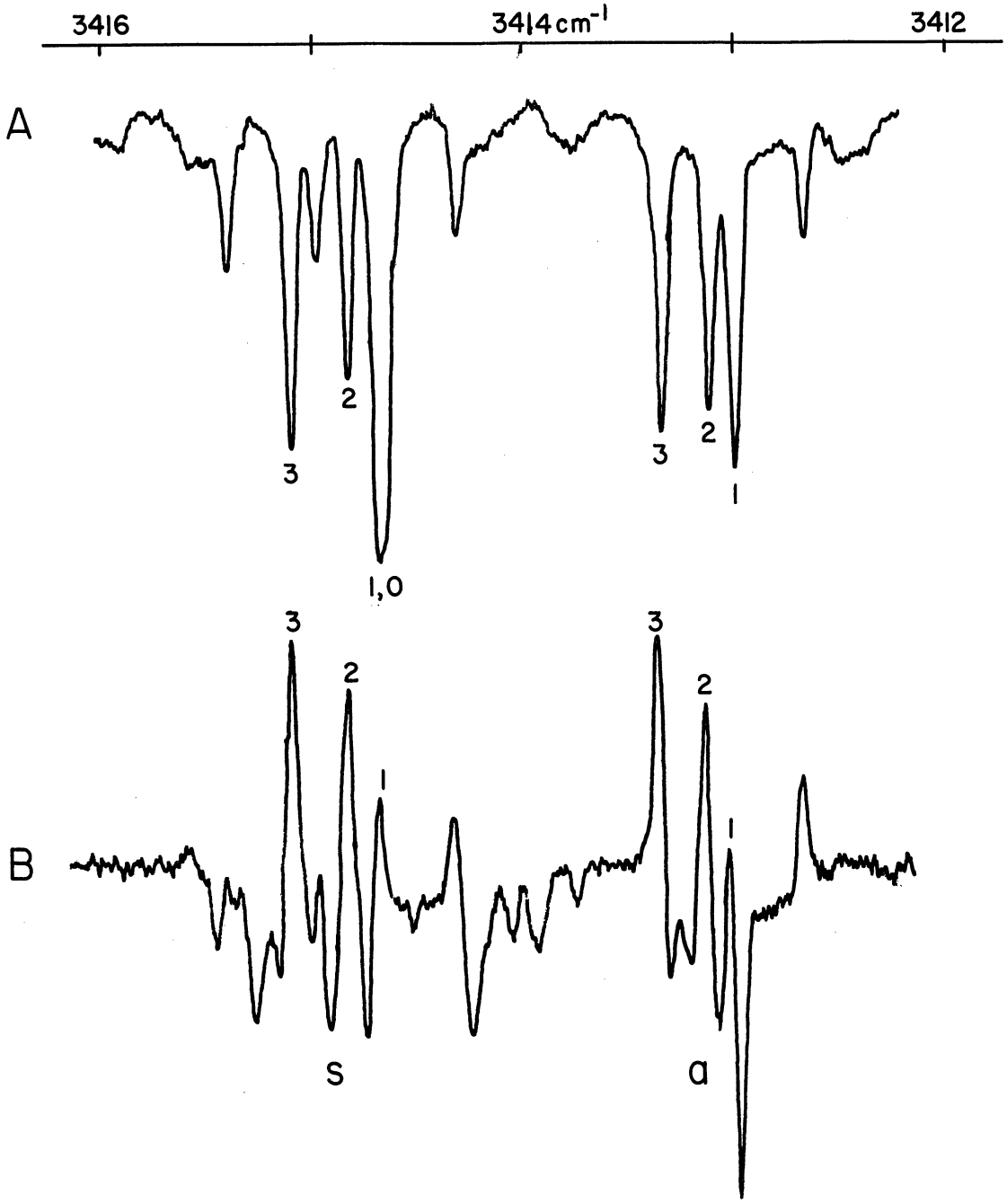

Figure 24 STARK EFFECT OF R(3) IN THE ν_1 FUNDAMENTAL OF AMMONIA.

A. Normal spectrum. K values indicated.

B. Stark difference signal. 20kV/cm. Negative signal implies greater absorption with field on.

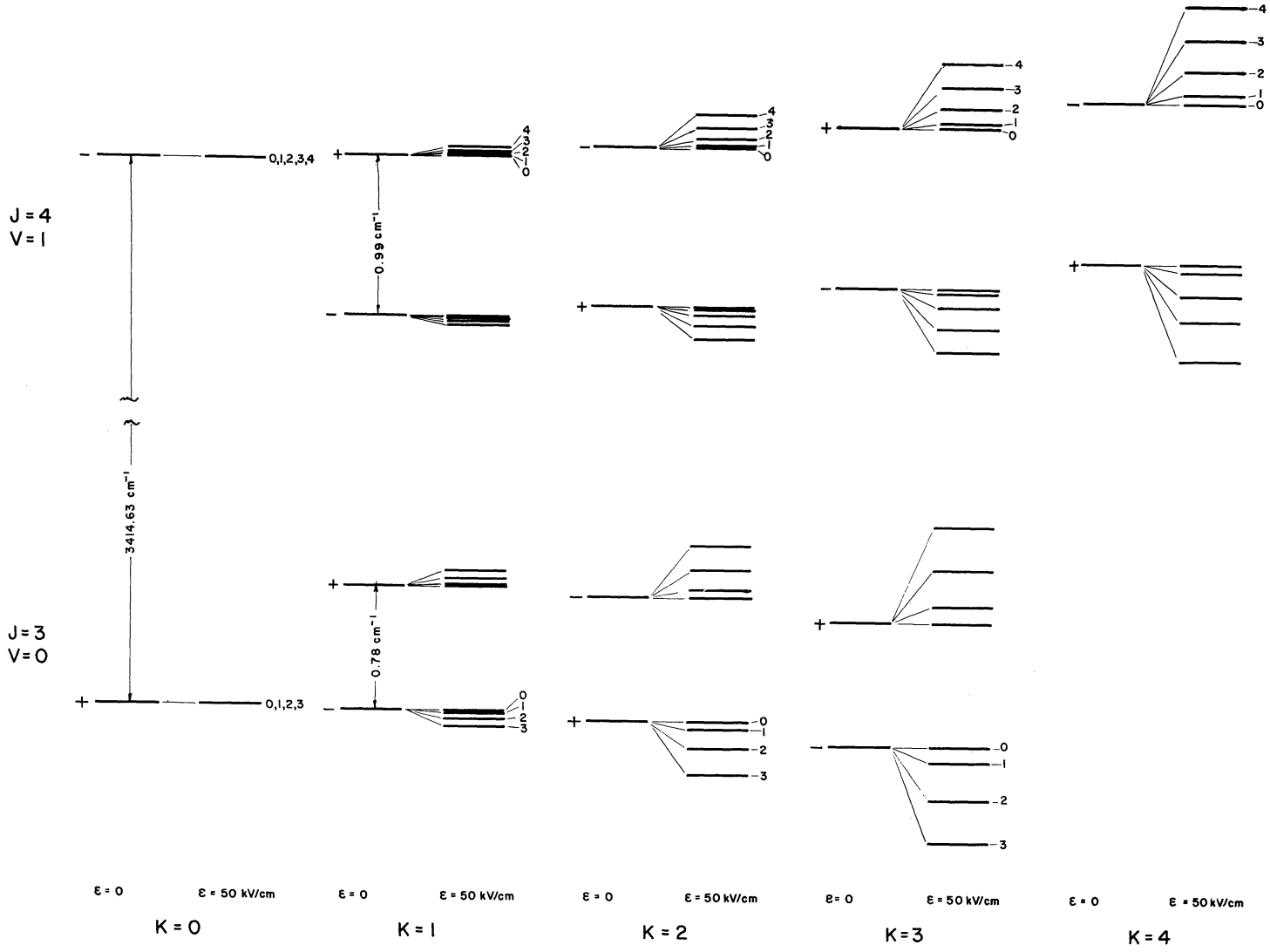

Figure 25 ENERGY LEVELS FOR THE R(3) TRANSITIONS IN THE ν_1 FUNDAMENTAL OF AMMONIA, WITH AND WITHOUT AN EXTERNALLY APPLIED ELECTRIC FIELD.

IM1 values are indicated. + and − refer to symmetry under I_{cm}. K dependence of the energy is suppressed, only the difference term between states of the same K being retained.

violation of this rule due to mixing of states in the presence of the field. Figure 26 shows the results of the 50 kV/cm run, together with another zero field trace of the region at maximum resolution. No attempts were made to correlate spectrum and theory!

5.5 Water

H_2O was selected as a representative case of an asymmetric top molecule in which to observe the Stark effect on the rotation-vibration spectrum.

A section of the Stark spectrum of water, obtained using the difference signal technique is reproduced in Figure 27. Table XI lists the prominent signals occurring in such a spectrum, giving both the relative intensities and the zero field transitions involved. It is seen that the largest Stark effects are not necessarily associated with states of low rotational energy, contrary to our previous experience. The two strongest signals arise from transitions involving rotational levels having $J \geq 4$. This implies the existence of closely spaced levels capable of interacting through an electric field perturbation.

A detailed theory of the Stark effect of asymmetric molecules, to second order in the perturbing fields, has been given by Golden and Wilson (33). They show that first order effects vanish identically, and are able to express the second order energy corrections as:

$$\Delta W_{J\tau M} = \frac{2\mathcal{E}^2}{A+C} \left[\begin{array}{l} \mu_x^2 \left(A_{J\tau}^{\bar{x}} + M^2 B_{J\tau}^{\bar{x}} \right) \\ + \mu_y^2 \left(A_{J\tau}^{\bar{y}} + M^2 B_{J\tau}^{\bar{y}} \right) \\ + \mu_z^2 \left(A_{J\tau}^{\bar{z}} + M^2 B_{J\tau}^{\bar{z}} \right) \end{array} \right] .$$

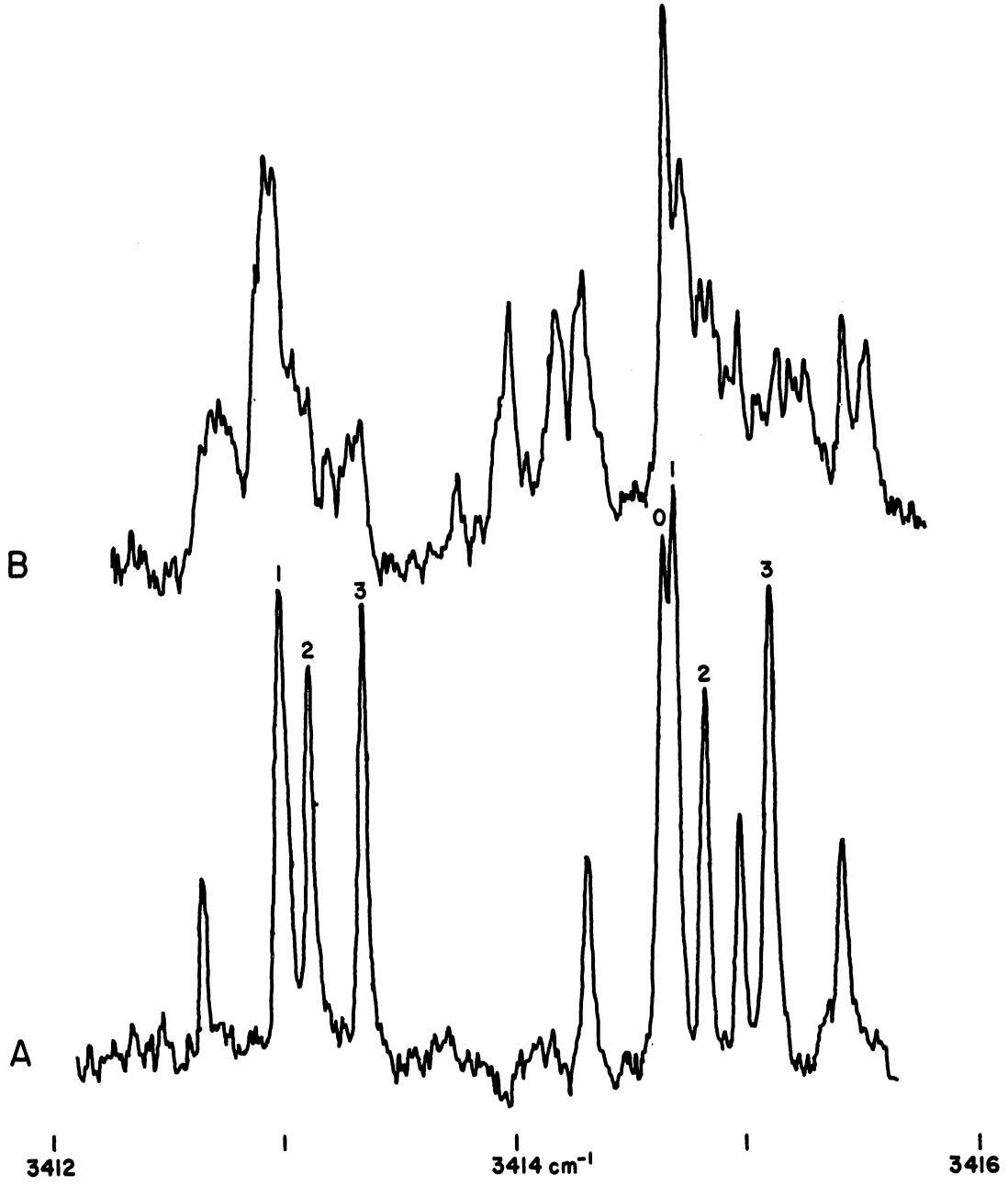

Figure 26 HIGH DC FIELD STARK EFFECT OF R(3) IN THE ν_1 FUNDAMENTAL OF AMMONIA.

A. Normal spectrum. K values indicated.

B. Spectrum with 50 kV/cm^{-1} DC field.

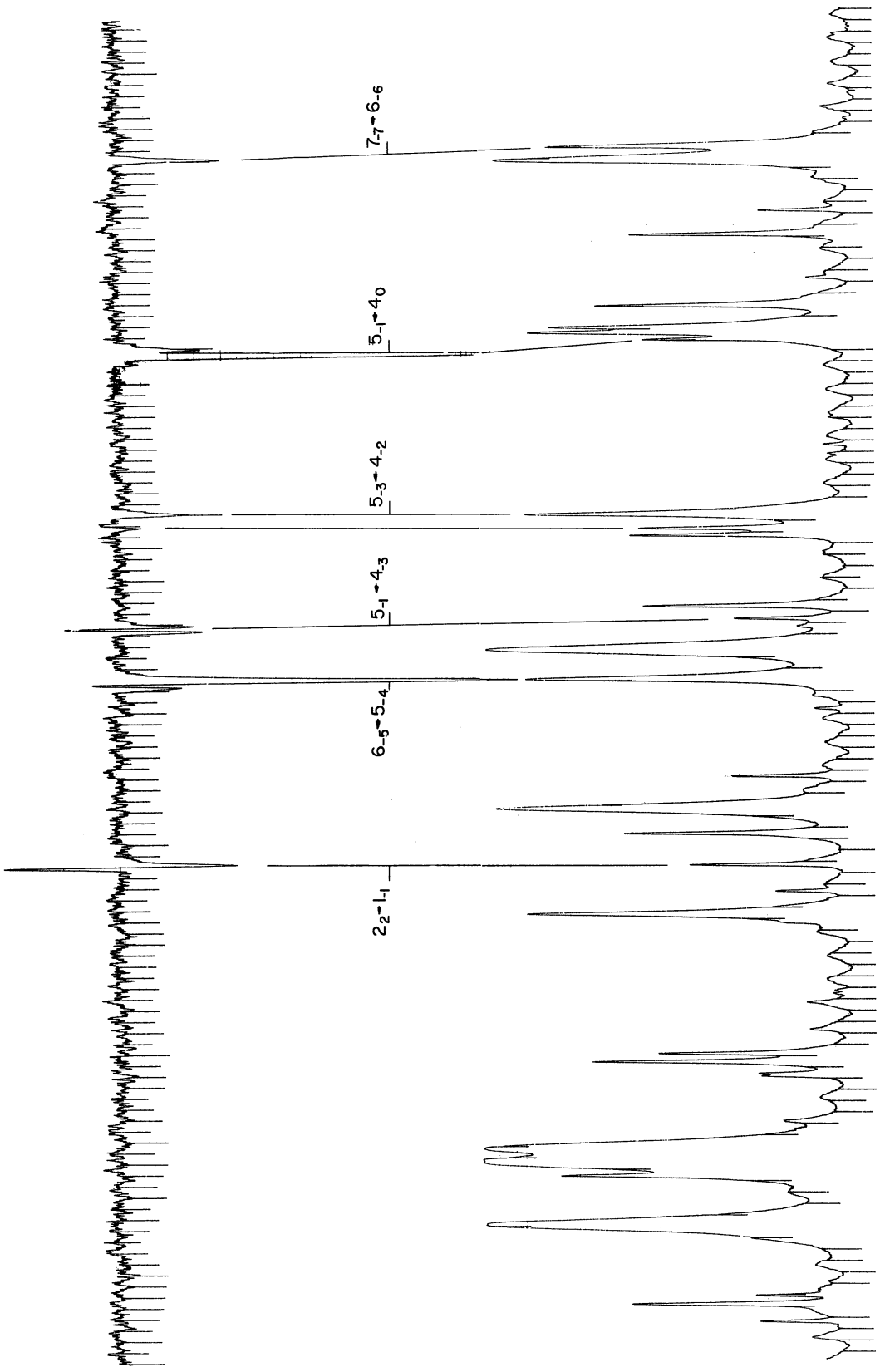

Figure 27 H_2O NEAR 3870 cm^{-1} 1 cm. press.

ABOVE: STARK DIFFERENCE SIGNAL, 10 $^{kv}/_{cm}$ BELOW: NORMAL SPECTRUM

TABLE XI

Summary of Stark Effects Observed in the Spectrum of H_2O

Frequency	Parent Transition J'	J''	Vib	Rel. Stark Sig.[a]	Orig. of Stark Sig.[b]
3880.07 cm^{-1}	5_{-1}	4_0	ν_3	10.5	B
3869.67	6_{-5}	5_{-4}	ν_3	9.5	B
3863.48	2_2	1_{-1}	ν_3	4.3	C
3871.65	5_{-1}	4_{-3}	ν_1	2.5	B
3973.98	5_{-1}	4_{-4}	ν_3	2.4	B
3779.41	1_{-1}	0	ν_3	2.3	C
	5_{-1}	5_{-2}	ν_3		B
3892.80	3_1	2_{-2}	ν_3	2.2	C
3711.09	2_{-1}	1_{-1}	ν_1	2.2	C
3885.77	7_{-6}	6_{-5}	ν_3	2.0	A
3696.22	5_{-1}	5_{-3}	ν_1	2.0	B
3629.53	4_0	3_{-3}	ν_3	1.8	X
3904.22	6_{-2}	5_{-1}	ν_3	1.7	A
3835.02	4_{-3}	3_{-2}	ν_3	1.7	B
3746.23	2_1	1_1	ν_1	1.4	C
3874.53	5_{-3}	4_{-2}	ν_3	1.3	B
3770.17	6_{-5}	5_{-5}	ν_1	1.3	B
3759.76	1_1	1_0	ν_3	1.3	C
3738.31	2_{-1}	2_0	ν_3	1.3	C
3637.99	1_{-1}	1_1	ν_1	1.2	C
3674.95	1_1	1_{-1}	ν_1	1.2	C
3709.16	2_1	2_{-1}	ν_1	1.2	C
	1_{-1}	2_{-2}	ν_3		C
3831.68	3_{-1}	2_0	ν_3	1.0	C
3785.01	7_{-7}	6_{-5}	ν_1	0.9	A
3823.09	5_{-3}	5_{-4}	ν_3	0.8	B
3749.49	2_1	2_2	ν_3	0.8	C

Table XI (Con't)

3819.88	3_0	3_{-3}	ν_3	0.7	X
3815.96	3_{-2}	2_{-1}	ν_3	0.7	C
3750.84	4_4	4_2	ν_1	0.7	X
3843.68	6_{-4}	6_{-5}	ν_3	0.6	A
3779.41	1_{-1}	0	ν_3	0.6	C
	5_{-1}	5_{-2}	ν_3		B
3701.45	1_1	2_0	ν_3	0.6	C
3820.65	3_{-3}	2_{-2}	ν_3	0.5	C

a. Simply the peak-to-peak Stark signal and only a crude estimate of the Stark shifts.

b. A Degenerate level in ground vibrational state

B Degenerate level in excited vibrational state

C Ordinary Stark shift of a strong transitions beteen low J(<2) levels. Independent of near degeneracies.

X Unexplained by A, B, or C.

Here A and C are the respectively largest and smallest rotational constants, and $\mu_{\bar{x}_i}$ is the $\bar{x}_i$ component of the molecular diople moment ($\bar{x}$ is defined as the axis of least moment of inertia, $\bar{z}$ that of the largest). The quantities $A_{J\tau}^{\bar{x}i}$ and $B_{J\tau}^{\bar{x}i}$ depend upon the quantum numbers and upon the molecular asymmetry parameters $\alpha = \frac{A-C}{A+C}$ and $K = \frac{2B-A-C}{A-C}$. A and B are listed in Table XII in terms of the quantum numbers, the state function expansion coefficients (34,35) using symmetric top eigenfunctions and the parity P_{x_i} of the state function for a rotation by 180° about $\bar{x}_i$. $A_{J\uparrow}^{\bar{x}i}$ and $B_{J\uparrow}^{\bar{x}i}$ have been numerically evaluated by Golden and Wilson (33) for all levels between $0 \leqslant J \leqslant 2$, entries being given for values of α ranging from 0.1 to 0.9 and for K from -0.9 to 0.9, both in steps of 0.2.

Let us compute, using Golden's tables, the second order perturbation correction to the ground rotational state W_{ooo} for water. Here, $\alpha = 0.48$ $K = -0.43$, $\frac{A+C}{2} = 18.4\ cm^{-1}$ and $\frac{2\mu^2 \mathcal{E}^2}{A+C} = 0.023\ cm^{-1}$ at $\mathcal{E}$ = 20 kV/cm. The permanent dipole moment of water lies along its $\bar{y}$ axis and thus

$$\Delta W_{ooo} = 0.023 A_{oo}^{\bar{y}} = 0.004\ cm^{-1}.$$

As in the case of linear and symmetric top molecules, the ground rotational state of asymmetric molecules is strongly affected by Stark fields. This computation then indicates that, barring accidental interacting degeneracies, field effects in H_2O will be very weak and individual Stark components cannot at present be resolved.

Golden and Wilson (33) have also considered the case of accidental doubly degenerate levels by first solving the double degenerate problem exactly, and then proceeding with the perturbation calculation as before.

The dipole moment of water lies along the $\bar{y}$ axis and changes sign under 180° rotation about either the $\bar{x}$ or $\bar{z}$ axes. The Stark perturbation, $-\bar{\mu} \cdot \bar{\mathcal{E}}$,

TABLE XII

Coefficients in the Perturbation Calculation for the Stark Effect of Asymmetric Rotors

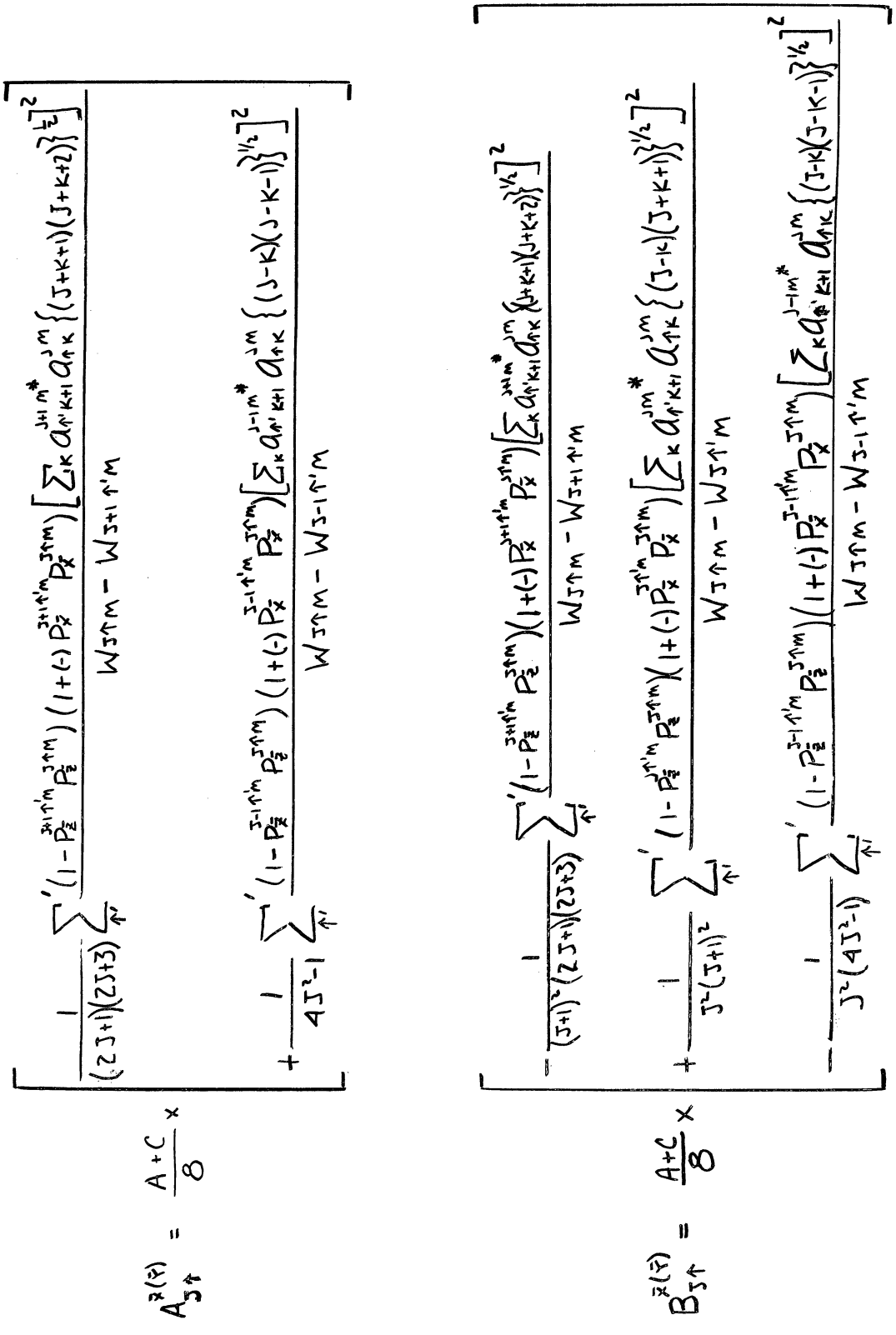

$$A^{\bar{z}}_{J\uparrow} = \frac{A+C}{8} \times \left[\frac{1}{(2J+1)(2J+3)} \sum_{\uparrow'}{}' \frac{(1+P^{J+1\uparrow'm}_{\bar{z}} P^{J\uparrow m}_{\bar{z}})(1-P^{J+1\uparrow'm}_{\bar{x}} P^{J\uparrow m}_{\bar{x}}) \left[\sum_K a^{J+1\,m*}_{\uparrow' K} a^{Jm}_{\uparrow K} \{(J+1)^2 - K^2\}^{\frac{1}{2}} \right]^2}{W_{J\uparrow m} - W_{J+1\uparrow' m}} \right.$$

$$\left. + \frac{1}{4J^2-1} \sum_{\uparrow'}{}' \frac{(1+P^{J-1\uparrow'm}_{\bar{z}} P^{J\uparrow m}_{\bar{z}})(1-P^{J-1\uparrow'm}_{\bar{x}} P^{J\uparrow m}_{\bar{x}}) \left[\sum_K a^{J-1\,m*}_{\uparrow' K} a^{Jm}_{\uparrow K} \{J^2 - K^2\}^{\frac{1}{2}} \right]^2}{W_{J\uparrow m} - W_{J-1\uparrow' m}} \right]$$

$$B^{\bar{z}}_{J\uparrow} = \frac{A+C}{8} \times \left[-\frac{1}{(J+1)^2(2J+1)(2J+3)} \sum_{\uparrow'}{}' \frac{(1+P^{J+1\uparrow'm}_{\bar{z}} P^{J\uparrow m}_{\bar{z}})(1-P^{J+1\uparrow'm}_{\bar{x}} P^{J\uparrow m}_{\bar{x}}) \left[\sum_K a^{J+1\,m*}_{\uparrow' K} a^{Jm}_{\uparrow K} \left[(J+1)^2 - K^2\right]^{\frac{1}{2}} \right]^2}{W_{J\uparrow m} - W_{J+1\uparrow' m}} \right.$$

$$+ \frac{1}{J^2(J+1)^2} \sum_{\uparrow'}{}' \frac{(1+P^{J\uparrow'm}_{\bar{z}} P^{J\uparrow m}_{\bar{z}})(1-P^{J\uparrow'm}_{\bar{x}} P^{J\uparrow m}_{\bar{x}}) \left[\sum_K a^{Jm*}_{\uparrow' K} a^{Jm}_{\uparrow K} K \right]^2}{W_{J\uparrow m} - W_{J\uparrow' m}}$$

$$\left. - \frac{1}{(4J^2-1)J^2} \sum_{\uparrow'}{}' \frac{(1+P^{J-1\uparrow'm}_{\bar{z}} P^{J\uparrow m}_{\bar{z}})(1-P^{J-1\uparrow'm}_{\bar{x}} P^{J\uparrow m}_{\bar{x}}) \left[\sum_K a^{J-1\,m*}_{\uparrow' K} a^{Jm}_{\uparrow K} \left[J^2 - K^2\right]^{\frac{1}{2}} \right]^2}{W_{J\uparrow m} - W_{J-1\uparrow' m}} \right]$$

will have the same symmetry properties. Thus two state functions having opposite parity under both of the rotations $\underline{C_2^x}$ and $\underline{C_2^z}$, and also satisfying $|\Delta J| \leq 1$, will interact in the presence of an applied electric field. Reference to the term values for water as given by Plyler (36) reveals that several pairs of states satisfying these conditions are degenerate to within 10 cm^{-1}. They are listed in Table XIII for the three vibrational states of interest $(\nu_1\nu_2\nu_3) = (000), (100), (001)$.

TABLE XIII

Summary of Nearly Degenerate Eigen States Having Connecting Dipole Moment Matrix Elements for the Water Molecule

Higher State J	Higher State Vib State	Lower State J	Lower State Vib State	Energy Separation cm^{-1}
6_{-5}	grnd	5_{-1}	grnd	0.74
6_{-5}	ν_1	5_{-1}	ν_1	0.18
6_{-5}	ν_3	5_{-1}	ν_3	0.16
5_{-4}	ν_1	4_{-3}	ν_3	0.08
5_0	ν_1	5_{-3}	ν_3	0.37
4_1	ν_1	3_2	ν_3	0.69
4_{-2}	ν_1	3_{-1}	ν_3	0.92

The interpretation given the observed spectra is immediately confirmed. The closest interacting degeneracy gave rise to the strongest observed effect. Indeed, every entry (with one exception) to the list of strong Stark signals as given in Table XI can be traced to either a transition involving an interacting degenerate level or to one involving levels of very small rotational energy.

VI. SUMMARY

A survey has been made of Stark effects in the vibration-rotation spectra of hydrogen cyanide, methyl fluoride, methyl iodide, ammonia and water.

The experiment depended entirely upon construction of a Stark cell which would permit application of fields between 10 and 100 kV/cm to vapor samples at several mm pressure. A light guide type cell was employed which had chromium front surfaced mirrors as plane parallel electrodes. The electrode separation of 0.2 to 0.5mm was evaulated by employing partially transparent mirror electrodes and examining the fringe systems produced upon passing light through the cell perpendicular to its transmission axis. A mean cell gap and a gap tolerance could in this way be determined. The voltage was established to ±0.1% and the gap tolerance held to ±1% so that the electric field was known to ±1%.

All of the observed field effects could be adequately explained on the basis of either perturbation theory, the theory of two interacting nearly degenerate states, or an exact solution to the problem of a symmetric top in an arbitrarily high electric field.

Hydrogen cyanide was found ideally suited to Stark effect studies. Its intense infrared absorption permitted use of minimum sample pressures and therefore of maximum electric fields. Its large dipole moment and reasonably small 'B' value gave rise to measurable frequency displacements. Its normal spectrum, that of a linear molecule and not seriously complicated by overlapping absorption bands, permitted identification of resolved Stark patterns. Careful measurement of certain splittings yielded a value for the dipole moment of hydrogen cyanide in its ν_3 vibrational state of 3.001 ±.007 debye

(as compared to 2.985 ±.005 in the ground state).

Isolation and identification of individual M components in the Stark effect patterns of methyl fluoride and methyl iodide was not possible because of the close spacing of lines in the normal spectra. Additionally, only modest fields could be applied since high sample pressures were needed to produce adequate absorption strengths. In the presence of a weak field, the individual absorption lines of a symmetric top molecule are broadened by an amount proportional to K/J^2. The intensity of a Stark difference signal will be proportional to this as well as to the usual factors. The Stark difference spectrum proved useful as an aid to making assignments in the zero field spectrum due to this new intensity modulation. At optimum field, some 70% of the transitions observed in the normal spectrum of methyl iodide were of negligible intensity in the Stark difference signal spectrum.

The inversion doubling of the ammonia molecule gave rise to interesting Stark effects in its spectrum. In the presence of an applied electric field, the wave functions describing adjacent inversion states mix and permit transitions previously forbidden in accordance with the selection rule $s \leftrightarrow a$, $s \not\leftrightarrow s$, $a \not\leftrightarrow a$. When extrapolated to zero field, the frequency separation between the 's' $\leftrightarrow$'s' and 'a' $\leftrightarrow$ 'a' 'field induced' absorptions equals the difference in the inversion splittings of the ground and excited vibrational states. These effects would prove helpful in understanding the spectra of the isotopic species NH_2D and NHD_2.

Accidental degeneracies, characteristic of the energy levels of asymmetric top molecules, led to the bulk of observable signals in the Stark difference spectrum of water. In addition, slight displacements were detected for transitions involving low J energy levels.

With present resolution and detectivity, observation of Stark effects in vibration-rotation spectroscopy remains limited to the spectra of carefully selected molecules. Increased luminosity of the source and a more sensitivity detector, as well as a Stark cell with higher transmission efficiency and higher breakdown voltage rating (conditions optimized as far as possible in the present experiments) would not greatly change this situation. A major improvement would result, however, from increased spectral resolution. With increased resolution, smaller frequency shifts could be detected and the lower sample pressures required to obtain adequate absorption strengths would enable higher electric fields to be applied without breakdown. In particular, the substantially greater resolving power of a Fabry Perot interferometer, if it could be incorporated into the experimental arrangement, would permit isolation and measurement of a great many Stark patterns which cannot currently be resolved.

BIBLIOGRAPHY

1. J. Stark, Berl. Akad, Wiss., 40, 932 (1913).

2. See, for instance, C. Townes, A. Schawlow, Microwave Spectroscopy, McGraw-Hill, New York (1955).

3. N. F. Ramsey, Molecular Beams, Oxford Clarendon Press, London (1956).

4. R. Terhune, C. Peters, J. Mol. Spect., 3, 138 (1959).

5. C. Costain, National Research Council of Canada, private communication.

6. M. Knoll, F. Ollendorff, R. Rompe, Gasentladungstabellen, 84, Springer-Verlag OHG, Berlin (1935).

7. H. Marshall, unpublished

8. D. Brown, High Resolution Infra-Red Spectroscopy, thesis, University of Michigan (1957).

9. D. Gates, C. Shaw, D. Beaumont, J. Opt. Soc. Am., 48, No. 2, 88 (1958).

10. J. Meek, J. Craggs, Electrical Breakdown of Gases, Oxford University Press, London (1953).

11. C. Church, High Resolution Electric Field Induced Infrared Absorption Spectra of H_2 and D_2, thesis, University of Michigan (1959).

12. D. Rank, G. Skorinko, D. Eastman, T. Wiggins, J. Opt. Soc. Am., 50, 421 (1960).

13. M. Born, H. Heisenberg, P. Jordan, Zeits. f. Physik 35, 565 (1925).

14. E. Whittaker, Analytical Dynamics, Cambridge University Press (1959).

15. F. Reiche, H. Rademaker, Zeits. f. Physik 41, 453 (1927).

16. W. Shaffer, J. Louck, J. Mol. Spec., 3, 123 (1959).

17. A. Edwards, Angular Momentum in Quantum Mechanics, Princeton University Press (1957).

18. J. H. Shirley, unpublished.

19. C. Schlier, Zeits. f. Physik 141, 16 (1955).

20. P. Kusch, V. W. Hughes, Handbuch der Physik XXXVII/I, 141 (1959).

21. D. Rank, A. Guenther, J. Shearer, T. Wiggins, J. Opt. Soc. Am., 47, 148, (1957).

22. B. N. Bhattacharya, W. Gordy, Phys. Rev., 119, 144 (1960).

23. G. Herzberg, Molecular Spectra and Molecular Structure, Van Nostrand, New York (1945).

24. S. Ghosh, R. Trambarulo, W. Gordy, J. Chem. Phys., 21, 308 (1953); Phys. Rev., 87, 172a (1952).

25. J. Pickworth, H. W. Thompson, Proc. Roy. Soc. London, A222, 443 (1954).

26. H. Edwards, Michigan State University, private communication.

27. K. T. Hecht, The University of Michigan, private communication.

28. C. E. Cleeton, N. H. Williams, Phys. Rev., 45, 234 (1934).

29. W. Weeks, Inversion Vibration and Inversion Rotation Interactions in the Ammonia Molecule, thesis, University of Michigan (1960).

30. D. M. Dennison, G. E. Uhlenbeck, Phys. Rev., 41, 313 (1932).

31. N. S. Benedict, E. K. Plyler, E. D. Tidwell, J. Chem. Phys., 32, 32 (1960).

32. C. C. Costain, Phys. Rev., 82, 108L (1951).

33. S. Golden, E. B. Wilson, J. Chem. Phys., 16, 669 (1948).

34. T. E. Turner, B. C. Hicks, G. Reitwiesner, Ballistics Research Laboratories Report No. 878 (Sept. 1953).

35. G. W. King, R. M. Hainer, P. C. Cross, J. Chem. Phys., 11, 27 (1943); J. Chem. Phys., 15, 89 (1947).

36. W. S. Benedict, E. K. Plyler, J. Res. Nat. Bur. Stds., 46, 246 (1951).

37. P. Jacquinot, R. Chabbal, J. Opt. Soc. Am., 46, 556 (1956).